Analytical Vortex Solutions to the Navier-Stokes Equation

Acta Wexionensia
No 114/2007
Theoretical Physics

Analytical Vortex Solutions to the Navier-Stokes Equation

Henrik Tryggeson

Växjö University Press

Analytical Vortex Solutions to the Navier-Stokes Equation.
Thesis for the degree of Doctor of Philosophy, Växjö University, Sweden 2007.

Series editor: Kerstin Brodén
ISSN: 1404-4307
ISBN: 978-91-7636-547-2
Printed by: Intellecta Docusys, Göteborg 2007

Abstract

Tryggeson, Henrik, 2007. *Analytical Vortex Solutions to the Navier-Stokes Equation*, Acta Wexionensia No 114/2007. ISSN: 1404-4307, ISBN: 978-91-7636-547-2. Written in English.

Fluid dynamics considers the physics of liquids and gases. This is a branch of classical physics and is totally based on Newton's laws of motion. Nevertheless, the equation of fluid motion, Navier-Stokes equation, becomes very complicated to solve even for very simple configurations. This thesis treats mainly analytical vortex solutions to Navier-Stokes equations. Vorticity is usually concentrated to smaller regions of the flow, sometimes isolated objects, called vortices. If one are able to describe vortex structures exactly, important information about the flow properties are obtained.

Initially, the modeling of a conical vortex geometry is considered. The results are compared with wind-tunnel measurements, which have been analyzed in detail. The conical vortex is a very interesting phenomenaon for building engineers because it is responsible for very low pressures on buildings with flat roofs. Secondly, a suggested analytical solution to Navier-Stokes equation for internal flows is presented. This is based on physical argumentation concerning the vorticity production at solid boundaries. Also, to obtain the desired result, Navier-Stokes equation is reformulated and integrated. In addition, a model for required information of vorticity production at boundaries is proposed.

The last part of the thesis concerns the examples of vortex models in 2-D and 3-D. In both cases, analysis of the Navier-Stokes equation, leads to the opportunity to construct linear solutions. The 2-D studies are, by the use of diffusive elementary vortices, describing experimentally observed vortex statistics and turbulent energy spectrums in stratified systems and in soap-films. Finally, in the 3-D analysis, three examples of recent experimentally observed vortex objects are reproduced theoretically. First, coherent structures in a pipe flow is modeled. These vortex structures in the pipe are of interest since they appear for Re in the range where transition to turbulence is expected. The second example considers the motion in a viscous vortex ring. The model, with diffusive properties, describes the experimentally measured velocity field as well as the turbulent energy spectrum. Finally, a streched spiral vortex is analysed. A rather general vortex model that has many degrees of freedom is proposed, which also may be applied in other configurations.

Keywords: conical vortex, Navier-Stokes equation, analytical solution, 2-D vortices, turbulence, vortex ring, stretched vortex, coherent structures.

.

Preface

This thesis is organised in the following way. First, an introduction to the subject is presented, together with a summery of the papers that this thesis is based on. Secondly, the papers are given in fulltext, and they are:

I. *Stationary vortices attached to flat roofs*
H. Tryggeson and M. D. Lyberg
Submitted to J. of Wind Eng. and Ind. Aero.

II. *Analytical Solution to the Navier-Stokes Equation for Internal Flows*
M. D. Lyberg and H. Tryggeson
Submitted to J. of Phys. A.

III. *Vortex Evolution in 2-D Fluid Flows*
H. Tryggeson and M. D. Lyberg
Submitted to Phys. Rev. Lett.

IV. *Analysis of 3-D Vortex Structures in Fluids*
M. D. Lyberg and H. Tryggeson
Submitted to Phys. Rev. Lett.

.

Contents

1 Introduction

Everyday we observe that liquids and gases in motion behave in a complex way. Even in very controlled forms, in a laboratory and with simple geometries considered, one finds that very complicated flow patterns arises. These phenomena are covered in the study of fluid dynamics or the equivalenty fluid mechanics. Fluid dynamics has important applications in such apart fields as engineering, geo- and astrophysics, and biophysics.

The French word *fluide*, and its English equivalent *fluid*, means "that which flows". So it is a substance whose particles can move around with total freedom (ideal fluids) or restricted freedom (viscous fluids). When fluid mechanics deals with liquids, in most cases meaning water, it becomes the mechanics of liquids, or hydrodynamics. When fluid consists of a gas, in most cases meaning air, fluid mechanics becomes the mechanics of gases, or aerodynamics.

It is difficult to make a short complete history of fluid dynamics but here is an attempt to name some of the main contributors, (for a more extended review see [1]). Archimedes (287-212 b.c.) was, perhaps, the first to study the internal structure of liquids. He produced two important concepts of classical fluid mechanics. Firstly, he claimed that a pressure applied to any part of a fluid is then transmitted throughout, and secondly that a fluid flow is caused and maintained by pressure forces. Archimedes founded fluid statics. Much later during the renaissance, Leonardo da Vinci (1452-1519) gave the first impulse to the renewed study of fluid statics. He presented, in philosophical words and in schetches and drawings, answers to a number questions concerning fluids. However it was Galileo Galilei (1565-1642) who laid the foundations of general dynamics, without which there would be neither fluid mechanics nor mechanics generally. He introduced the important concepts of inertia and momentum.

It is impossible to select any particular contribution from Isaac Newton (1642-1727) to fluid mechanics, for almost all the fundamental fluidmechanic concepts are built upon Newton's basic laws. For example, Navier-Stokes equation is just Newton's second law applied to fluids. His *Philosophiae Naturalis Principia Mathematica* became the guide of all the branches of mechanics. Later, the mathematican Lagrange named the work "the greatest production of the human mind". Then we have Leonhard Euler (1707-83) who may be named the founder of fluid mechanics, its mathematical architect. Earlier, there was a problem of the term "point" as an element of geometry because it has no extension, no volume and consequently lacks mass. And therefore momentum, used in Newton's laws, could not be defined. Euler was the first to overcome this fundamental contradiction by the introduction of his historic fluid particle, thus giving fluid mechanics a powerful instrument for physical and mathematical analysis.

The rapidly growing fluid mechanics demanded a more general solution of the problem of viscosity. Above all, it was necessary to establish the

most general equations of motion of real, viscous, fluids. Euler was the creator of hydrodynamics, but he failed to include viscosity. Instead, this was provided by Claude Navier (1785-1836) who devised a physical model for viscosity. He proceeded with the mathematical study of viscous flows and developed the famous Navier equation. About the same time the equation, but in a different form, was also obtained by Sir George Gabriel Stokes (1819-1903), a British mathematician and physicist. Therefore, it is often called the Navier-Stokes equation. The basic mathematical philosophy of fluid mechanics was thus complete.

In practical terms only the simplest cases can be solved so that an exact solution is obtained. For more complex situations, solutions of the Navier-Stokes equations may be found with the help of computers. A variety of computer programs (both commercial and academic) have been developed to solve the Navier-Stokes equations using various numerical methods [2, 3, 4].

The focus of this thesis is investigation and understanding of vortex structures. That is, trying to find mathematical descriptions for different objects of vorticity that satisfy Navier-Stokes equation. By studying the geometrical symmetries and boundary conditions for the vortices, a guidance for the choise of coordinates and mathematical functions is obtained. Also, it is helpful to consider Navier-Stokes equation in detail to find simplified cases and symmetries, but not compromise with the restriction of exact analytical solutions. Vortex motion and dynamics has been summerized in the literature, for example by Saffman [5], who almost entirely considers the special case of inviscid vortex motion. Ogawa [6] discusses vortices in engineering applications, such as chemical and mechanical technology. A more recent, and very rigorous summery of vorticity and vortex dynamics is given by Wu *et. al* [7].

The vortex models in this thesis are designed to find a connection between modern experiments and the observed results. One phenomenon which satisfyies the criteria is the conical vortex that rolls up near the roof corner on buildings with flat roofs. Such buildings correspond to many of the industrial building complexes. It is well known that, of all building surfaces, the zones of a flat roof close to the the roof corners experience the highest lift-off wind forces. That is just what the conical vortex is responible for. Another vortex feature with a respective experimental and theoretical history is the axis-symmetric vortex ring. From starting jets to volcanic eruptions or the propulsive action of some aquatic creatures, as well as the discharge of blood from the left atrium to the left ventricular cavity in the human heart, vortex rings (or puffs) can be identified as the main flow feature.

Turbulence is one of the most common examples of complex and disordered dynamical behaivor in nature. Yet the way in which turbulence arises and sustains itself is not understood, even in the controlled laboratory experiments. The first study of this kind was undertaken by Reynolds in 1883 [8]. He investigated transition to turbulence in a pipe flow. The theoretical investigation of the origin of turbulence is adressed to stability analysis of

perturbated solutions to a linerized Navier-Stokes equation, so called Orr-Sommerfeld equation [9, 10, 11]. In this thesis neither stability analysis nor the transition is considered. Instead, vortex modeling of coherent structures in turbulence is presented. Numerical simulations [12, 13] as well as experiments [14] indicate that, in turbulent flows, vorticity is concentrated in localized regions in the form of filaments. This recognition have led to interest in the dynamical behaivour of vortex structures with concentrated vorticity. A process occuring naturally in turbulent flows is the stretching of the vorticity field, strongly enhancing the vorticity [15]. In this thesis a new stretched vortex model is proposed with different properties than earlier studies [16, 17].

Recently, experimental observations of coherent structures in pipe flows in the range where transition to turbulence is expected suggests that the dynamics associated may indeed capture the nature of fluid turbulence [18, 19, 20]. In addition a large number of numerical simulations confirms coherent states in pipe flows [21, 22, 23]. The thesis provide studies of an exact coherent structures consisting of downstream vortices and associated streaks which are regulary arranged in circumferential direction.

In the last two decades laboratory studies of 2-D turbulence have appeared. So far only two schemes for generating 2-D turbulence have emerged. In one of them turbulence is generated in a relative thin layer of conducting fluid, with a spatially and temporally varying magnetic field applied perpendicular to this layer. The first such experiment was performed by Sommeria [24] and later by a series of studies by Tabeling and his collaborators [25, 26, 27, 28]. About the same time as Sommeria's experiments appeared, Couder demonstrated that vortex interactions and turbulence of 2-D type can also be generated in soap films [29, 30]. Furter extended studies by the use of soap films where made by Kellay and others [31, 32, 33, 34, 35]. In this thesis, a work of modeling these experiment results is presented.

The first part of this thesis presents an introductory section, where a basic theoretical background is given to fluid dynamics, turbulence and specially vortex modeling. The second part contains a presentation of the papers. In Paper I a model of a conical vortex inducing low pressures and suction on flat roofs is given. Paper II contains a new theoretical approach to attac the non-linear Navier-Stokes equation for internal flows. Then, in the following two papers, Paper III and Paper IV, a reproduction of experimental results are given for vortices in 2-D and 3-D, repectively.

2 Physics of Fluids

In this chapter, an elementary introduction to the physical ideas and the governing equations in fluid dynamics is reviewed. It is based on standard textbooks at undergraduate and graduate level such as [36, 37, 38, 39, 40]. Also, here is a discussion about boundary conditions, which is connected to the essence of Paper II. This Paper gives, by physical argumentation about vorticity production at boundaries, a suggestion for a solution procedure of the fluid flow equations of internal flows.

2.1 Concepts and Equations

The macroscopic properties of matter (solids, liquids and gases) are directly related to their molecular structure and to the nature of the forces between the molecules. Different molecular properties implies different thermodynamic states. The manner in which some of the molecular properties of a liquid stand between those of a solid and those of a gas is shown in Table 2.1. Before one can formulate basic equations, certain preliminary ideas are needed. Starting by making the assumtion of the applicability of continuum mechanics or the continuum hypothesis. Suppose that we can associate with any volume of fluid, no matter how small, macroscopic properties, for example the temperature with that of the fluid in bulk. This assumption is not correct if we go down to molecular scales, so a fluid particle thus must be large enough to contain many molecules. It must still be effectively a point with respect to the flow as a whole. Thus the continuum hypothesis can be valid only if there is a length scale, L_2, which we can think of as the size of a fluid particle, such that $L_1 \ll L_2 \ll L_3$ where the meaning of L_1 and L_3 is illustrated by Fig. 2.1. When the volume is so small that it contains only a few molecules and is characterized with a length scale L_1, there are large random fluctuations, associated with a Brownian motion. At the other extreme, the volume may become so large that it extends to regions where the temperature is significantly different. So L_3 is a typical length over which the macroscopic properties vary appreciably.

Now to the actual formulation of equations. The fundamental axioms of fluid dynamics are the conservation laws. Consider first the representation of mass conservation, often called the continuity equation. This is given by

$$\partial_t \rho + \nabla \cdot (\rho \boldsymbol{u}) = 0 \ , \tag{2.1}$$

where $\rho(\boldsymbol{r}, t)$ is the density and $\boldsymbol{u}(\boldsymbol{r}, t)$ is the velocity of the fluid. A fluid problem is called compressible if the pressure variations in the flow field are large enough to effect substantial changes in the density of the fluid. Flows of liquids with pressure variations much smaller than those required to cause phase change (cavitation), or flows of gases involving speeds much lower than the isentropic sound speed are termed incompressible. The continuity equation Eq. (2.1) then reduces to

	Intermolecular forces	Molecular arrangement	Type of statistics needed
solid	strong	ordered	quantum
liquid	medium	partially ordered	quantum + classical
gas	weak	disordered	classical

Table 2.1: Some molecular properties of solids, liquids and gases. Notice how the properties of liquids stand between the other two.

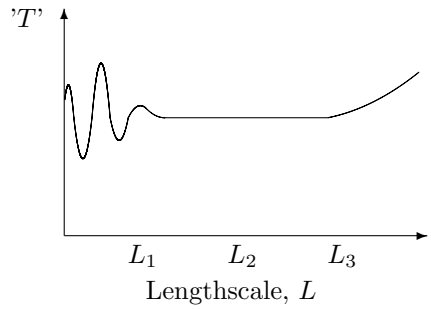

Figure 2.1: Schematic variation of average energy of molecules with length scale.

$$\nabla \cdot \boldsymbol{u} = 0 \ . \tag{2.2}$$

The next equation to be considered is the represenatation of Newton's second law of motion for fluids. It states that the rate of change of momentum of a fluid particle is equal to the net force acting on it. This is called Navier-Stokes equation and may be written

$$\partial_t \boldsymbol{u} + (\boldsymbol{u} \cdot \nabla)\boldsymbol{u} = -\rho^{-1}\nabla p + \nu \nabla^2 \boldsymbol{u} + \boldsymbol{F} \ , \tag{2.3}$$

where $p(\boldsymbol{r}, t)$ is the pressure, ν is a property of the fluid called the kinematic viscosity and the term $\boldsymbol{F}(\boldsymbol{r}, t)$ represents externally imposed forces. There are two types of forces acting on fluid particles. The surface forces, such as pressure and viscous forces, are given by the first two terms on the right hand side. Secondly, we have body forces, for example gravity, centrifugal, Coriolis and electromagnetic forces. Furthermore, notice that the equation is a non-linear partial differential equation in $\boldsymbol{u}$ (the second term on the left hand side). This is called the convective term. The non-linearity is responsible for much of the mathematical difficulty of fluid dynamics. The continuity equation and Navier-Stokes equation provide one scalar equation and one vector equation, effecively four simultaneous equations. The correspnding variables to be determined are one scalar variable (the pressure p)

and one vector variable (the velocity $\boldsymbol{u}$), effectively four unknown quantities, so in that sense the set of equations is closed.

The kinematic viscosity, ν, is effectively a diffusivity for the velocity $\boldsymbol{u}$, having the same dimensions $[length] \times [velocity]$ like all diffusivities. Values of ν and the equivalent dynamic viscosity $\mu = \nu/\rho$ for some common fluids at 15°C and one atmosphere pressure are presented in Table 2.2.

There are several ways to reformulate Eq. (2.3) with the use of vector identities. For example, we may write Eq. (2.3) as

$$\partial_t \boldsymbol{u} + \boldsymbol{\omega} \times \boldsymbol{u} + \frac{1}{2}\nabla \boldsymbol{u}^2 = -\rho^{-1}\nabla p - \nu \nabla \times \boldsymbol{\omega} + \boldsymbol{F} \ , \tag{2.4}$$

where $\boldsymbol{\omega} = \nabla \times \boldsymbol{u}$. This appearance of Navier-Stokes equation will be helpful for the analysis in Ch. 3.2.

2.2 Reynolds Number

In fluid dynamics, Reynolds number, Re, is an important non-dimensional number and it implies a rough estimation of the relative magnitudes of two key terms in the equation of motion, Eq. (2.3). which is the ratio

$$\frac{|\text{inertia term}|}{|\text{viscous term}|} = \frac{|(\boldsymbol{u} \cdot \nabla)\boldsymbol{u}|}{|\nu \nabla^2 \boldsymbol{u}|} = \frac{O(U^2 L^{-1})}{O(\nu U L^{-2})} = O\left(\frac{UL}{\nu}\right) = O(\text{Re}) \ . \tag{2.5}$$

Stokes flow is a flow at very small Reynolds numbers, such that inertial forces can be neglected compared to viscous forces. Solutions of this problem are reversible in time, i.e. still make sense when reversing the motion. On the contrary, high Reynolds numbers indicate that the inertial forces are more significant than the viscous (friction) forces. Therefore, we may assume the flow to be an inviscid flow, an approximation in which we neglect the viscosity as compared to the inertial term. The standard equations of inviscid flow are called the Euler equations. Another often used model, especially in computational fluid dynamics, is to use the Euler equations far from the body and the boundary layer equations, which incorporate viscosity, close to the body. The Euler equations can be integrated along a streamline to get the well known as Bernoulli's equation. When the flow is everywhere irrotational (contains no vorticity, see Ch. 3.1) as well as inviscid, Bernoulli's equation can be used throughout the field. A complication at high Reynolds number is that steady flows are often unstable to small disturbances, and may, as a result, become turbulent.

2.3 Boundary Conditions

Since the governing equations of fluid motion are differential equations, the specification of any problem must include the boundary conditions. There are various types of boundaries, but we restrict ourself to the most common type of boundary to a fluid region, the rigid impermeable wall. One applying condition is obiously the requirement that no fluid should pass through

	μ [g cm^{-1} s^{-1}]	ν [cm^2 s^{-1}]
air	0.00018	0.15
water	0.011	0.011
mercury	0.016	0.0012
olive oil	0.99	1.08
glycerine	23.3	18.5

Table 2.2: Dynamic viscosity and kinematic viscosity for some common fluids.

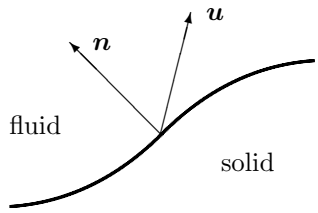

Figure 2.2: Velocity vectors of solid and fluid particles immediately next to its surface.

the wall. The condition on the tangential component of velocity to be zero at solid boundaries is known as the no-slip or adherence condition, and it holds for a fluid of any viscosity $\nu \neq 0$. In the language of partial differential equations the no slip case corresponds to a Dirichlet-type boundary condition. Summing up, we have the following relations for the velocity of fluid, $\boldsymbol{u}$, at solid boundaries at rest, with a unit normal $\boldsymbol{n}$ to the surface (see Fig. 2.2)

$$\boldsymbol{u} \cdot \boldsymbol{n} = \boldsymbol{u} \times \boldsymbol{n} = 0 \ . \tag{2.6}$$

Some remarks about the boundary conditions may be noticed. About two centuries ago Navier proposed a more general boundary condition that allows slip at the surface. The boundary condition states that the tangential component of the velocity at the surface is proportional to the tangential stress at the surface. For a flat wall, the boundary condition reduces to $v_t = \lambda_0 \partial_n v_t$, where v_t is the tangential velocity, $\partial_n v_t$ is its normal derivative, and λ_0 is the slip length. Currently there is a major interest in slip flows in microfluids, where slip lengths heve been measured [42, 41]. Also, there are recent theoretical studies on streamline patterns when the slip-parameter λ_0 is changed [43, 44].

In paper II we discuss how the no-slip boundary condition acts as a source of vorticity in fluid flows. Then, one needs to add to the right-hand side of Eq. (2.3) the forces acting on the system boundaries. They are of the form of an externally applied pressure at inlets and outlets and viscous stress (vorticity) at solid walls. The velocity field may be calculated explicitly and shown to depend on boundary conditions only.

3 Vorticity

The subject of vorticity and vortices is of general interest in mechanical engineering, chemical engineering and also in powder technology. The studies of vortices also has a respectable history. For example, Leonardo da Vinci depicted very interesting drawings of various kinds of vortex and eddy flows.

Traditionally, fluid motion is described by Navier-Stokes equation, which is written in terms of the fluid velocity at every point and expresses Newton's law that force equals mass times acceleration. In this chapter the voticity equation for determining fluid flow is presented. Then an introduction of velocity potentials is made, together with a discussion about simplifications of the flow equations used in the papers. Further, some examples of vortex models is presented. Finally, the 2-D flow around a cylinder is studied and a solution based on method given in Paper II is proposed.

3.1 Concepts and Equations

The vorticity, $\boldsymbol{\omega}(\boldsymbol{r}, t)$, of a fluid motion is defined as

$$\boldsymbol{\omega} = \nabla \times \boldsymbol{u} \ . \tag{3.1}$$

This quantity corresponds to rotation of the fluid. Flow without vorticity is called irrotational flow. An equation for the vorticity in incompressible flow is obtained by applying the curl operation to the Navier-Stokes equation, Eq. (2.3),

$$\partial_t \boldsymbol{\omega} + (\boldsymbol{u} \cdot \nabla)\boldsymbol{\omega} = (\boldsymbol{\omega} \cdot \nabla)\boldsymbol{u} + \nu \nabla^2 \boldsymbol{\omega} \ . \tag{3.2}$$

The first term of the right-hand side of Eq. (3.2) represents the action of velocity variations on the vorticity. The signifigance of the second term on the right-hand side is the action of viscosity which produces diffusion of vorticity. The second term on the left-hand side descibes the convective transport of vorticity. The vorticity transport equation may also be casted in the form

$$\partial_t \boldsymbol{\omega} + \boldsymbol{u} \times \Delta \boldsymbol{u} - (\nabla_u - \nabla_\omega)(\boldsymbol{u} \cdot \boldsymbol{\omega}) = \nu \nabla^2 \boldsymbol{\omega} \ , \tag{3.3}$$

where the symbol ∇_u indicates that the derivatives are with respect to the components of $\boldsymbol{u}$ only. The vortex motion in 3-D space differs from 2-D in several ways. The most important result is vortex stretching and the consequent of non-conservation of vorticity. In 2-D flows, the velocity is perpendicular to the vorticity, so $\boldsymbol{u} \cdot \boldsymbol{\omega} = 0$.

When the external force is only the gravitational force, the fluid flow describes an irrotational motion. Such a rotational motion is called a free vortex motion or natural vortex motion and the circumferential velocity $u_\theta \sim 1/r$. When one considers the motion of a viscous fluid, the viscosity gives the resistance force to the motion of fluid while the external force is the gravitational force. Indeed, when there is the very high deformation,

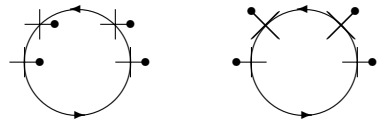

(a) $u_\theta \sim 1/r$ (b) $u_\theta \sim r$

Figure 3.1: A crude vorticity meter's behaviour when immersed in a line vortex flow (a) and a uniformly rotating flow (b).

the frictional force becomes very high. Then, if one assumes the fluid to be a nearly perfect, it is impossible to create the free vortex motion near the center of the axis due to the high deformation of the fluid particles. Therefore it is assumed that the center axis rotates as a solid body, $u_\theta \sim r$.

By organizing the two flows in Fig. 3.1 together in the following way

$$u_\theta = \begin{cases} \Omega r & r < a \\ \frac{\Omega a^2}{r} & r > a \ , \end{cases} \tag{3.4}$$

one obtains a so-called Rankine vortex, which serves as a simple model for a real vortex. The circumferential velocity u_θ and the vorticity ω for a Rankine vortex are shown in Fig. 3.2. Real vortices are typically characterized by fairly small vortex cores in which the vorticity is concentrated, while outside the core the flow is essentially irrotational. The core is not usually exactly circular, nor is the vorticity uniform within it.

For an arbitrary closed circuit C in a fluid flow, the circulation Γ is defined as

$$\Gamma = \oint_C \boldsymbol{u} \cdot d\boldsymbol{s} \ . \tag{3.5}$$

The circulation is related to the vorticity by Stokes theorem

$$\oint_C \boldsymbol{u} \cdot d\boldsymbol{s} = \iint (\nabla \times \boldsymbol{u}) \cdot d\boldsymbol{S} = \iint \boldsymbol{\omega} \cdot d\boldsymbol{S} \ . \tag{3.6}$$

There must be vorticity within a loop round which circulation occurs. The existence of closed streamlines in a flow pattern implies that there are loops for which $\Gamma \neq 0$ and thus that the flow is not irrotational everywhere. However, the converse may not apply.

3.2 Velocity Potentials and Stream Function

If we have the continuity equation of the form in Eq. (2.2) one may apply Helmholtz decomposition [45]. That is, the velocity $\boldsymbol{u}$ may be uniquely

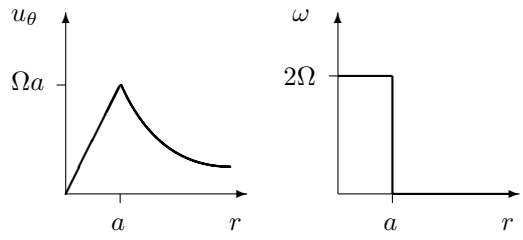

(a) (b)

Figure 3.2: Distribution of (a) circumferential velocity u_θ and (b) vorticity ω in a Rankine vortex.

defined by a rotational part $\boldsymbol{u}_{rot}$ determined by a vector potential $\boldsymbol{A}$, and a potential part $\boldsymbol{u}_{pot}$ determined by a scalar potential ϕ as

$$\boldsymbol{u} = \boldsymbol{u}_{rot} + \boldsymbol{u}_{pot} = \nabla \times \boldsymbol{A} + \nabla\phi \ . \tag{3.7}$$

It also follows from the continuity equation, Eq. (2.2), that ϕ has to satisfy the Laplace equation $\Delta\phi = 0$, if there are no sources and sinks. The vorticity is determined from the vector potential as $\boldsymbol{\omega} = \nabla(\nabla\cdot\boldsymbol{A}) - \Delta\boldsymbol{A}$. It is possible to choose $\boldsymbol{A}$ such that $\nabla \cdot \boldsymbol{A} = 0$, a gauge condition.

A particular kind of simple solutions to the flow equation is when the non-linear terms are explicitly zero due to properties of the solution. In finding solutions of this kind, one may be guided by the observation that non-linear terms disappear from the vorticity equation if:

1. the velocity is parallel to the vorticity, as seen from Eq. (2.4), or
2. the velocity is orthogonal to the vorticity and $\Delta\boldsymbol{u}$ is parallel to $\boldsymbol{u}$, as seen from Eq. (3.3).

The vorticity then satisfies the vector Helmholtz equation $\partial_t\boldsymbol{\omega} = \nu\Delta\boldsymbol{\omega}$. This result has been used in Paper I, III and IV to formulate vortex models. For 2-D or axisymmetric flows, only one component of $\boldsymbol{A}$ is non-zero. In this case, Eq. (2.2) can always be satisfied by introducing ψ such that

$$u_x = \partial_y\psi, \quad u_y = -\partial_x\psi \ , \tag{3.8}$$

where ψ is known as the stream function, since it is constant along a streamline. The stream function corresponds then to the only non-zero component of $\boldsymbol{A}$.

Now, suppose we have that $\nabla \cdot \boldsymbol{A} = 0$ everywhere, the equation for $\boldsymbol{A}$ is $\Delta\boldsymbol{A} = -\boldsymbol{\omega}$ of which a solution is

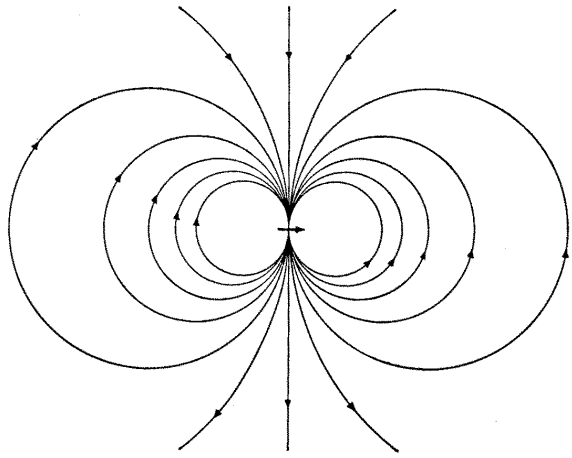

Figure 3.3: Streamlines for the 2-D solenoidal flow associated with a line vortex doublet. The stream function increases by the same amount between each pair of neighbouring streamlines. The horizontal arrow in the center is the dipole vector $\boldsymbol{\lambda}$.

$$\boldsymbol{A}(\boldsymbol{r}) = -\frac{1}{4\pi}\iiint \frac{\boldsymbol{\omega}(\boldsymbol{r})}{|\boldsymbol{r}-\boldsymbol{r'}|}dV' \ . \tag{3.9}$$

By substituting Eq. (3.9) into the definition of the vector potential, one can obtain the following equation for the velocity field as

$$\boldsymbol{u}(\boldsymbol{r}) = -\frac{1}{4\pi}\iiint \frac{\boldsymbol{\omega}(\boldsymbol{r})\times(\boldsymbol{r}-\boldsymbol{r'})}{|\boldsymbol{r}-\boldsymbol{r'}|^3}dV' \ . \tag{3.10}$$

This equation corresponds to the Biot-Savart's law which is a measure of a magnetic field generated by electric current. As an example consider a line of singularity of the vorticity distribution which is specified entirely by the strength κ and the position of the line. This may be called a line vortex singlet or a monopole vortex. The velocity distribution is found from Eq. (3.10). In the very simple case of a straight line vortex of infinite length, the velocity is everywhere in the circumferential direction about the line vortex and has magnitude $|\boldsymbol{u}| = \frac{\kappa}{2\pi|\boldsymbol{r}-\boldsymbol{r'}|}$ at distance $|\boldsymbol{r}-\boldsymbol{r'}|$ from the line vortex.

Other singularties can be constructed from line vortices. We obtain a line vortex doublet or dipole vortex by placing a straight line vortex of strength κ at position $\boldsymbol{r'}+\delta\boldsymbol{r'}$ and another of strength -κ at $\boldsymbol{r'}-\delta\boldsymbol{r'}$, and by allowing κ to increase and $|2\delta\boldsymbol{x'}|$ to approach zero in such way that $2\kappa\delta\boldsymbol{r'}$ tends to the finite limit $\boldsymbol{\lambda}$ (the dipole vector). The streamlines of a vortex doublet is presented in Fig. 3.3.

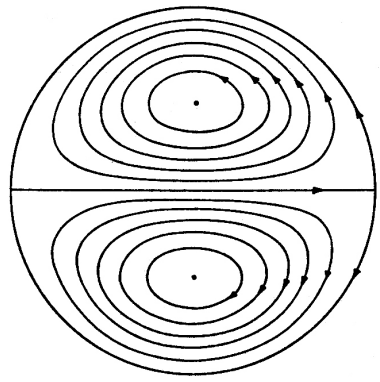

Figure 3.4: Streamlines in the region $r \leq a$ for the steady flow due to vorticity proportional to $J_1(kr)\sin\theta$ ($r \leq a$, $ka = 3.83$) and a uniform stream function with suitable chosen speed at infinity.

3.3 Classical Vortex Motions and Models

Here follows a presentation of some models of vortices. A couple of them are of historical interest, others are examples of special cases where simple solutions may be obtained. There are comments in the examples how to relate them to the present work in the papers.

Lamb-Chaplygin dipole vortex

One of the first nontrivial vortical solution, the translating circular dipole, was suggested independently more then a century ago by Lamb [46] and Chaplygin [47]. Since that time, most of the research in the dynamics of localized distributed vortices has been associated with monopoles and dipoles or their combinations. The Lamb-Chaplygin dipole model assumes a linear relation between vorticity and the stream function $\omega = k^2\psi$ (with k a constant) within an isolated circular region with radius $r = a$, and a potential flow $\omega = 0$ in the exterior region ($r > a$). The solution in terms of the stream function of the flow, relative to a comoving frame with velocity U, is

$$\psi = \begin{cases} -\frac{2U}{kJ_0(ka)} J_1(kr)\sin\theta & r < a \\ U\left(r - \frac{a^2}{r}\right)\sin\theta & r > a \end{cases}, \tag{3.11}$$

where J_0 and J_1 are the zero- and first-order Bessel functions, and ka is a root of J_1. The latter means that there is a countable spectrum of allowed values of ka and, correspondingly, a countable set of interior solutions matching the same exterior solution. When the first root of J_1 is taken as ka, the solution represents a true dipole (see Fig. 3.4).

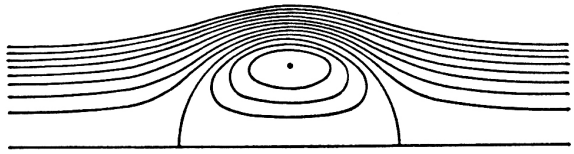

Figure 3.5: Streamlines of the steady flow relative to a Hill's spherical vortex, with equal intervals of ψ. The lower horizontal line is the axis of symmetry.

Hill's spherical vortex

Hill's spherical vortex may be described as a vortex sphere advancing with constant velocity through a inviscid fluid which is at rest at infinity [48]. The flow in the whole field is symmetrical about the line of motion. The vorticity inside the sphere is proportional to the distance from the axis of symmetry, while the motion outside is the same as the irrotational motion outside a moving solid sphere. Let us suppose that a region $r < a$ is filled with fluid. One finds the solution for the stream function as

$$\psi = -\frac{3}{4}Ur^2\left(1 - \frac{r^2}{a^2}\right)\sin^2\theta \ . \tag{3.12}$$

This spherical vortex will travel through stationary fluid with uniform speed U. The corresponding streamlines are illustrated in Fig. 3.5. Hill's spherical vortex was used in the pioneering work [49] where a statistical theory of homogenous isotropic turbulence was developed. The turbulent fluctuations was modeled as due to Hill's vortices moving about chaotically. It is perhaps best viewed not as a model of the fine structure but the modelling of the large energy containing eddies. Due to the absence of internal structure or a continuous dissipation mechanism, its use in calculating turbulence properties of the inertial and dissipation ranges is limited.

Lamb-Oseen type vortices

Another vortex model was given by Lamb [46] and also by Oseen [50]. It represent a solution to the laminar Navier-Stokes equations with an axisymmetric solution for the swirl velocity together with the assumption that the axial and radial velocities are zero, for the initial condition $\omega(r,0) = \Gamma\delta(x)\delta(y)$. The Lamb-Oseen vortex model for the circumferential velocity is

$$u_\theta = \frac{\Gamma}{2\pi r}\left[1 - \exp\left(-\frac{r^2}{4\nu t}\right)\right] \ . \tag{3.13}$$

The viscous core radius is the radial location where the swirl velocity is a maximum. Actually, the Lamb-Oseen vortex is just a special case of a more general class of 2-D vortex solution derived from a solenoidal vector potential given in Paper III, namely

$$\boldsymbol{A}(\boldsymbol{r},t) = A(r,\theta,t)\boldsymbol{e} = \frac{r^n \cos n\theta}{(\nu t)^\beta} F\left(\frac{r}{\sqrt{\nu t}}\right)\boldsymbol{e}\ , \tag{3.14}$$

where n is an integer giving the order of the vortex multiplet, $\boldsymbol{e}$ is a unit vector, β is a parameter characterizing the dynamic behaviour, F is a function of the diffusive variable $\frac{r}{\sqrt{\nu t}}$. In [51] another model of Lamb-Oseen type, originally found by Taylor [52], is used to descibe the decay of monopolar vortices in a stratified fluid which was investigated experimentally. This model may also be generated from the general vector potential in Eq. (3.14).

Burgers' vortex

In 1938 Taylor also recognised the fact that the competition between stretching and viscous diffusion of vorticity must be the mechanism controlling the dissipation of energy in turbulence [53]. A decade later Burgers obtained exact solutions describing steady vortex tubes and layers in locally uniform straining flow where the two effects are in balance [54]. Burgers introduced this vortex as "a mathematical model illustrating the theory of turbulence", and he noted particularly that the vortex had the property that the rate of viscous dissipation per unit length of vortex was independent of viscosity in the limit of vanishing viscosity (i.e. high Reynolds number). The discovery of the exact solutions stimulated the development of the models of the dissipative scales of turbulence as random collections of vortex tubes and/or sheets. The intermittent nature of the vorticity field was observed in experiments by taking statistical measurements which indicated the existence of the small-scale localised structures [55].

The exact solution of a 3-D vortex satifying the Navier-Stokes equation given by Burgers is in cylindrical coordinates

$$u_r = -\frac{\alpha r}{2}, \quad u_\theta = \frac{\Gamma}{2\pi r}\left[1 - \exp\left(-\frac{\alpha r^2}{4\nu}\right)\right], \quad u_z = \alpha z \tag{3.15}$$

where $\alpha > 0$ and Γ are constants. The vorticity is given by

$$\boldsymbol{\omega} = \frac{\alpha\Gamma}{4\pi\nu}\exp\left(-\frac{\alpha r^2}{4\nu}\right)\boldsymbol{e}_z \tag{3.16}$$

The Burgers' vortex provides an excellent example of a balance between convection, intensification and diffusion of vorticity. It is essentially the vortex to the left in Fig. 3.6. but with outward diffusion of vorticity countered by a secondary flow which sweeps the vorticity back towards the axis and intensifies the vorticity by stretching fluid elements in the z-direction. The circumferential velocity u_θ is shown to the right in Fig. 3.6. However the streching $\partial_z u_z$ of such velocity fields remains radially constant, a feature which departs from what is observed in experimental streched vortex filaments [56]. The last work in Paper IV proposes a streched vortex model which includes a nonuniform stretching in the radial direction that is clearly

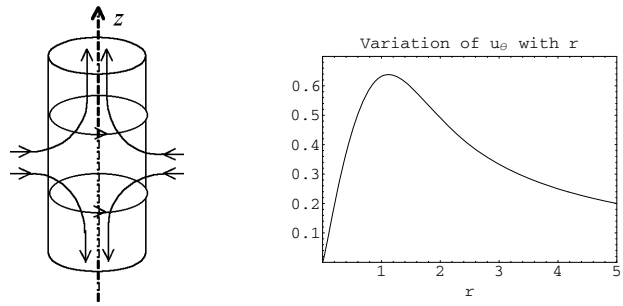

Figure 3.6: (left) Picture of Burgers' vortex. (right) The variation of u_θ with r.

present in real flows, as well as the slow variation of velocity profiles along the vortex axis.

Vortex ring

The motion of a vortex ring shows interesting phenomena for the physical process for which the fundamental investigation was already established by Kelvin, Maxwell and Lamb [57, 58, 46]. A more recent review is given in [59]. Vortex rings can be formed by ejecting a puff of smoke suddenly from the mouth through rounded lips and which travels forward steadily with a smoke-filled core. The essential requirement for the production of a vortex ring is that linear momentum should be imparted to the fluid with axial symmetry. One of the observed properties of all vortex rings in uniform fluid is the approximate steadiness of the motion relative to the ring when the ring is well clear of the generator and this has been proved for inviscid vortex rings [60]. There is some decay of the motion always, presumably due to the action of viscosity, but the decay is less for larger rings, suggesting that the motion should be truly steady at infinite Reynolds number. In [61], the velocity field inside a viscous vortex ring is obtained on the basis of an existing solution of the Stokes equation for the velocity in a moving coordinate system (see Fig. 3.7). Their study generated a expression for the velocity in terms of modified Bessel functions and exponential functions which where approximated by polynoms. In Paper IV an exact solution based on a Greens function for the diffusion equation in spherical coordinates is found,

$$\boldsymbol{u}(\boldsymbol{r},t) = e^{-\frac{(r^2-R^2)}{4\nu t}}(4\pi\nu t)^{-\frac{3}{2}}\left[\frac{\cot\theta}{r}I_1\left(\frac{rR}{2\nu t}\right)\boldsymbol{e}_r\right.$$

$$\left.+\left(\frac{r}{2\nu t}I_1\left(\frac{rR}{2\nu t}\right)-\frac{R}{2\nu t}I_0\left(\frac{rR}{2\nu t}\right)\right)\boldsymbol{e}_\theta+0\ \boldsymbol{e}_\phi\right], \qquad (3.17)$$

where I_0 and I_1 are modified Bessel functions. The solution is compared

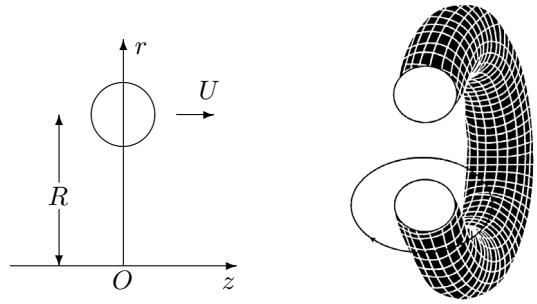

Figure 3.7: (left) Coordinate system of a cross section of a vortex ring of radius R propagating with a speed U. (right) Schematic picture of a vortex ring.

with very recent experimental observations [62, 63] of the velocity and vorticity field, together with the turbulent energy spectrum and they show a good agreement.

A general expression for the propagation velocity U of a viscous vortex ring valid for arbitrary vorticity, ω, and stream function distributions, ψ, was found by Saffman [64] (cylindrical coordinates)

$$U = \frac{\int_0^\infty \int_{-\infty}^\infty (\psi + 6zr\nu)\omega dz dr}{2\int_0^\infty \int_{-\infty}^\infty r^2 \omega dz dr} \tag{3.18}$$

In [64] Eq. (3.18) was derived using the Lamb transformation [46] for the velocity of a ring in an ideal fluid and the validity of its application to a viscous fluid was proved. Continued calculations with the solution in Eq. (3.17) may be done for the propagation velocity and compared with experiments in [65].

Furthermore, the reduction of Navier-Stokes equation to diffusion type equation, $\partial_t \boldsymbol{\omega} = \nu \Delta \boldsymbol{\omega}$, may be solved in toroidal coordinates [66]. An exact solution can be obtanied containing trigonometric and Legendre functions for the space varibles. A limitation here is that only an exponential decay in time is possible. Diffusive coordinates can not be used due to a non-separable diffusion equation in toroidal coordinates.

Trailing vortex

The vortices generated at the edge of the wings of an airplane are called trailing vortex or the wing tip vortex. The prediction of the induced velocities and circulation history of the tip vortices as they trail behind an aircraft has been the subject of much research over the past decades, for a review of see for example [67, 68, 69]. The trailing vortex is generated by the intrusion of the stream around the wing tip from the high static pressure on the lower surface of the wing to the low static pressure on the upper surface due to the static pressure difference between both surfaces of the

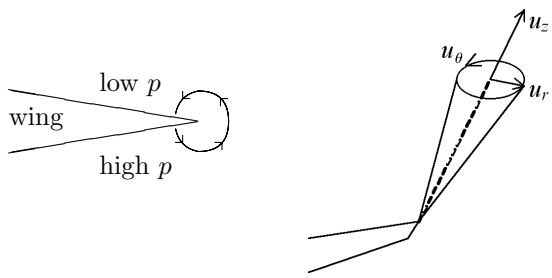

Figure 3.8: (left) The fluid is transported from below to the upper side of the wing where there is a lower pressure. This induces the formation of a trailing vortex. (right) Coordinate system for a simple model of a trailing vortex.

wing during flight. A schematic illustration is shown to the left in Fig. 3.8. The trailing vortex contributes not only a decline of the lift coefficient of the wing but also an uninvited accident of the airplane which is swallowed up by this vortex. The persistence of aircraft tip vortices poses a wake-hazard problem for any following aircraft, and this is a major factor limiting the capacity of large airports.

In order to make the mathematical analysis, the flow in a single trailing vortex may be assumed to be axis-symmetric. This assumption is actually satisfied at the distances far downstream from the aerofoil. Newman made an simple model with a assumtions that the axial velocity deficiency $U - u_z$ and the circumferential velocity u_θ are small compared with the free stream velocity U, the radial velocity is very small compared with the free stream velocity and finally that the Reynolds number of the main flow is large [70]. The solution is as follows (see the coordinates to the right in Fig. 3.8)

$$u_\theta = \frac{\Gamma}{2\pi r}\left[1 - \exp\left(-\frac{Ur^2}{4\nu z}\right)\right] \tag{3.19}$$

$$u_r = -\frac{ar}{2z^2}\exp\left(-\frac{Ur^2}{4\nu z}\right) \tag{3.20}$$

$$u_z = U - \frac{a}{z}\exp\left(-\frac{Ur^2}{4\nu z}\right) \ . \tag{3.21}$$

Here the the solution of u_θ is identical with that given by Lamb and Oseen for the development with lapse of time of a 2-D viscous vortex when the time is replaced by z/U.

A further investigation of a solution of the same structure as for the stretched vortex in Paper IV may be applied to this problem. One needs to study the different boundary conditions for the case of a trailing vortex but since the vortex solution possesses degrees of freedom, that will probably not be a problem.

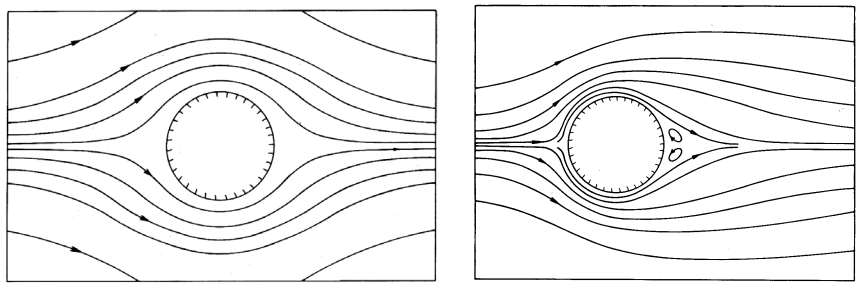

Figure 3.9: (left) Low Reynolds number flow past a circular cylinder. (right) As Re is increased vortices is created and the upstream-downstream symmetry breaks.

3.4 Flow Past a Circular Cylinder

Introduction

A cylinder is placed with its axis normal to a flow of free stream speed U, that means that U is the speed that would exist everywhere if the cylinder was absent. The cylinder is so long compared with the diameter that its ends have no effect, we can then think of it as an infinite cylinder. Also, the boundaries to the flow are so far away that they have no effect. An entirely equivalent situation exists when a cylinder is drawn perpendiculary to its axis through a fluid otherwise at rest. The only difference between the two situations is in the frame of reference from which the flow is being observed. The description of the flow patterns is based almost entirely on experimental observations. Only for the lowest Re can the flow as a whole be determined analytically (see Fig. 3.9 to the left).

As Re is increased the upstream-downstream symmetry disappears. Two attached eddies appears behind the cylinder (see Fig. 3.9 to the right), and these becomes larger with increasing Re. At even higher Re, the flow settles into an unsteady but highly structured form in which vortices are shed alternately from the two sides of the cylinder, giving the remarkable von Karman vortex street. As for transition to turbulence in a pipe, this unsteadiness arises spontaneosly even though all the imposed conditions are being held steady. Concentrated regions of rapidly rotating fluid form two rows on either side of the wake. All the vortices on one side rotate in the same sense, those on the opposite side in the opposite sense. The whole pattern of vortices travels downstream, but with a speed rather smaller than U.

A simple model of a fully developed vortex street, in the complex plane, may be given by one set of line vortices of strength Γ at $z = na$, and another set of strength $-\Gamma$ at $z = \left(n + \frac{1}{2}\right) a + ib$, with $n = 0, \pm 1, \pm 2, \ldots$ (see Fig. 3.10). Consider any of these vortices. The local flow velocity due to the others in the same row is zero, because their contributions cancel

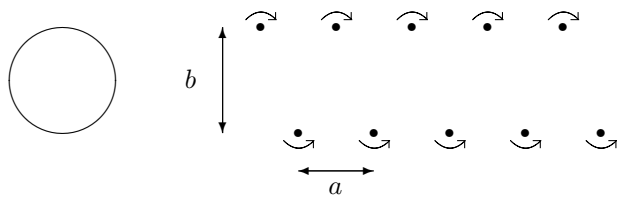

Figure 3.10: Line vortex representation of a Karman vortex street in the wake of a cylinder. Note the relative positions of the vortices.

in pairs. The y-components of velocity due to those in the other row also cancel in pairs, but the x-components reinforce each other to give a velocity V to the left if $\Gamma > 0$. One can show that the whole vortex street moves to the left with speed $V = \frac{\Gamma}{2a} \tanh\left(\frac{\pi b}{a}\right)$ [39].

Solution by the method given in Paper II

This problem may be analyzed by the techique proposed in Paper II. We start by considering a velocity field determined by a vector potential $\boldsymbol{A}$ in cylindrical coordinates r and θ and time t

$$\boldsymbol{A}(\boldsymbol{r},t) = \left(r + \frac{1}{r} - 2\right) \sum_{n,m} r^{-n} \left[\alpha_{n,m}(t') \cos m\theta + \beta_{n,m}(t') \sin m\theta\right] \delta(t-t')\boldsymbol{e}_z$$

$$= \sum_{n,m} r^{-n+1} \left[a_{n,m}(t') \cos m\theta + b_{n,m}(t') \sin m\theta\right] \delta(t-t')\boldsymbol{e}_z \ . \qquad (3.22)$$

The r-dependent factor in front of the sum is included to satisfy the no-slip boundary condition at $r = 1$. The coefficients α and β are assumed to oscillate slightly around a mean value and the indices n and m run from zero and upwards. We take $m \leq n$, which may be motivated by considering the potential as a function of the complex variables z and z^* and invoking symmetry arguments. To facilitate the notation and practical calculations, it is convenient to introduce the sets of coefficients a and b that are linear combinations of the coefficients α and β. These relations are easily derived from Eq. (3.22). The resulting velocity components are

$$u_r = \sum_{n.m} r^{-n} m \left[-a_{n,m} \sin m\theta + b_{n,m} \cos m\theta\right] \qquad (3.23)$$

$$u_\theta = \sum_{n.m} r^{-n} (n-1) \left[a_{n,m} \cos m\theta + b_{n,m} \sin m\theta\right] \ . \qquad (3.24)$$

We start by considering the quasi-static part of the velocity field possessing the property of an instantaneous adaptation to changing boundary conditions and obeying the equation derived from the Navier-Stokes equation

$$u_r u_\theta = -\partial_r \iint G(|\boldsymbol{r}-\boldsymbol{r}'|) d\boldsymbol{S}'\cdot\nabla u_\theta - r^{-1}\partial_\theta \iint G(|\boldsymbol{r}-\boldsymbol{r}'|) d\boldsymbol{S}'\cdot\nabla u_r \ , \quad (3.25)$$

where the first term on the right-hand side vanishes as the derivative in the radial direction of u_r is zero on the boundary as seen from the equation of continuity and the fact that the velocity satisfies the no-slip condition. The Green's function G has been defined in Paper II.

We assume that just outside the boundary the vector potential is given by

$$\boldsymbol{A}(\boldsymbol{r},t) = \sum_m \left[f_m(r,t')\cos m\theta + g_m(r,t')\sin m\theta\right]\delta(t-t')\boldsymbol{e}_z \ , \quad (3.26)$$

so that on the boundary one may write

$$\partial_r u_r = \sum_m m\left[-c_m(t')\sin m\theta + d_m(t')\cos m\theta\right] \ , \quad (3.27)$$

giving, after integration, the right-hand side of Eq. (3.24) equal to

$$\sum_m r^{-n} m^2 \left[c_m(t')\cos m\theta + d_m(t')\sin m\theta\right]\delta_{n-2,m} \ . \quad (3.28)$$

Calculating the product of the velocity components and identifying with Eq. (3.27) gives the equations below, Eq. (3.29) and Eq. (3.30). They are to be interpreted in the following manner. The equations are given for fixed values of the indices n and m. Put the index $N = n+m+1$. The left-hand side of the equations contain terms where in each product of two coefficients, one of the coefficients has an index N while the other coefficient has a lower index. The right-hand side only contains terms where all coefficients have an index smaller than N. Thus, the Eq. (3.28) constitutes a system of equations if one includes all equations where n and m take values such that their sum equals $N-1$. By increasing successively the value of N by 1, may one calculate the value of all coefficient a and b given the coefficients c and d and the coefficients of a and b with the smallest index. For a cylinder exposed to a homogenous cross flow, these coefficients would be $a_{0,1} = 0$ and $b_{0,1} = -1$

$$\sum_{k=0}^{n-2}\left[a_{k,k+1}a_{n-k,m+k+1} + b_{k,k+1}b_{n-k,m+k+1}\right](n-k-1)(k+1) =$$

$$-\sum_{n'=0}^{n-2}\sum_{m'=0}^{N-n'}\left[a_{n',m'}a_{n-n',m+m'} - b_{n',m'}b_{n-n',m+m'}\right](n-n'-1)m'$$

$$-\sum_{n'=0}^{n-2}\sum_{m'=0}^{N-n'}\left[a_{n',m'}a_{n-n',m-m'}-b_{n',m'}b_{n-n',m-m'}\right](n-n'-1)m'$$
$$+(n-2)^2 d_{n-2}\delta_{m,n-2}\ , \tag{3.29}$$

$$\sum_{k=0}^{n-2}\left[b_{k,k+1}a_{n-k,m+k+1}+a_{k,k+1}b_{n-k,m+k+1}\right](n-k-1)(k+1)=$$
$$-\sum_{n'=0}^{n-2}\sum_{m'=0}^{N-n'}\left[b_{n',m'}a_{n-n',m+m'}-a_{n',m'}b_{n-n',m+m'}\right](n-n'-1)m'$$
$$-\sum_{n'=0}^{n-2}\sum_{m'=0}^{N-n'}\left[b_{n',m'}a_{n-n',m-m'}-a_{n',m'}b_{n-n',m-m'}\right](n-n'-1)m'$$
$$+(n-2)^2 c_{n-2}\delta_{m,n-2}\ . \tag{3.30}$$

We know turn to the velocity field determined by the equation

$$\boldsymbol{v}(\boldsymbol{r},t)=\frac{1}{\mathrm{Re}}\int^t dt'\partial_r\iint K(|\boldsymbol{r}-\boldsymbol{r}'|,t-t')d\boldsymbol{S}'\cdot\nabla\boldsymbol{u}(\boldsymbol{r}',t')\ , \tag{3.31}$$

where the diffusive Green's function is defined in Paper II. Inserting the velocity derivative from Eq. (3.27), one obtains after integration over the boundary the velocity field

$$\boldsymbol{v}(\boldsymbol{r},t)=\frac{1}{\mathrm{Re}}\int^t dt'\sum_m \exp\left[-\frac{\mathrm{Re}(r^2+1)}{4(t-t')}\right]I_m\left(\frac{\mathrm{Re}\,r}{2(t-t')}\right)$$
$$\times\left[c_m(t')\sin m\theta-d_m(t')\cos m\theta\right]\ , \tag{3.32}$$

where I_m is a modified Bessel function of index m.

It remains to satisfy boundary conditions for this velocity field. This is achieved by subtracting from the right hand side of Eq. (3.32) an identical expression with r equal to 1. One may study periodic solutions by introducing the Fourier transformed coefficients

$$\tilde{c}_m(\omega)=\frac{1}{2\pi}\int dt\exp(i\omega t)c_m(t)\ , \tag{3.33}$$

and similarly for the d-coefficient. After integration over time, one obtains

$$\boldsymbol{v}(\boldsymbol{r},t)=\frac{1}{2\pi}\int d\omega\exp(i\omega t)\sum_m\left[\tilde{c}_m(\omega)\sin m\theta-\tilde{d}_m(\omega)\cos m\theta\right]$$

$$\times \left[K_m \left(\frac{r\,\mathrm{Re}}{\sqrt{2i\omega}} \right) - K_m \left(\frac{\mathrm{Re}}{\sqrt{2i\omega}} \right) \right] I_m \left(\frac{\mathrm{Re}}{\sqrt{2i\omega}} \right) \ , \tag{3.34}$$

where K_m is the other modified Bessel function and one should take the real part of this expression.

4 Turbulence

The most common form of fluid flow in nature is of an irregular and chaotic form. This is because in real flows, a number of disturbing sources exist which interact with the main flow field. An growing instability is normally the first stage of a sequence of changes in the flow, where the final result is that the flow becomes turbulent.

In this chapter, a summary of the basics in turbulence theory is given. It is primary based on classical textbooks such as [71, 72, 73, 74]. The last subsection is concerning the topic of coherent structures in turbulence. The first part of Paper IV, and the main of Paper III may be classified as studies of coherent structures in pipe flow and 2-D turbulence, respectively.

4.1 Concepts and Correlations

No short but complete definition of turbulence seems to be possible. One can formulate a brief summary, rather than formal definition. Perhaps the best description is that turbulence is *a state of continuous instability*. Each time a flow changes as a result of an instability, the ability to predict the details of the motion is reduced. When successive instabilities have reduced the level of predictability so much that it is appropiate to describe a flow statistically, rather than in every detail, then one says that the flow is turbulent.

In the analysis of turbulence, one usually follows the procedure devised by Reynolds [75] and divides the velocity into a mean and a fluctuating part, $U_i + u_i$. Due to the random behavior of a turbulent field, one has to devise an averaging process to obtain deterministic quantaties from some available experimental or theoretical data. Average values can be determined in various ways, time average, space average and ensamble average. For stationary and homogenous processes one expects all three averaging procedures to lead to the same result. This is known as the ergodic hypothesis.

A major and important part of the subject of fluid turbulence is to analyze and understand the internal structure of the turbulent flow fields. This is done in studies of various velocity correlations between points of the field, and it play an essential role in both theoretical and experimental studies of turbulence. To illustrate how they can indicate the scale and structure of a turbulent motion, consider now typical properties of double correlations. Given the second order probability distribution $P(u_1, u_2)$, we form the mathematical expectation or average of the product $u_1 u_2$ as

$$\overline{u_1 u_2} = \int_{-\infty}^{\infty} \int_{-\infty}^{\infty} u_1 u_2 P(u_1, u_2) du_1 du_2 \ , \tag{4.1}$$

which is called the double correlation. When u_1 and u_2 are velocities at different positions but at the same instant, $\overline{u_1 u_2}$ is known as a space correlation. Most attention is usually given to longitudinal and lateral correla-

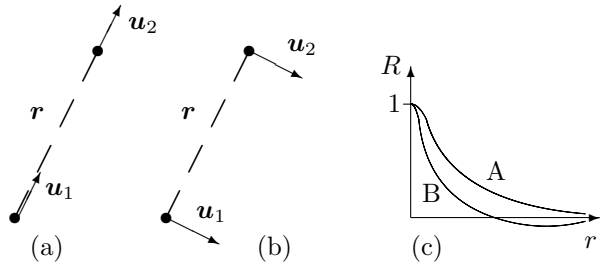

Figure 4.1: Schematic representation of longitudinal double velocity correlation (a) and the lateral double velocity correlation (b). In (c) typical correlation curves for homogenous isotropic turbulence is shown. The longitudinal curve is A and the lateral is B.

tions given in Fig. 4.1 (a) respectively (b). Different behaivour in different directions may provide information about the structure of the turbulence.

A special case of turbulence is the concept of homogenous, isotropic turbulence. It is turbulence of which the statistical properties do not vary with position and have no prefered direction. An approximation to such motion can be obtained far downstream behind a grid in a wind-tunnel. The turbulence is supposed to be generated at an initial instant and then to decay as time proceeds. Typical curves of correlation coefficient $R \sim \overline{u_1 u_2}$ for homogenous isotropic turbulence is shown in (c).

Taylor [53] reduced the problem of measurement of isotropic turbulence to a much simpler level by introducing a hypothesis that the mean flow U_1 acts as the carrier of turbulent fluctuations such that a sequence of changes in velocity at a fixed point is simply the passage of the unchanging pattern of turbulent motion at that point. That is $u_i(\boldsymbol{r}, t) = u_i(\boldsymbol{r} - U_1 t, 0)$. Hence, a local time derivative could be replaced by a convective derivative, $\partial_t = -U_1 \partial_1$.

4.2 Averaged Equations

The equation of mean turbulent flow are obtained through the Navier-Stokes equation by preforming the ensamble or the time average on each term of the equations. The mean and fluctuating parts of the velocity field, U_i and u_i, individually satisfy the usual form of the continuity Eq. (2.2). A division, also applied to the Navier-Stokes equation, Eq. (2.3), yields

$$\partial_t(U_i + u_i) + (U_j + u_j)\partial_j(U_i + u_i) = -\rho^{-1}\partial_i(P + p) + \nu\partial_j^2(U_i + u_i) \ . \quad (4.2)$$

Carrying out a averaging process throughout this equation, with the aid of the continuity equation, gives

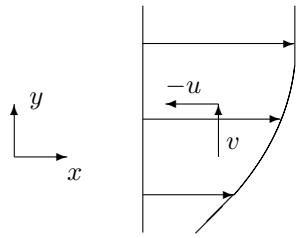

Figure 4.2: Illustration of the generation of a Reynolds stress in a mean gradient.

$$U_j \partial_j U_j = -\rho^{-1} \partial_i P + \nu \partial_j^2 U_i - \partial_j \left(\overline{u_i u_j} \right) \ , \tag{4.3}$$

where attention has been restricted to steady mean conditions. Eq. (4.3) for the mean velocity U_i differs from the laminar flow equation by addition of the last term. This term represents the action of the velocity fluctutions on the mean flow arising from the non-linearity of the Navier-Stokes equation. Write the last two terms of Eq. (4.3) as

$$\rho^{-1} \partial_j (\mu \partial_j U_i - \rho \overline{u_i u_j}) \ . \tag{4.4}$$

This shows that the velocity fluctuations produce a stress on the mean flow. The quantity $-\rho \overline{u_i u_j}$ is called Reynolds stress. The Reynolds stress arises from the correlations of two components of the velocity fluctuation at the same point (see Fig. 4.2). A non-zero value of this correlation implies that the two components are not independent of one another.

One encounters what is known as the closure problem, a consequence of the non-linearity of the equation. The appearance of second order correlations (the Reynolds stresses) in the averaged equations call for a technique to specify these unknowns in terms of dependent variables of the equations. In formulating an equation for the double correlation, it involves tripple correlations, an equation for these involves forth-order ones, and so on. At no point will this procedure balance the number of unknown and equations. Based on physical grounds, this is not a particulary suprising situation. After all, such operations are strictly mathematical in nature, and introduce no additional physical principles. In essence, Reynolds averaging is a crude simplification that loses much of the information contained in the Navier-Stokes equation.

The earliest known attempt to model the Reynolds stresses in terms of the derivatives of mean velocity components is due to Boussinesq [76]. The process is in general (but not in detail) analogous the the Brownian motion of molecules giving rise to fluid viscosity. The analogy has led to the definition of a quantity ν_T such that

$$\overline{u_i u_j} = \nu_T \partial_j U_i \ . \tag{4.5}$$

ν_T is called the eddy or turbulent viscosity. It is important to realize that ν_T is a representation of the action of the turbulence on the mean flow and not a property of the fluid. In recent times the intensive area of turbulence modeling is to devise approximations for the unknown correlations in terms of flow properties that are known, such that a sufficient number of equations exist. In making such approximations, the system of equations is closed.

4.3 Energy Spectrum

Another method of discovering the structures associated with turbulent motion is Fourier analysis. A introduction of Fourier analysis gives a relatively simple picture of the physics of turbulence. The technicalities of Fourier transforming the equations is straightforward. The effect will be to replace each differential operator by its analogous wavenumber operator. The nonlinear term must be treated by the convolution theorem. In addition, one can define a wave number spectrum, Fourier transforms of the space correlations. Defining a quantity $E(k)$, where k is the magnitude of the wave number, such that

$$K(\boldsymbol{r}, t) = \int_0^\infty E(\boldsymbol{r}, k, t) dk \ , \tag{4.6}$$

where $K(\boldsymbol{r}, t)$ is the turbulent energy per unit mass. Physically k has the dimension of $[length]^{-1}$. Hence, small and large eddies are represented by large and small wave numbers, respectively. $E(k)$ indicates the distribution of energy over different length scales. It is an important parameter in many theoretical treatments of turbulent motion. However, it cannot be measured experimentally, one would need simoultanous information from every point of the flow. When applicable, Taylor's hypothesis can be used to derive a spatial spectrum from an observed time spectrum (see Ch. 4.1). However, this is an one-dimensional spectrum with respect to the component of the wave number in the mean flow direction, and so not in general a complete determination of the spectral characteristics or of $E(k)$.

Let us now consider the energy relations that occur in turbulent flows. Because of the dissipative nature of such flows, a continuous supply of energy is necessary to maintain the turbulence, certainly for a steady flow. Energy fed into the turbulence transfers primarily into the larger eddies. (In grid turbulence this happens during the initial generation.) From these process, smaller and smaller eddies are generated. The process continues until the length scale is small enough for viscous action to be important and dissipation to occur. This sequence is called the energy cascade and is schematically described in Fig. 4.3. The dynamics of the energy cascade and the dissipation is assumed to be governed by the energy per unit time (per unit mass) supplied to it at the large (low wavenumber) end. This is, of course, equal to the energy dissipation ϵ defined by

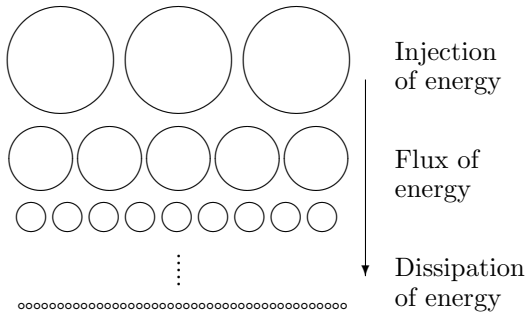

Figure 4.3: Schematic figure of the energy cascade which goes from larger to smaller eddies.

$$\epsilon = -\frac{dK}{dt} \ . \tag{4.7}$$

This suggests that the spectrum function E is independent of the energy production processes for all wavenumbers large compared with those at which the production occurs. Then E depends only on the wavenumber, the dissipation, and the viscosity, $E(k, \epsilon, \nu)$. If the cascade is long enough, there may be an intermediate range in which the action of viscosity has not yet occured, that is, $E = E(k, \epsilon)$. Dimensional analysis then gives $E = A\epsilon^{\frac{2}{3}}k^{-\frac{5}{3}}$, where A is a numerical constant. This is a famous result, known as the Kolmogorov $-\frac{5}{3}$ law [77].

4.4 Coherent Structures

In recent years it has been increasingly evident that turbulent flows are not just random or chaotic but can contain more deterministic features, known as coherent structures. We are now considering some discernible patterns in the flow, which may have random features but nevertheless occur with sufficient regularity, in space or time, to be recognizable as quasi-periodic or near-deterministic. Quite a variety of structures has been identified, such as vortices, waves, streaks etc. Here our task is vortex modeling of fully developed turbulence in 2-D and developed structures in pipe flows.

An example of the later one, the visualization of turbulent flows and boundary layers via sophisticated experimental methods like particle imaging velocimetry has led to the indentification of a rich variety of prominent coherent structures [78, 79, 80, 81]. Recently, experimental studies of transitional pipe flow has shown the existence of coherent flow structures that are dominated by downstream vortices [19, 20]. Downstream vortices transport liquid across the mean shear gradient and create regions of fast or slow mov-

ing fluid, so-called high- and low-speed streaks. In the first part of Paper IV a model of these objects is presented.

The first study of a physical model of vortices describing fully developed turbulence appears to be the work of Synge and Lin [49] in 1943 who represented isotropic turbulence as a random superposition of Hill spherical vortices which was mentioned in Ch. 3.3. Later, the idea that the small-scale structures of turbulence might be representable in terms of a random distribution of vortex sheets or tubes was taken up by Townsend [55] in 1951. Townsend showed that a random distribution of vortex sheets would give rise to an energy spectrum proportional to k^{-2} (multiplied by an exponential viscous cut-off factor). A random distribution of vortex tubes gave rise to a power-law k^{-1} (again modified by an exponential cut-off), this slower fall-off with k being associated with the more singular behaviour in physical space associated with a line vortex. In 1982 Lundgren [16] adapted this method to model the fine structure of turbulence by replacing the steady Burgers vortices in the Townsend ensamble with unsteady stretched spiral vortices. The dual properties of axial straining combined with a nonaxis-symmetric vorticity structure give the model a rich predictive capability. Further investigations and reformulations of Lundgren's model has been done [82, 83, 84].

2-D turbulence has provided a remarkable context for the study of coherent structures and the interplay with classical energy cascade theories. Coherent structures can often be visualized directly from the vorticity field as long-lived objects of generally circular topology, with a very simple structure, cleary distinguishable from the background within which they evolve. In Paper III statistics of the coherent structures in freely decaying and forced 2-D turbulence is presented.

The division of a turbulent motion into interacting motions on various length scales is useful since the different scales play rather different roles in the dynamics of the motion. However, it must be mentioned that an eddy differs from a Fourier component in the following way. A single Fourier component, no matter how small its wavelength, extends over the whole flow. But an eddy is localized and its extent is indicated by its length scale.

5 Summary of Papers

A short summary of each paper included in the second part of this thesis is presented below. They all concern vortex motions and vortex solutions to the Navier-Stokes equation.

5.1 Paper I

During cornering winds at buildings, dual conical vortices form in the separated flow along the leading edges of flat roofs. These vortices cause the most extreme wind suction forces found anywhere on the building, so it is important to predict them accurately. Therefore, in this paper a model of a conical vortex is proposed. The first experimental and modeling of conical vortices where related to wing-tip, or trailing, vortices [85, 86] (see Ch 3.3 for trailing vortices). Theoretical considerations of vortices attached to flat roofs has mostly been of semi-analytical or hueristic nature [87, 88, 89].

The derivation here is made in spherical coordinates. Assumptions made in the calculations are that the vortex possess a perfect rotational symmetry (no ϕ-dependence) and that the impact flow is uniform (no atmospheric boundary layer) and quasi-stationary. In the model, the vorticity is parallel to the velocity so the flow equation is reduced to a diffusion type of equation containing no non-linear terms. The radial parametrization of the flow field contains a spherical Bessel function with index l as a free parameter. The θ-dependece of velocity field is represented by a linear combination of Legendre functions of the first and second kind. By this choise, the boundary condition of the radial velocity at the edge of the cone, $u_r(\theta = \theta_0) = 0$, can be fulfilled. The other boundary values for the velocities on the surface of the cone, u_θ and u_ϕ, are calculated from simple boundary layer theory.

In the model for the flow field there is no implicit dependence on the Reynolds number. However, there is still a Re-dependence from the boundary conditions. With the velocity determined, the pressure on the boundary of the cone may be derived by an integration of Navier-Stokes equation, giving Bernoulli equation. Comparison with pressure measurements show good agreement.

5.2 Paper II

This paper is a mathematical and theoretical study of the Navier-Stokes equation. A solution to the Navier-Stokes equation for internal flow systems is proposed by considering the vorticity generated at the boundaries of the system. There are experimental evidence for the major impact the no-slip boundary conditions has on the whole flow considered [90]. The solid boundaries act as a source of vorticity, which spread into the flow domain.

The Navier-Stokes equation describes the flow in a free space, but it contains no information how to take into account boundary conditions. The forces acting on boundaries of the flow domain that have to be included in the equation are: pressure applied at inlets and outlets and viscous forces

at solid boundaries. Then Navier-Stokes can be rewritten in the form of a divergence and integrated. The resulting equation may be split into two equations: its symmetric and skew-symmetric part. Further, the diagonal elements of the symmetric equation gives a relation from which the pressure may be calculated in the flow. The off-diagonal elements of the symmetric equation gain a non-linear but purely algebraic equation for the velocity components.

Now, continued studies of the skew-symmetric equation show it is a linear differential equation for a vector potential $\boldsymbol{A}$. A solution consisting of an integral kernal similar to such used for the diffusion may be applied. This describes vorticity generated at solid boundaries as well as contained in fluid leaving or entering the system. Still left undetermined are boundary values of the velocity and its gradients (vorticity).

The final part of the paper presents a suggestion about inquiring information about the velocity and velocity gradients (vorticity) at the boundaries. By the use of the equation of continuity a velocity field $\boldsymbol{v}_Q$ from sources and sinks in a infinte space is obtained. Then, $\boldsymbol{v}_Q$ has to be modified such that it satisfies the normal and tangential boundary conditions. This gives two surface integrals (one from the normal and one from the tangential condition) with specified kernals that will be subtracted from infinte space velocity $\boldsymbol{v}_Q$.

5.3 Paper III

In Paper III the vortex evolution and connection to turbulence in 2-D flows is described. There exist two common methods to generate 2-D vortical flows, namely in soap films and in stratified systems. See [91, 92] for a rewiew. The statified flow is generated in a plastic cell under which permanent magnets are located, orientated such that to have a vertical magnetization axis. The cell is filled with two layers of a solution which has different densities. The heavier solution is on the bottom and the density difference of the interface acts to prevent vertical velocities, and thus a bidimensionalization of the flow. The magnets are placed to create a 8×8 array of vortices wiht nearest neighbors counter-rotating.

We have used vortex solutions derived from a solenodial vector potential $\boldsymbol{A}$. The vector potential is characterized by three parameters, n the order of vortex multiplet, the dynamic behaivor β and j which is the lower summation index of a sum over a diffusive variable $\frac{r}{\sqrt{\nu t}}$. Evolution of the vorticity fields are calculated and statistics for average vortex radius and number of vortices are compared with messurements [27]. Vortex singlets do not contribute to the energy spectrum so dipoles are used to compare with the measured turbulent energy spectrum in [28].

Now we turn to the situation of soap films. Two vertical combs are placed along the channel walls. The teeth of the vertical combs perpetually generate small vortices, which then are quickly swept into the center of the channel by larger vortices. A forced, steady turbulent state is created.

We model the flow by a combination of vortex doublets of the same type as in the stratified layer case, and a stationary part assumed to consist of a uniform flow. The no-slip boundary condition at the channel walls is satisfied by this choise of combination.

The main results we obtain for the energy spectral function $E(k)$ is that it scales with $k\sqrt{\nu t}$ and that it has an amplitude that is proportional to νt. Also, we display that $E(k)$ scales as k^{-3}. These results are in good agreement with experimental results of soap films shown in [34].

5.4 Paper IV

In Paper IV the focus is on vortex structures in 3-D. We give three examples of recent experimental observations where we find solutions that reproduces the measurements. First, travelling vortex structures experimentally observed in a pipe flow at Re close to transition from laminar to turbulent flow is considered [19, 20]. These vortex structures has stremwise orientation creating local anomalies in the streamwise velocity, called streaks. The flow in the spanwise direction is weaker but may still be critical for the flow pattern. Our solutions, which are found in spherical coordinates, possesses the property that the velocity and vorticity are parallell so they are exact solutions to the non-linear vorticity transport equation. A superposition of such vortices, which still is a exact solution, describes flow patterns observed in [19, 20].

Secondly, vortex rings are studied. New experimental observations made in water are reported in [62, 63]. The vortex rings are generated by pushing water through the cylindrical nozzle of a pipe submerged in an aquarium. By the use of planar laser induced flourescence and particle image velocimetry, the velocity and vorticity profiles together with the energy spectral function for the vortex structure are obtained. We model the vortex ring by elementary vortices with diffusive properties, again in sperical coordinates, where the flow field has the property that the velocity is perpendicular to the vorticity. Elementary vortices are placed around a circle and integrated to obtain the total flow.

Finally, a stretched vortex experimentally obtained in a water channel [56, 93] is modelled. A small bump on the bottom wall of the channel induces the initial boundary vorticity to roll up in a vortex. Then the vortex is strongly enhanced by stretching which is produced by sucking the flow through a hole on each lateral wall. We model the vortex by an elementary vortex structure where the vorticity and velocity is parallel as for the travelling vortex in a pipe. A distribution of elementary vortices are placed along the stretching axis and we are able to satisfy the boundary conditions. The resulting velocity field reproduces the experimental data with good agreement [56, 93].

6 Acknowledgements

First of all I will thank my supervisor, docent Mats D. Lyberg, for bringing me into the interesting field of fluids. I will also thank him for all the support and encouragement during the years of the work. Secondly, I will thank everyone at the Physics Department at Växjö University for the nice enviroment to work in. Finally, I will thank my family, especially Helena, for all your support.

Bibliography

[1] G.A. Tokaty, *A History and Philosophy of Fluid Mechanics*, Dover Publications, New York, (1971).

[2] D. Gottlieb and S.A. Orszag, *Numerical Analysis of Spectral Methods: Theory and Applications*, SIAM, Philadelphia, (1977).

[3] G.D. Smith, *Numerical Solution of Partial Differential Equations: Finite Difference Methods*, 3rd ed., Clarendon Press, Oxford, (1985).

[4] O.C. Zienkiewicz and R.L. Taylor, *The Finite Element Method – Vol. 2: Solid and Fluid Mechanics*, McGraw-Hill, New York, (1991).

[5] P.G. Saffman, *Vortex Dynamics*, Cambridge University Press, Cambridge, (1992).

[6] A. Ogawa, *Vortex Flow*, CRC Press, Boca Ranton, Florida, (1993).

[7] J.Z. Wu, H.Y. Ma and M.D. Zhou, *Vorticity and Vortex Dynamics*, Springer-Verlag, Heidelberg, (2006).

[8] O. Reynolds, Philos. Trans. **174**, 935 (1883).

[9] P.G. Drazin and W.H. Ried, *Hydrodynamic Stability*, Cambridge University Press, Cambridge, (1981).

[10] S. Chandrasekhar, *Hydrodynamic and Hydromagnetic Stability*, Dover Publications, New York, (1981).

[11] P.J. Schmid and D.S. Henningson, *Stability and Transition in Shear Flows*, Springer-Verlag, New York, (2001).

[12] E.D. Siggia, J. Fluid Mech. **107**, 37 (1981).

[13] A. Vincent and M. Meneguzzi, J. Fluid Mech. **225**, 1 (1991).

[14] O. Cadot, D. Douady and Y. Couder, Phys. Fluids **7**, 630 (1995).

[15] Y. Cuypers, A. Maurel and P. Petitjeans, Phys. Rev. Lett. **91**, 1945 (2003).

[16] T.S. Lundgren, Phys. Fluids **25**, 2193 (1982).

[17] J.C. Vassilicos and J.G. Brasseur, Phys. Rev. E **54**, 467 (1996).

[18] B. Hof, A. Juel and T. Mullin, Phys. Rev. Lett. **91**, 2445 (2003).

[19] B. Hof, C.W.H. van Doorne, J. Westerweel, F.T.M. Nieuwstadt, H. Faisst, B. Eckhardt, H. Wedin, R. R. Kerswell and F. Waleffe, Science **305**, 1594 (2004).

[20] B. Hof, C.W.H. van Doorne, J. Westerweel and T.M. Nieuwstadt, Phys. Rev. Lett. **95**, 2145 (2005).

[21] H. Faisst and B. Eckhardt, Phys. Rev. Lett. **91**, 2245 (2003).

[22] F. Waleffe, Phys. Fluids **15**, 1517 (2003).

[23] H. Wedin and R. Kerswell, J. Fluid Mech. **508**, 333 (2004).

[24] J. Sommeria, J. Fluid Mech. **170**, 139 (1986).

[25] O. Cardoso, D. Marteau and P. Tabeling, Phys. Rev. E **49**, 454 (1994).

[26] J. Paret and P. Tabeling, Phys. Rev. Lett. **79**, 4162 (1997).

[27] A.E. Hansen, D. Marteau and P. Tabeling, Phys. Rev. E **58**, 7261 (1998).

[28] J. Paret, M-C. Jullien and P. Tabeling, Phys. Rev. Lett. **83**, 3418 (1999).

[29] Y. Couder, J. Physique Lett. **42**, 429 (1981).

[30] Y. Couder, J. Physique Lett. **45**, 353 (1984).

[31] H. Kellay, X.L. Wu and W.I. Goldburg, Phys. Rev. Lett. **74**, 3975 (1995).

[32] X.L. Wu, B. Martin, H. Kellay and W.I. Goldburg, Phys. Rev. Lett. **75**, 236 (1995).

[33] B. Martin, X.L. Wu, W.I. Goldburg and M.A. Rutgers, Phys. Rev. Lett **80**, 3964 (1998).

[34] M.A. Rutgers, Phys. Rev. Lett. **81**, 2244 (1998).

[35] H. Kellay, X.L. Wu and W.I. Goldburg, Phys. Rev. Lett. **80**, 277 (1998).

[36] G.K. Batchelor, *An Introduction to Fluid Dynamics*, Cambridge University Press, Cambridge, (1967).

[37] D.J. Tritton, *Physical Fluid Dynamics*, Oxford University Press, Oxford, (1988).

[38] Z.U.A. Warsi, *Fluid Dynamics, Theoretical and Computational Approaches*, 2nd ed., CRC Press, Boca Ranton, (1999).

[39] D.J. Acheson, *Elementary Fluid Dynamics*, Oxford University Press, Oxford, (1990).

[40] L.D. Landau and E.M. Lifshitz, *Fluid Mechanics*, 2nd ed., Pergamon Press, Oxford, (1987).

[41] C.-H. Choi, J.A. Westin and K.S. Breuer, Phys. Fluids **15**, 2897 (2003).

[42] E. Lauga and H.A. Stone, J. Fluid Mech. **489**, 55 (2003).

[43] L. Tophøj, S. Møller and M. Brøns, Phys. Fluids **18**, 3102 (2006).

[44] M. Brøns, Adv. Appl. Mech. **41**, 38 (2006).

[45] G. Dassios and I.V. Lindell, J. Phys. A **35**, 5139 (2002).

[46] H. Lamb, *Hydrodynamics*, 6th ed., Cambridge University Press, Cambridge, (1932).

[47] S.A. Chaplygin, Trans. Phys. Sect. Imperial Moscow Soc. Friends of Natural Sci. **11**, 11 (1903).

[48] M.J.M. Hill, Proc. of the Roy. Soc. of London **55**, 219 (1894).

[49] J.L. Synge and C.C. Lin, Trans. R. Soc. Can. **37**, 45 (1943).

[50] C.W. Oseen, Ark. J. Mat. Astrom. Fys. **7**, 14 (1912).

[51] R.R. Trieling and G.J.F. van Heijst, Fluid Dyn. Research **23**, 27 (1998).

[52] G.I Taylor, Reports and Memoranda **598**, 73 (1918).

[53] G.I Taylor, Proc. R. Soc. London A **164**, 476 (1938).

[54] J.M. Burgers, Adv. Appl. Mech. **1**, 197 (1948).

[55] A.A. Townsend, Proc. R. Soc. A **208**, 534 (1951).

[56] P. Petitjeans, J.H. Robres, J.E. Wesfreid and N. Kevlahan, Euro. J. Mech. B. /Fluids **17**, 549 (1998).

[57] Lord Kelvin, Trans. R. Soc. Edinb. **25**, 217 (1869).

[58] J.C. Maxwell, *A Treatise on Electricity and Magnetism – Vol. 2*, 3rd ed., Dover Publications, New York, (1954).

[59] K. Shariff and A. Leonard, Annu. Rev. Fluid Mech. **24**, 235 (1992).

[60] L.E. Fraenkel, Proc. R. Soc. Lond. A **316**, 29 (1970).

[61] F.B. Kaplanskii and Y.A. Rudi, Fluid Dynamics **36**, 16 (2001).

[62] A. Dazin, P. Dupont and M. Stanislas, Exp. in Fluids **40**, 383 (2006).

[63] A. Dazin, P. Dupont and M. Stanislas, Exp. in Fluids **41**, 401 (2006).

[64] P.G. Saffman, Stud. Appl. Math. **49**, 371 (1970).

[65] A.H.M. Eisenga, R. Vericco and G.J.F. van Heijst, J. Fluid Mech. **354**, 69 (1998).

[66] H. Tryggeson and M.D. Lyberg, in preparation.

[67] S. E. Widnall, Annu. Rev. Fluid Mech. **7**, 141 (1975).

[68] P. R. Spalart, Annu. Rev. Fluid Mech. **30**, 107 (1998).

[69] L. Jacquin, Int. J. Heat and Fluid Flow **26**, 843 (2005).

[70] B.G. Newman, Aeronaut. Q. **1**, 167 (1959).

[71] G.K. Batchelor, *The Theory of Homogenous Turbulence*, Cambridge University Press, Cambridge, (1982).

[72] J.O. Hinze, *Turbulence*, McGraw-Hill, New York, (1975).

[73] W.D. McComb, *The Physics of Fluid Turbulence*, Oxford University Press, Oxford, (1991).

[74] U. Frisch, *Turbulence: The Legacy of A.N. Kolmogorov*, Cambridge University Press, Cambridge, (1995).

[75] O. Reynolds, Phil. Trans. R. Soc. A **186**, 123 (1895).

[76] J. Boussinesq, Mém. prés. par div. savant à l'acad. sci. Paris **23**, 46 (1877).

[77] A.N. Kolmogorov, Dokl. Akad. Nauk S.S.S.R. **32**, 19 (1941).

[78] S. Robinson, Annu. Rev. Fluid Mech. **23**, 601 (1991).

[79] P. Holmes, J.L. Lumley and G. Berkooz, *Turbulence, Coherent Structures, Dynamical Systems and Symmetry*, Cambridge University Press, Cambridge, (1998).

[80] B. Podvin and J. Lumley, J. Fluid Mech. **362**, 121 (1998).

[81] R. Panton, Prog. Aerospace Sci. **37**, 341 (2001).

[82] D.I. Pullin and P.G. Saffman, Phys. Fluids **5**, 126 (1993).

[83] D.I. Pullin, J.D. Buntine and P.G. Saffman, Phys. Fluids **6**, 3010 (1994).

[84] D.I. Pullin and P.G. Saffman, Annu. Rev. Fluid Mech. **30**, 31 (1998).

[85] N.C. Lambourne and D.W. Bryer, Aero. Res. Coun., Dokument 477, (1959).

[86] M.G. Hall, J. of Fluid Mech. **11**, 209 (1961).

[87] H. Kawai and G. Nishimura, J. Wind Eng. Ind. Aero. **60**, 211 (1996).

[88] C.W. Williams and C.J. Baker, J. Fluids and Structures **11**, 767 (1997).

[89] D. Banks and R.N. Meroney, Wind and Structures **4**, 227 (2001).

[90] G.J.F. van Heijst, H.J.H. Clercx and D. Molenar, J. Fluid Mech. **554**, 411 (2006).

[91] H. Kellay and W. I. Goldburg, Rep. on Progr. in Phys. **65**, 845 (2002).

[92] P. Tabeling, Phys. Rep. **362**, 1 (2002).

[93] M. Rossi, F. Bottausci, A. Maurel and P. Petitjeans, Phys. Rev. Lett. **92**, (2004).

I

Stationary vortices attached to flat roofs

Henrik Tryggeson* and Mats D. Lyberg

Physics Dept., Växjö Univ., S-35195 Växjö, Sweden

Abstract

This paper treats the topic of a conical vortex attached to a plane, horizontal surface. Data have been collected from measurements on freely suspended cubes in a wind-tunnel. Data are analyzed and some vortex properties derived. The pressure coefficient is found to decrease as the inverse of the square root of the distance from the corner. Experimental results are used to construct an analytical model of the conical flow derived from a solution to the non-linear vorticity transport equation and the resulting flow is predicted. This flow is used to calculate the pressure suction on the attached surface. An application would be pressure on flat roofs of high-rise buildings subjected to an adverse wind.

Keywords: Conical vortex, High-rise building, Flat roof, Wind-tunnel test, Mean pressures

*Corresponding author
E-mail adresses: htr@msi.vxu.se (H. Tryggeson)

1 Introduction

This paper contains measurements on and a mathematical model of conical vortices adjacent to flat surfaces. The first thorough experimental studies and modeling of conical vortices were related to wing tip vortices (Lambourne and Bryer, 1959; Hall, 1961). This was somewhat later followed by studies of conical vortices attached to walls (Davenport, 1960; Leufheusser, 1965) and has seen a continuous development of more refined experiments and theoretical models (Simiu, 1978; Wirén, 1970, 1985, 1990; Lee and Evans, 1984; Kind, 1986; Kramer and Gerhardt, 1991; Doligalski et al, 1994; Tieleman et al, 1996) and, in recent years, by a large number of studies (for example, Banks and Meroney, 2001; Kawai, 1997; Lin et al, 1995; Bienkiewicz and Ham, 2003; Wu et al, 2001) .

Below follows a brief overview of the main physical and mathematical background of the topic treated. Some experimental results of the main problem are presented in Sections 2 and 3. In Section 4 appears the derivation of the mathematical model applied. Section 5 treats the connection between model and what results are to be expected from theory for wall boundary layers rolling up into a vortex. Section 6 contains results and a discussion.

The main aim of this paper is to find a simple description of a conical vortex attached to a planar horizontal surface. The velocity field will be the desired output, from which the pressure may be determined. The input is measured data of the incoming flow, which will serve as boundary conditions to solutions of the differential equations governing a flow.

Suppose we have an incompressible newtonian fluid. The Navier-Stokes equation and the equation of continuity govern its motion. These equations contain all the dynamic information about a fluid in motion. We will use spherical co-ordinates applied to a cone with the z-axis of the co-ordinate system along the principal axis.

A conical vortex appears, for example, close to the edge at the roof of buildings, as in Fig. 1. The airflow released from the vertical side rolls up into two conical vortices (Kramer and Gerhardt, 1991; Banks et al, 2000; Banks and Meroney, 2001; Wu et al, 2001), as is schematically indicated in Fig. 2. The presence of the cones bring about suction on the roof below the vortices. The pressure is lowest at the tip of a conical vortex and its magnitude decreases along the symmetry line.

The vortices have been observed not to be stationary. In laboratory experiments, the symmetry axis of a vortex may be swaying back and forth several degrees (Kawai and Nishimura, 1996), even in a smooth flow (Banks et al, 2000). The relative strength of the two conical vortices may fluctuate in a periodic manner (Kawai, 1997). In the field, wind gusts will affect properties of the conical vortices.

The pressure distribution over the planar top depends mainly on the flow at the leading edge (Wirén, 1970, 1985; Zhao et al, 2002). This flow, in its turn, is determined by the following properties: the main flow angle with the leading edge, the leading edge velocity profile and the characteristic length of the configuration.

If the leading edge is sharp, a separation of the flow appears and the vortex sheet arriving at the edge rolls up into a concentrated vortex (Lin et al, 1995; Banks et al, 2000). The core of the conical vortex makes an angle of 11° to 14° with the leading edge in wind tunnel studies (Lin et al, 1995; Kawai 1997; this study) and somewhat larger in full-scale studies (Cochran,

1992). The smaller angle is for large Reynolds numbers, Re. Re is the non-dimensional number defined from Re=UL/ν, where U is a characteristic velocity of the system, L is a characteristic length and ν is the kinematic viscosity. We have identified U with the free-stream velocity. The choice of L is discussed below. The high flow speed effect is most notable when the incoming flow makes a 45° angle with the leading edge. The strongest suction occurs for a smooth flow (Lin et al, 1995; Kawai 1997). If the leading edge is rounded or phased, the strength of the vortices is decreased and so is the suction on the roof (Wirén, 1970; Franchini et al, 2005; Fu et al, 2005; Ahmad and Kumar, 2002).

The influence of the characteristic length on the top pressure is important as borne out by experimental results. The characteristic length is an important scaling parameter while the Reynolds number influence turns out to be less pronounced.

A characteristic that has only a small influence on final pressure suction on the roof, is the height of the ground boundary layer relative to the model height (Simiu et al, 1978). It is predominantly the turbulence and the vertical mean velocity gradient of the ground boundary layer that contribute to pressure fluctuations and other dynamic instabilities on the sides of the building (Leufheusser, 1965; Letchford and Marwood, 1997).

2 Experimental pressure data

Pressure measurements have been carried out in an aerodynamic wind-tunnel by the Department of Aeronautics at the Royal Institute of Technology, Stockholm. The objects consisted of cubes freely suspended at mid height of the tunnel cross section with an angle of attack of 45°. Consequently, there was no boundary layer. Two vortices formed on top of the cube (see Fig. 1). The side of the cube was 2a=300 or 150 mm. Air velocities up to 80 m/s could be attained. Pressure measurements were carried out in the Reynolds number range of $0.63\ 10^5<Re_a<6.9\ 10^5$. Here, the Reynolds number is based on half the side of the cube, a.

Holes to measure the pressure have been situated at stations at x=5, 10, 15, 20, 25, 30, 40, 50, 75, 100, 125 and 145 mm. For each value of x there were holes at y=5, 10, 15, 20, 30, 40, 50, 75, 100 and 145 mm. With this resolution, the pressure data obtained were those of the vortex adjacent to the y-axis, not along the x-axis of the top of the cube (see Fig. 3). An example is given in Fig. 4. The pressure data have been invoked to calculate the pressure coefficient, C_p. This coefficient is defined from

$$C_p = \left(p - p_\infty\right) \Big/ \left(\rho U^2/2\right), \qquad (2.1)$$

where ρ is the density of the fluid and p_∞ is the pressure at infinity.

3 Boundary values and characteristic flow parameters

To model the conical vortex we need some characteristic flow parameters and boundary values. When we construct our model we need boundary values, in particular,

1. the characteristic length,
2. the top angle of the cone,

3. the radial velocity on the boundary of the cone,
4. the azimuthal velocity on the boundary of the cone, and
5. the circumferential velocity on the boundary of the cone.

The length over which a boundary layer develops before rolling up is an important parameter when modeling roof vortices, the non-dimensionalizing length of choice (Lin et al, 1995). For a freely suspended cube, it would seem natural to take half the side length, a, as the characteristic length. However, maybe due to buoyancy effects, the level where the velocity is horizontal is shifted upwards from the mid-height of the cube for small Reynolds numbers. Therefore, we have taken the distance between the top of the cube and the level where the velocity is horizontal as the characteristic length, h. This resulted in more coherent results regarding scaling and reduced the apparent dependence on the Reynolds number.

For a low-rise building, there may not be a height where the velocity along a wall is horizontal, other than the ground level. If this is so, the only characteristic length is the building height (Lin et al, 1995). For those high-rise buildings where the height is much larger than the width, the situation may be different. It may be of importance if the width is large enough or not for the conical vortex to reattach to the roof (Lin et al, 1995). If the stream pattern close to the top is similar to the one observed for a cube in this experiment, one should, for a building resembling a pillar, base the Reynolds number on a characteristic length more related to the width than to the height of the building.

To determine what is the relation between h, a and the Reynolds number Re_a, we used pictures showing streamlines on the sides of the cube. Fig. 5 shows a side view photograph where the stream patterns may be seen. The result from a fit is given in Fig. 6. It is of the form

$$h/a = 1 - \exp\left[-1/2\left(Re_a\, 10^{-5}\right)^{3/4}\right]. \qquad (3.1)$$

From now on we use r/h as the dimensionless length variable and the Reynolds number Re_h based on the characteristic length h.

Below the symmetry axis of the cone, the roof pressure falls off roughly as the square root of the distance from the corner (see Fig. 7). This is in accordance with observations in other experiments (Lin et al, 1995). The cone top angle $2\theta_0$ is practically constant when considered as functions of r/h and independent of the Reynolds number, see Fig. 8.

From pictures such as Fig. 5 one may also determine the angle α between the vertical direction and the flow at the top of the cube side. An example is shown in Fig. 9. The angle α is very small. From this one may infer that, at the boundary of the cone, the radial velocity component (as the top angle is small, this is essentially the velocity component directed parallel to the symmetry axis) may be put equal to zero.

4. A model of a conical vortex.

Theoretical considerations leads to the conclusion that there are many candidates when formulating models of a rolled up vortex based on analytic properties (Lundgren, 1982). One particular model for the early stages of formation of a stretched cylindrical vortex is that of a logarithmic spiral (Vassilicos and Brasseur, 1996). Experimental observations confirm this

behavior (Petitjeans et al, 1996; Rossi et al, 2004). The kind of vortices considered in this paper differs from these cylindrical vortices in one respect. For a conical vortex, there is a strong axial velocity component removing fluid that has been injected into the cone closer to the tip.

The axial velocity component in a vortex induces an axial strain, favoring exchange of fluid in the direction perpendicular to the axis of symmetry. This leads to an enhanced and more rapid mixing of the rolled boundary layers for a conical vortex compared to a cylindrical vortex. It then seems reasonable that, when modeling conical vortices, one may assume that the vortex possesses a cylindrical symmetry, maybe with the exception of the outermost layer. This kind of models is common when modeling conical vortices (Banks et al, 2001). We have chosen to base our model of a conical vortex on this assumption. However, some flattening of the vortex has been experimentally observed (Banks and Meroney, 2001).

We seek a solution to the flow equations satisfying the boundary conditions that have been derived in the previous sections. In the analysis, we will use spherical coordinates (r, θ, φ) with the origin at the building top corner. Thus, r will be the distance from this corner. The velocity in the r-direction is approximately parallel to the symmetry axis as the cone top angle is small. The azimuthal velocity (the θ-direction) is perpendicular to the envelope of the cone and defines the flux of fluid into it. The circumferential velocity (the φ-direction) defines the rotation of the vortex. The velocity components relative the roof have been defined in Fig. 3.

The boundary conditions for the velocity components that we will consider have been determined as follows.

1. As noted above (Fig. 7), below the symmetry axis of the cone, the roof pressure falls off roughly as the square root of the distance from the corner. If the pressure is essentially determined by the square of the velocity u on the boundary, this velocity behaves as

$$u(r,\theta=\theta_0)\propto(r/h)^{-1/4}. \tag{4.1}$$

2. The radial velocity, u_r, is almost zero on the boundary $\theta=\theta_0$ (see Fig. 9).

The relevant flow equations are the Navier-Stokes equation and the equation of continuity for an incompressible fluid,

$$\partial_t\bar{u}+\bar{\omega}\times\bar{u}+\nabla\left(\bar{u}^2/2+p\right)-Re^{-1}\Delta\bar{u}=0, \tag{4.2}$$

$$\nabla\cdot\bar{u}=0. \tag{4.3}$$

In these equations, velocities are normalized by the free-stream velocity U, length coordinates by h (see Section 3), time by h/U and pressure by $\rho U^2/2$. Taking the rotation of eq. (4.2), one of the non-linear terms (the gradient term) disappears. The other non-linear term, the one stemming from $\bar{\omega}\times\bar{u}$, disappears if the velocity $\bar{u}$ and the vorticity $\bar{\omega}$ are parallel. However, this prescription needs to be cast in the form of an explicit equation to be useful. Such an equation is provided by the circumstance that the rotation of eq. (4.2) may be written in the form

$$\partial_t \bar{\omega} + \bar{u} \times \Delta \bar{u} - \left(\nabla(\bar{u}) - \nabla(\bar{\omega})\right)\left(\bar{u} \cdot \bar{\omega}\right) = \mathrm{Re}^{-1} \Delta \bar{\omega}\,. \tag{4.4}$$

Here, the symbol $\nabla(\bar{u})$ indicates that the derivatives of the nabla operator are to be applied to the components of $\bar{u}$ only. This equation and its equivalents are often referred to as the vorticity equation or the vorticity transport equation. As the non-linear terms on the left-hand side disappear if the vorticity is parallel to the velocity, the remaining terms must satisfy the diffusion type equation

$$\partial_t \bar{\omega} = \mathrm{Re}^{-1} \Delta \bar{\omega}\,. \tag{4.5}$$

This is possible if the velocity or the vorticity can be factorized with regard to space coordinates and time. For example, a vortex left to decay from time t=0 will have a factor $\exp(-t/\mathrm{Re})$ and a shear flow starting at time t=0 will create a growing vortex with a factor $\left[1-\exp(-t/\mathrm{Re})\right]$. Denote the time dependent factor by f(t). A velocity field satisfying the above requirements is given by

$$\begin{aligned} u_r(r,\theta,t) &= -C\,\ell(\ell+1)\,r^{-1}\,j_\ell(r) R_\ell^0(\theta) f(t) \\ u_\theta(r,\theta,t) &= -C\left[j_{\ell-1}(r) - \ell r^{-1}\,j_\ell(r)\right] R_\ell^1(\theta)\, f(t) \\ u_\varphi(r,\theta,t) &= C\, j_\ell(r)\, R_\ell^1(\theta)\, f(t)\,. \end{aligned} \tag{4.6}$$

Here, C is a constant, j_ℓ is a spherical Bessel function and R_ℓ^m with m=0, 1 is an associate Legendre function. This velocity field satisfies the eq. (4.4). As a matter of fact, any linear combination of velocity fields of the form of eq. (4.6) but displaced from the origin to any other point or time will also satisfy eq. (4.6) (Lyberg and Tryggeson, 2007). This circumstance allows a description of a dynamical vortex, such as the swaying of the main axis, or the influence on the vortex from gusts. Consider the simple example of a vortex driven by a wind of constant direction but of varying speed U(t). In this case, the factor f(t) above would take the form

$$f(t) = \int_{-\infty}^{t} \exp\left[-(t-t')/\mathrm{Re}\right] U(t')\,dt'. \tag{4.7}$$

The relevant associated Legendre functions of eq. (4.6) may not have any zeros for arbitrary values of the parameter ℓ. However, the second boundary condition stated above may be satisfied by making the angular factors of $\bar{u}$ a linear combination of Legendre functions of the first and second kind

$$R_\ell^m(\theta) = Q_\ell^0(\theta_0) P_\ell^m(\theta) - P_\ell^0(\theta_0) Q_\ell^m(\theta), \tag{4.8}$$

where m=0 or 1. From the velocity field given by eq. (4.6), one may now calculate the pressure from eq. (4.2)

$$p = -\bar{u}^2/2 + p_\infty + \mathrm{Re}^{-1} \int_{\infty}^{\bar{r}} \Delta \bar{u} \cdot d\bar{r}, \tag{4.9}$$

and thereby the pressure coefficient C_p. To evaluate the integral of eq. (4.9), select a path of integration along a ray on the envelope of the cone. One then obtains (in non-dimensional units)

$$\int_{\infty}^{\bar{r}} \Delta\bar{u}\cdot d\bar{r} = Re\,\partial_t \int_{\infty}^{r} u_r(r,\theta=\theta_0)\,dr = 0, \qquad (4.10)$$

as the radial velocity component is assumed to be zero on the cone envelope. This justifies using the Bernoulli equation to calculate the pressure. It still remains to determine the parameter ℓ in such a manner that the pressure falls off with the square root of the distance to the corner. However, from eq. (4.6) it is obvious that the azimuthal and circumferential velocity components do not have the same dependence on r. To determine the parameter ℓ, one then needs an estimate of the r-dependence for one of the velocity components.

5 Check with boundary layer theory.

We want to carry out an independent consistency check to see if the velocity field given by eq. (4.6) is compatible with simple assumptions regarding properties of the boundary layer on the vertical wall. Such a check will provide information about the relation between the azimuthal and the circumferential velocity components at the cone boundary.

To determine the azimuthal velocity u_θ one needs to make some assumptions. It will be assumed that the mass flux of the boundary layer on the vertical side of the cube is fed into the vortex (see Fig. 2). The simplifying assumption is made that the influx to the cone is uniformly distributed at the boundary independent of the circumferential angle φ. The velocity u_θ may then be determined from the relation $\sin\theta_0\, 2\pi r\, u_\theta = \dot{q}$ where $\dot{q}$ is the mass flux contained in the boundary layer. One then needs an estimate of this mass flux.

During the trip along the wall, the flow is accelerated due to the pressure gradient, and vorticity is created. The path length of the boundary layer flow is assumed to be that of the trajectory along the vertical side. The path length may be determined from pictures such as Fig. 5. Pictures like this one show diffuse trajectories that may be hard to follow. Increasing the black and white picture contrast or color coding by computer algorithms facilitates tracing stream-lines. However, it would have been more efficient to record the streamline pattern in the form of pixels containing information in the form of a grey-scale. Computer algorithms for pattern recognition then could have been applied to identify streamlines.

The estimation of the boundary layer thickness is based on the theory of turbulent boundary layers, with or without pressure gradient. We apply Prandtl's conjecture that if there is a transition to a turbulent boundary layer, the boundary layer then behaves as if it had been turbulent from the leading edge (Schlichting, 1960).

The boundary layer is then derived from the momentum integral equation and the assumption that the velocity profile over the boundary layer thickness may be approximated by a suitable empirical profile. Up to $Re<3.6\ 10^6$ one may, for flow along a flat plate, use a power law

$$u/U = (y/\delta)^{1/n}, \qquad (5.1)$$

where n is a constant depending on Re, U is the flow velocity outside the boundary layer and δ is the boundary layer thickness. Taking n=7 should be valid for an interval in Re from 10^5 to $3.2\ 10^6$ and includes our experimental data interval. We will assume that this power law profile is valid.

In the presence of a pressure gradient, the boundary layer gets thinner than in the case of a zero pressure gradient. However, in this approximate estimate, we will assume that the boundary layer may be treated as the one for a flat plate. We have chosen to identify the boundary layer thickness by the momentum thickness δ_2. It is defined as

$$\delta_2 = \int_0^\infty u(y)/U\,(1 - u(y)/U)\,dy, \tag{5.2}$$

where U is the flow velocity outside the boundary layer. A calculation using the eq. (5.1) and (5.2) yields the result that the boundary layer thickness after a path length s is

$$\delta(s) = 0.37\,Re_h^{-1/5}(s/h)^{4/5}h\ . \tag{5.3}$$

The trajectory lengths have been determined from side view photographs. One finds that the length s of trajectories such as those of Fig. 5 then depends on the distance r in the form of a power law,

$$s/h = 1.24(r/h)^{0.91}. \tag{5.4}$$

This result is displayed in Fig. 10. Subsequently, we have therefore used the results of eq. (5.4) in all calculations.

Consider the volumetric flux, $\dot{q}$, that is fed into the cone. The amount fed in must for a fixed r be equal to the volume that the boundary layer contains at the edge of the wall for the same r,

$$\dot{q} = \int_0^\delta u(y)\,dy = \int_0^\delta U\,(y/\delta(s))^{1/n}\,dy = U\,\delta(s)\,n(n+1). \tag{5.5}$$

The above assumptions that the flux of the boundary layer is fed into the vortex then leads to

$$\sin\theta_0\ u_\theta(r, \theta = \theta_0)\,2\pi r\,dr = U\,0.37\,Re_h^{-1/5}(s/h)^{4/5}h\,n(n+1)\,dr\,. \tag{5.6}$$

The velocity u_θ, may then be estimated assuming that the free stream velocity U is approximately the same as the flow velocity outside the boundary layer along the wall. This is not an exact relation as the fluid is accelerated when moving along the wall. The blocking effect when inserting the bluff body into the wind-tunnel was 4%, which increases the velocity outside the wall. The actual velocity enhancement rather was somewhat more than 10%.

Inserting the result of eq. (5.4) into eq. (5.5) yields

$$\sin\theta_0\ u_\theta(r, \theta = \theta_0)/U \propto (r/h)^{-0.27}, \tag{5.7}$$

which is almost the same exponent as in eq. (4.6). A number of simplifying assumptions have been made in the calculation above, so this result should not be taken as a confirmation of the validity of eq. (4.6), but it gives an indication that the model is a sound one.

It remains to fix the value of the parameter ℓ, which determines the r-dependence of the velocity components. Guided by eq. (5.7), we put ℓ=3/4, giving the azimuthal velocity the dependence $u_\theta \propto r^{-1/4}$. Fixing the value of this parameter, one may now calculate the two angular functions $R_\ell^m(\theta)$, m=0, 1 defined in eq. (4.8). The result is shown in Fig. 11.

6 Results and Discussion

In Section 4 the solution method was presented and from the calculations the velocity field was determined. From that point of view the whole problem is solved, and to receive the wanted output, it is possible to determine the velocity field, the pressure field, and the vorticity. In the previous sections, a number of approximations and assumptions have been made regarding the character of the flow. A listing thereof includes the following items.

1. The vortex has been assumed to possess a rotational symmetry, neglecting any layered structure and flattening.
2. The characteristic length chosen is the distance between the roof and the height at which the wall boundary layer reaching the top commences its journey.
3. No effects of an atmospheric boundary layer are considered.
4. In the model derived from a solution to the flow equations, there is no implicit dependence on the Reynolds number, Re, except for the dependence on time. However, notice that we have still a Re-dependence from the boundary conditions.
5. The pressure is found to decrease as the inverse of the square root of the distance from the corner, r, motivating a dependence of the azimuthal velocity as $u_\theta \propto r^{-1/4}$.
6. With the model chosen, the pressure on the boundary of the cone may be derived from the Bernoulli equation.
7. The external flow driving the vortex has been assumed to be quasi-stationary.

The static pressure coefficient, C_p, may be derived from equation (4.7).

Figure 12 shows the theoretically calculated values of $-C_p$ and the experimentally measured ones for a value of Re=1.8 10^5 for a freely suspended cube. They agree remarkably well for values up to r/h=1, that is up to r=h in dimensional coordinates.

There are some remarks to be made. First, the boundary conditions are calculated from a theory of a simple boundary layer description involving the momentum thickness δ_2. A second remark is that our characteristic length, h, is dependent on Re, if the characteristic length used in the definition of Re is related to the side length of the cube. It establishes the boundary conditions, and data has been taken from a freely suspended cube. But the general model itself is not Re-dependent. The conclusion is that there is no simple scaling in C_p for Re, but it depends on details of the boundary layer rolling up to become a conical vortex.

References

Ahmad S., Kumar K., 2002. Wind pressures on low-rise hip roof buildings. Wind and Structures 5, 493-514.

Banks D., Meroney R.N., Sarkar P.P., Zhao Z., Wu F. 2000. Flow visualization of conical vortices on flat roofs. J. Wind Eng. Ind. Aerodyn. 84, 65-85.

Banks D., Meroney R.N., 2001. A model of roof top surface pressures produced by conical vortices. Wind and Structures 4, 227-246.

Bienkiewicz B., Ham H.J., 2003. Wind tunnel modelling of roof pressure and turbulence effects on the TTU test building. Wind and Structures 6, 91-106.

Cochran L.S. 1992. Wind tunnel modeling of low rise structures. Ph.D. Thesis, Civil Engineering, Colorado State University, CO.

Davenport, A.G., 1960. Wind Loads on Structures. NRCC 5576, Division of Building Research, National Research Council of Canada, Ottawa, Canada.

Dogigalski, T.L., Smith, C.R., Walker, J.D.A., 1994. Vortex interactions with walls. Ann. Rev. Fluid Mech. 26, 573-616.

Franchini, S., Pindado, S., Meseguer, J., Sanz-Andres, A., 2005. A parametric, experimental analysis of conical vortices on curved roofs of low-rise buildings. J. Wind Eng. Ind. Aerodyn. 93, 639-650.

Fu J.Y., Li Q.S., Xie Z.N., 2005, Wind effects on a large cantilevered flat roof. Wind and Structures 8, 357-372.

Hall, M. G., 1961. A theory for the core of a leading-edge vortex. J. Fluid Mech. 11, 209-228.

Kawai H., Nishimura G., 1996. Characteristics of fluctuating suction and conical vortices on a flat roof in oblique flow. J. Wind Eng. Ind. Aerodyn. 60, 211-225.

Kawai H., 1997. Structure of conical vortices related with suction fluctuation on a flat roof. J. Wind Eng. Ind. Aerodyn. 69-71, 579-588.

Kawai H., 2002. Local peak pressure and conical vortex on building. J. Wind Eng. Ind. Aerodyn. 90, 251-263.

Kind, R.J., 1986. Worst suctions near edges on flat rooftops on low-rise buildings, J. Wind Eng. Ind. Aerodyn. 25, 31-47.

Kramer C., Gerhardt, H.J., 1991. Wind pressures on roofs of very low and very large industrial buildings. J. Wind Eng. Ind. Aerod. 38, 285-295.

Lambourne, N.C., Bryer, D.W., 1959. Some measurements in the vortex flow generated by a sharp leading edge having 65° sweep. Aero. Res. Coun., Document 477.

Lee, B.E., Evans, R.A., 1984. The measurements of wind flow patterns over building roofs. Building and Environment 4, 235-241

Letchford, C.W., Marwood, R., 1997. On the influence of v and w component turbulence on roof pressures beneath conical vortices. J. Wind Eng. Ind. Aerodyn. 69-71, 567-577.

Leufheusser, H.J., 1965. Pressure distributions on a cube at various degrees of boundary layer immersion. Univ. of Toronto. U 1 Mec TP 6502.

Lin, J.X., Surry, D., Tieleman, H.W., 1995. The distribution of pressure near roof corners of flat roof low buildings, J. Wind Eng. Ind. Aerodyn. 56, 235-265.

Lundgren, T.S., 1982. Strained spiral vortex model for turbulent fine structure. Phys. Fluids 25, 2193-2203.

Lyberg, M.D., Tryggeson, H., 2007. Analysis of 3-D vortex structures in fluids. Submitted to Phys. Rev. Lett.

Marwood R. 1996. An investigation of conical roof edge vortices. Ph.D. Thesis, Lincoln College, Univ. of Oxford, Oxford, U.K.

Petitjeans P., Robres J.H., Wesfreid J.E., Kevlahan N., 1998. Experimental evidence for a new type of stretched vortex. Eur. J. Mech. B./Fluids 17, 549-560.

Rossi M., Bottausci F., Maurel A., Petitjeans P., 2004. A nonuniformly stretched vortex. Phys. Rev. Lett. 92, 4504-4507.

Schlichting, H., 1960. Boundary-layer theory. Mc-Graw-Hill.

Simui, E., Scanlan, R.H., 1978. Wind effects on structures: An introduction to wind engineering. A Wiley-Interscience publication.

Tieleman, H.W., Surry, D., Metha, K.C., 1996. Full-model scale comparison of surface pressures on the Texas Tech experimental building. J. Wind Eng. Ind. Aerodyn. 61, 1-23.

Vassilicos J.C., Brasseur J.G., 1996. Self-similar spiral flow structure in low Reynolds number isotropic and decaying turbulence. Phys. Rev. E 54, 467-485.

Wirén, B., 1970. Wind-tunnel investigation of the pressure distribution on a flat roof for various roof edges (in Swedish). The National Swedish Institute for Building Research. Rapport R35.

Wirén, B.,1985. Effects of Surrounding Buildings on Wind Pressure Distributions and Ventilation Losses for Single-Family Houses. Part I. The National Swedish Institute for building research. Bulletin M85.

Wirén, B.,1990. Wind effects on structures, Lecture Notes on Building Aerodynamics (in Swedish). The National Swedish Institute for Building Research.

Wu F. Sarkar P.P., Mehta K.C., 2001. Full scale study of conical vortices and roof corner pressures. Wind and Structures 4, 131-146.

Zhao Z., Sarkar P.P., Mehta K.C., Wu F., 2002. Wind flow characteristics and their loading effects on flat roofs of low-rise buildings. Wind and Structures 5, 25-48.

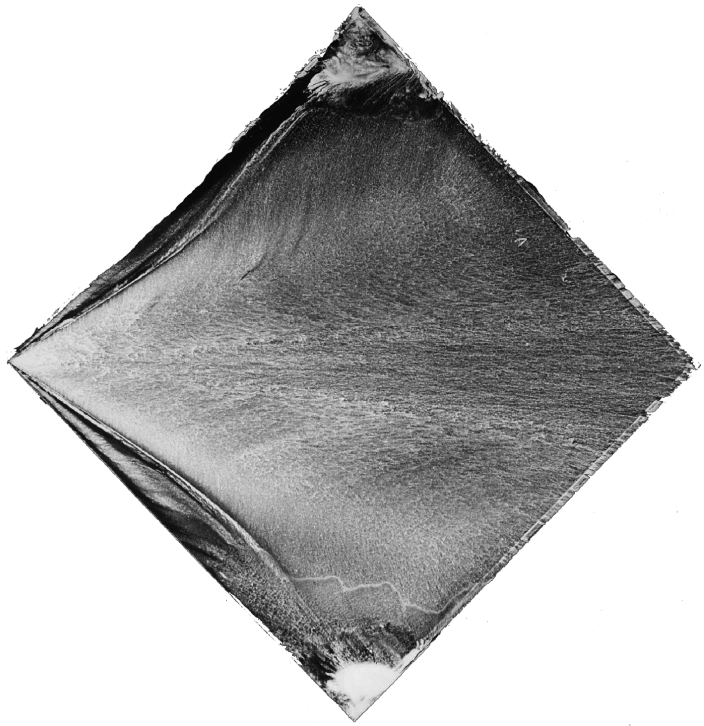

Fig. 1: *The flow above the horizontal top of a cube at $Re=10^5$. The incoming flow is from the left. The two conical vortices are close to the edges.*

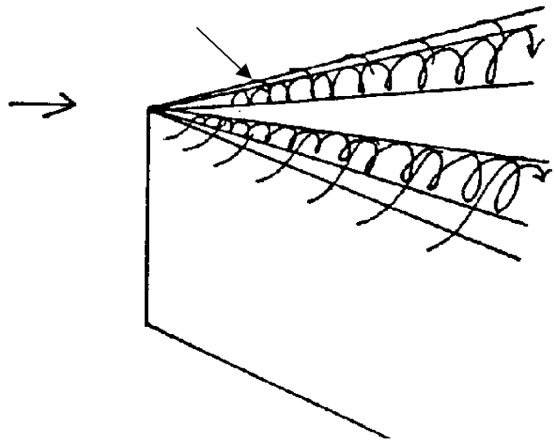

Fig. 2: *Sketch of conical vortices. The horizontal arrow indicates the wind direction. The other arrow indicates the leading edge.*

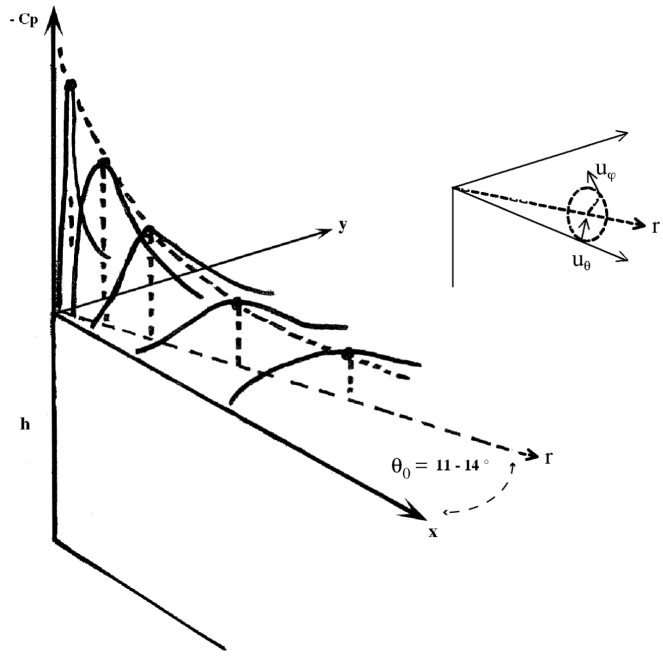

Fig. 3: *The pressure coefficient on a roof and definition of the x- and y- coordinate axes. Half the top angle of the conical vortex usually takes a value between 11 and 14 degrees in building aerodynamics. To the upper right, the velocity components in spherical coordinates are indicated.*

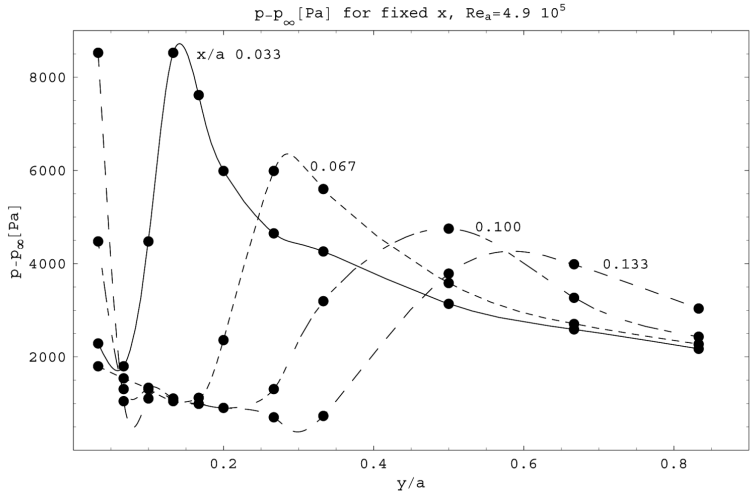

Fig. 4: *Pressures measured below a vortex on top of a freely suspended cube. The curves have been obtained from a cubic spline fit. The pressure minimum is determined from the maximum of the curves. Data refer to the vortex close to the y-axis (see Fig. 3).*

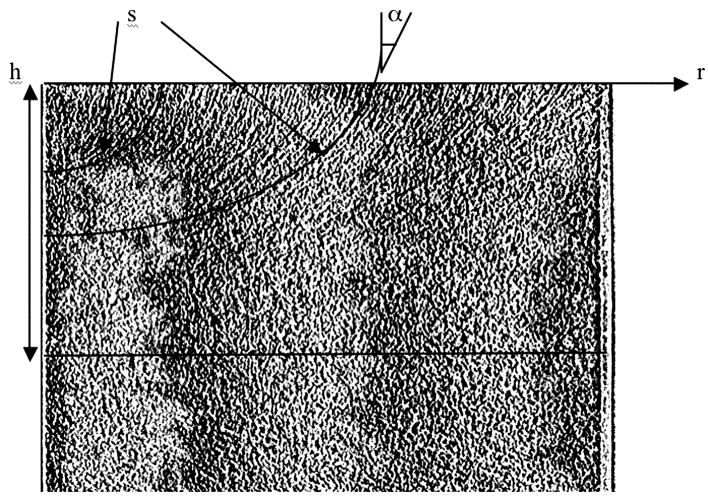

Fig 5: *Computer-modified picture of he flow along the wall at $Re=10^5$. The characteristic length h is the distance between the top and the symmetry line of the cube. The symbol α indicates the angle between the boundary layer velocity and the normal to the top for the flow leaving the edge.*

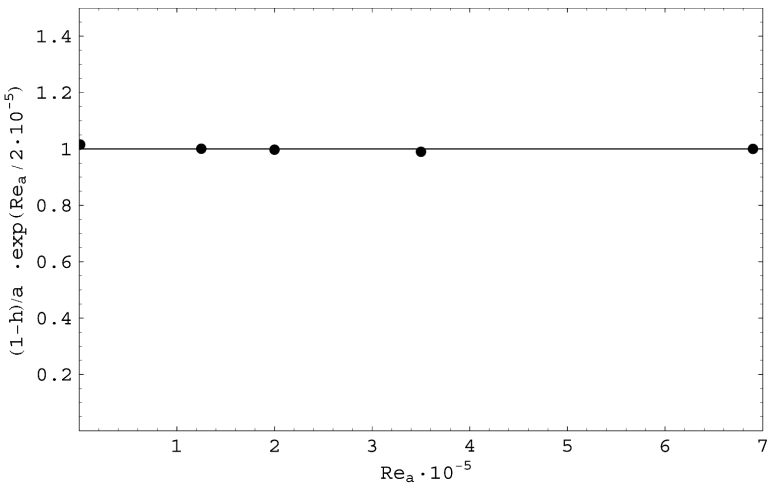

Fig. 6: *A relation between the characteristic length and the half side of a cube, a, for various values of the Reynolds number Re_a. The values of h have been determined from Schlieren photographs such as the one presented in Fig. 5.*

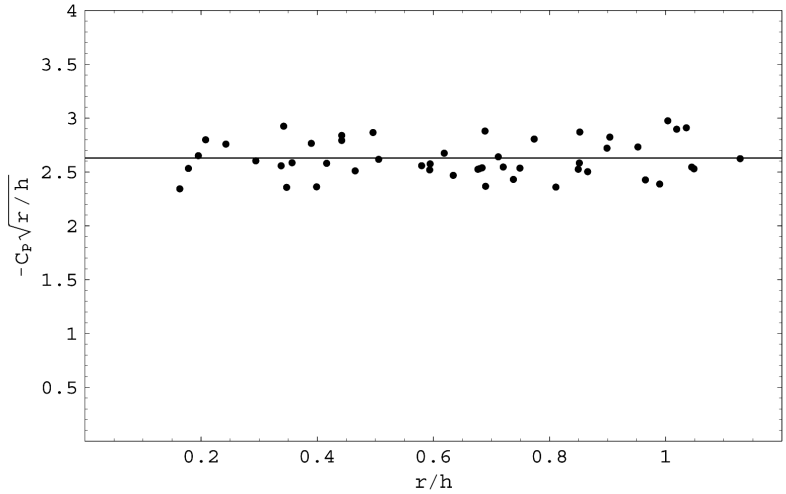

Fig. 7: *The value of $-C_p\sqrt{r/h}$ as dependent on r/h for Reynolds numbers Re_h in the range 0.2<Re_h 10^{-5}<6.0. There is no systematic dependence on r/h found. The scatter around the average value is about 7%.*

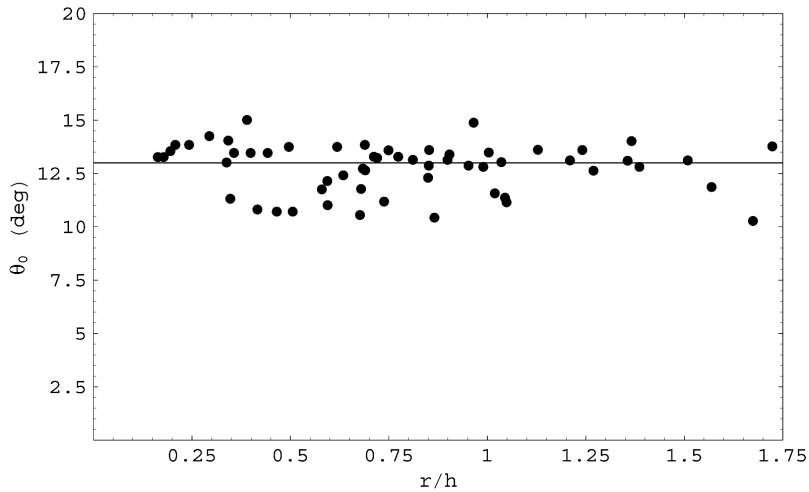

Fig. 8: *The dependence of half the vortex top angle on distance r/h. The average here is 13 degrees.*

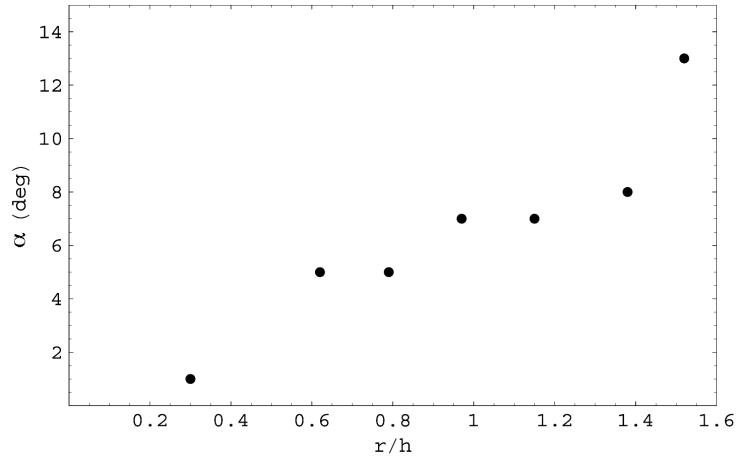

Fig. 9: *The direction of the flow leaving the wall. The angle α is the deviation from the vertical direction.*

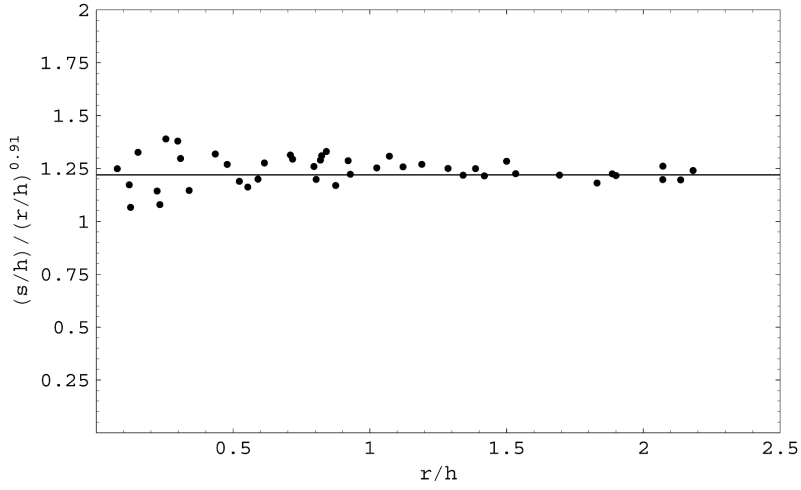

Fig. 10: *A relation between the trajectory length as a function of r/h for various Reynolds numbers $0.2<Re\ 10^{-5}<6.1$. The values have been obtained from Schlieren photographs.*

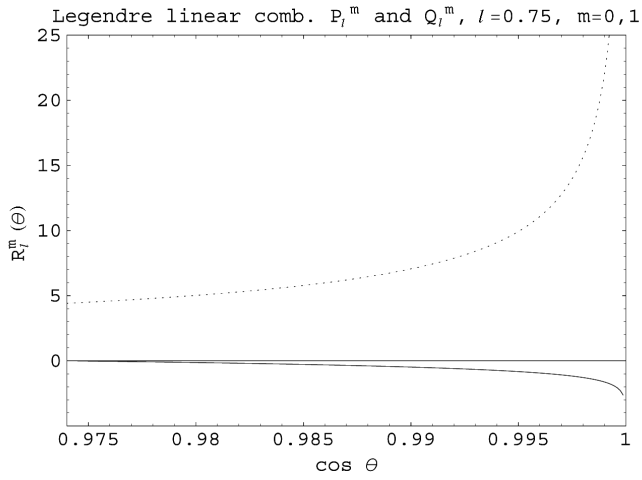

Fig. 11: *The radial functions $R_\ell^m(\theta)$, m=0,1, for angles between 0 and θ_0=13°, or 0.975<cosθ<1. The solid line is m=0.*

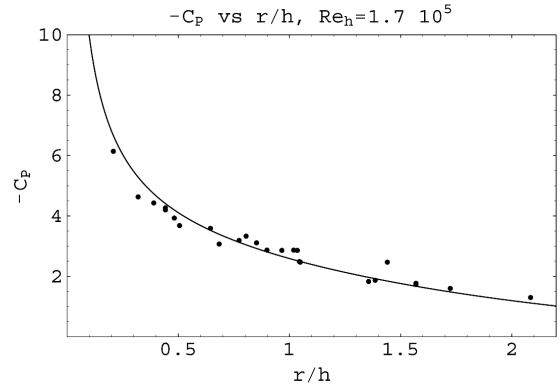

Fig. 12: *A comparison between theoretical and experimental values of -C_p as a function of r/h. The curve gives the pressure coefficient below the symmetry axis of the conical vortex at an angle of incidence equal 45°.*

II

Analytical Solution of the Navier-Stokes Equation for Internal Flows

Mats D. Lyberg and Henrik Tryggeson

Department of Physics, Växjö University, 35195 Växjö, Sweden.

E-mail: Mats.Lyberg@msi.vxu.se, htr@msi.vxu.se

Abstract. This paper derives a solution to the Navier-Stokes equation by considering vorticity generated at system boundaries. The result is an explicit expression for the velocity. The Navier-Stokes equation is reformulated as a divergence and integrated, giving a tensor equation that splits into a symmetric and a skew-symmetric part. One equation gives an algebraic system of quadratic equations involving velocity components. A system of non-linear partial differential equations is reduced to algebra. The velocity is then explicitly calculated and shown to depend on boundary conditions only. This removes the need to solve the Navier-Stokes equation by a 3-D numerical computation, replacing it by computation of 2-D surface integrals over the boundary.

PACS numbers: 47.10.-g, 47.10.A-, 47.10.ab, 47.10.ad

A major obstacle for detailed calculations of fluid flows is the time consuming 3-D calculations characteristic of solving differential equations numerically, or using integral methods involving the calculation of entire 3-D domain integrals. For the latter approach, various methods have been presented that attempt to reduce the computational task. In the boundary element method one applies potential theory to lower the dimension of the problem by one order. However, this property is lost if vorticity is considered. An extended version of the method [1], transforms local boundary conditions into global conditions integrated over the boundary. The velocity is divided into a potential and a rotational part. This leads to a system of coupled boundary integral equations to be solved iteratively. The property of the reduced dimension is preserved. Other methods, commonly applied to vibration analysis, also transforming domain integrals into boundary integrals include the dual reciprocity method [2], and the particular integrals technique [3]. The application of these latter methods is limited to small values of the Reynolds number [4, 5].

Laboratory experiments indicate the significant role played by the no-slip boundary condition in the formation of vortex filaments affecting the flow evolution. Recently, [6], detailed studies of vortex filaments in 2-D turbulent flows reveal that their influence may have dramatic effects on the flow, not only in the vicinity of the wall but extending over the full flow domain

It is a common assumption that to describe quantitatively turbulent flows in the presence of solid boundaries, it is necessary to have a quantitative model of the vorticity creation rate [7]. Based on this assumption, the boundary vorticity dynamics model has developed [8], describing the vorticity creation from solid boundaries and the reaction of the created vorticity to the boundaries. In this model, the velocity field is decomposed into two parts. One part, derived from a scalar potential, describes the longitudinal compression. The other part, derived from a vector potential, describes the transverse shearing process.

None of the methods or models listed in the previous paragraphs yields a closed expression for the velocity in the flow in terms of conditions at the system boundary. Such an expression is presented in this work. We do not a priori assume any explicit model of vorticity formation, or that the velocity field may be split into a potential and a rotational part.

From a strictly mathematical point of view, it may not be straightforward how to solve a set of non-linear partial differential equations and include boundary conditions. From a physical point of view, the situation is simpler. The Navier-Stokes equation describes the acceleration of a fluid subjected to interior forces. If the validity of the equation is extended to include also the boundary, the external pressure and viscous forces at the boundary have to be included in the equation. It then describes the acceleration in a system exposed to interior and external forces. A common procedure then is to integrate the equation. We have done just that.

The Navier-Stokes is recast in the form of a divergence that is zero, permitting immediate integration. By invoking symmetry properties, the resulting expression may

be partitioned into two equations that may be solved separately. One equation gives a linear partial differential equation for the velocity potential, permitting the calculation of a rotational part of the velocity field. The other equation reduces to a quadratic algebraic equation for components of a velocity field. These two solutions may be added, giving in closed form an expression only depending on externally applied pressure and the value of the velocity and the derivatives of the velocity at the boundary.

The flow of an incompressible fluid of velocity $\boldsymbol{u}(\boldsymbol{r},t)$ is governed by the Navier-Stokes equation (1) and by the equation of continuity (2). These equations are most often formulated as

$$\rho\partial_t\boldsymbol{u}+\rho\left(\boldsymbol{u}\cdot\nabla\right)\boldsymbol{u}\equiv\rho\partial_t\boldsymbol{u}+\rho\boldsymbol{\omega}\times\boldsymbol{u}+\frac{1}{2}\nabla\rho\boldsymbol{u}^2=-\nabla p-\mu\nabla\times\boldsymbol{\omega}\ , \tag{1}$$

$$\rho\nabla\cdot\boldsymbol{u}=Q(\boldsymbol{r}',t')\delta(\boldsymbol{r}-\boldsymbol{r}')\delta(t-t')\ . \tag{2}$$

Here, $\boldsymbol{\omega}=\nabla\times\boldsymbol{u}$ is the vorticity, p the pressure, ρ the density, μ the viscosity, and $Q(\boldsymbol{r}',t')$ the amount of fluid injected into sources or removed by sinks from the system at a specified point and time. If the vorticity is considered as a skew-symmetric tensor, $\omega^{ji}=\partial^j u^i-\partial^i u^j$, a conjugate variable is the rate of strain, σ, defined from $\sigma^{ji}=\partial^j u^i+\partial^i u^j$. The Navier-Stokes equation is the law of force where the left hand side contains the acceleration and the right hand side the forces acting in the system. The density and the viscosity will be treated as constants. It follows from Eq. (2) that the Helmholtz decomposition applies, the velocity $\boldsymbol{u}$ is uniquely defined from an rotational part $\boldsymbol{u}_{rot}$ determined by a vector potential $\boldsymbol{A}$, and a potential part $\boldsymbol{u}_{pot}$ determined by a scalar potential ϕ as

$$\boldsymbol{u}=\boldsymbol{u}_{rot}+\boldsymbol{u}_{pot}=\nabla\times\boldsymbol{A}+\nabla\phi\ . \tag{3}$$

Here, ϕ has to satisfy the Laplace equation $\Delta\phi=0$ if there are no sources and sinks. The vorticity is determined from the vector potential as $\boldsymbol{\omega}=\nabla(\nabla\cdot\boldsymbol{A})-\Delta\boldsymbol{A}$. It is possible to choose $\boldsymbol{A}$ such that $\nabla\cdot\boldsymbol{A}=0$ (see [9], for a discussion on the uniqueness of the Helmholtz decomposition).

The Eq. (1) describes the flow in a free space, but contains no information about how to take into account boundary conditions. We will integrate Eq. (1) and therefore include on its right hand side the forces acting on the fluid at the boundary. These forces include pressure applied at inlets and outlets and viscous forces at boundaries.

We rewrite Eq. (2) to describe fluid entering or leaving the system at points $\boldsymbol{r}_Q$ on the boundary

$$\rho\nabla\cdot\boldsymbol{u}(\boldsymbol{r},t)=2\Delta(\boldsymbol{r})\iint d\boldsymbol{S}_Q\cdot\boldsymbol{u}(\boldsymbol{r}_Q,t')\rho G(\boldsymbol{r}-\boldsymbol{r}_Q)\delta(t-t')\ . \tag{4}$$

The integration is over all surfaces Q of inlets and outlets where the entrance, or exit, flow velocity is $\boldsymbol{u}(\boldsymbol{r}_Q)$. Here, G is the kernel, or Green's function, $G(\boldsymbol{r})=(4\pi r)^{-1}$. As we are considering an incompressible fluid, the system responds instantaneously to any dynamical change of external pressure or the flow from sources. This justifies the use of a stationary Greens function in Eq. (4) satisfying the Laplace equation $\Delta G(\boldsymbol{r})=-\delta(\boldsymbol{r})$.

This would give a minus sign to the right hand side of Eq. (4). However, another minus sign enters because the surface element vector $d\boldsymbol{S}_Q$ points away from the system. The factor of 2 enters because when positioning point sources from Eq. (2) on a boundary surface, only half the flux will enter the system, the other half "on the other side of the wall" will contribute to the environment. We rewrite Eq. (4) as

$$\rho\partial_j u^j(\boldsymbol{r},t) - \partial_j\partial^j 2\iint d\boldsymbol{S}_Q\cdot\boldsymbol{u}(\boldsymbol{r}_Q,t')\rho G(\boldsymbol{r}-\boldsymbol{r}_Q)\delta(t-t') = 0\ . \tag{5}$$

Here, we have applied a convention, a summation is to be carried out over identical upper and lower indices. Next, we multiply this equation by the i-component of the velocity. Using simple derivation rules and applying the fact that the second term of Eq. (5) is zero except at inlets and outlets, one arrives at

$$\rho u^j\partial_j u^i = \rho\partial_j(u_j^j u^i) - \partial_j\partial^j 2\iint d\boldsymbol{S}_Q\cdot\boldsymbol{u}(\boldsymbol{r}_Q,t')u^i(\boldsymbol{r}_Q,t')\rho G(\boldsymbol{r}-\boldsymbol{r}_Q)\delta(t-t')\ . \tag{6}$$

The left hand side of Eq. (6) is identical to the second non-linear term of Eq. (1). If one performs one of the derivations of the integral of Eq. (6) and then performs a partial integration, the resulting expression will contain partial derivatives of the velocity components.

We continue by adding to the right hand side of Eq. (1) the forces acting on the system at the boundary in the form of an externally applied pressure at inlets and outlets, and viscous stress acting at the boundary. Suppose we maintain at a point $\boldsymbol{r}_Q$, belonging to an inlet or outlet, a pressure $p(\boldsymbol{r}_Q,t')$ applied in the direction $-\boldsymbol{n}_Q$ if $\boldsymbol{n}_Q$ is directed from the fluid. One should then complement Eq. (1) on the right hand side with a term $-\boldsymbol{n}_Q p(\boldsymbol{r}_Q,t')\delta(\boldsymbol{r}-\boldsymbol{r}_Q)\delta(t-t')$.

The force from viscous stress at surface element $d\boldsymbol{S}_B$ at a point $\boldsymbol{r}_B$ on the boundary is given by the term $\mu d\boldsymbol{S}_B\times[\nabla\times\boldsymbol{u}(\boldsymbol{r},t)\delta(\boldsymbol{r}-\boldsymbol{r}_B)] = \mu\nabla[\boldsymbol{u}(\boldsymbol{r},t)\delta(\boldsymbol{r}-\boldsymbol{r}_B)\cdot d\boldsymbol{S}_B] - \mu[d\boldsymbol{S}_B\cdot\nabla]\boldsymbol{u}(\boldsymbol{r},t)\delta(\boldsymbol{r}-\boldsymbol{r}_B) = \mu d\boldsymbol{S}_B\cdot\nabla\boldsymbol{u}(\boldsymbol{r},t)\delta(\boldsymbol{r}-\boldsymbol{r}_B)$, an expression defining the dynamic viscosity μ. The last equality is obtained if the boundary conditions are satisfied. Writing these two contributions to the right hand side of Eq. (1) with the help of Green's functions, one arrives at the contribution

$$\partial_j\partial^j 2\iint G(\boldsymbol{r}-\boldsymbol{r}_Q)p(\boldsymbol{r}_Q,t)d\boldsymbol{S}_Q - \mu\partial_j\partial^j 2\iint G(\boldsymbol{r}-\boldsymbol{r}_B)d\boldsymbol{S}_B\cdot\nabla\boldsymbol{u}(\boldsymbol{r}=\boldsymbol{r}_B,t)\ , \tag{7}$$

where the surface integrals are to be performed over the interior of the system boundary. One may now collect terms from Eq. (6) and (7) by defining the tensors P, S and Ω

$$P^{ji} = -2\partial^j\iint p(\boldsymbol{r}_p,t)G(\boldsymbol{r}-\boldsymbol{r}_p)dS_p^i\ , \tag{8}$$

$$R^{ji} = \partial^j\iint G(\boldsymbol{r}-\boldsymbol{r}_B)d\boldsymbol{S}_B\cdot(\mu\nabla-\rho\boldsymbol{u})u^i(\boldsymbol{r}_B,t)\ , \tag{9}$$

$$\Omega^{ji} = R^{ji} - R^{ij} = \epsilon^{ijk}\Omega_k \quad\text{and}\quad S^{ji} = R^{ji} + R^{ij}\ . \tag{10}$$

The tensor Ω is skew-symmetric and is related to the amount of vorticity transferred to the system, or generated, at boundaries. The first relation of Eq. (10) defines the vector $\mathbf{\Omega}$. The tensor S is symmetric and related to to the amount of rate of strain transferred to the system, or generated, at boundaries. The tensor P may be shown to be approximately diagonal if the pressure force as well as the bulk flow is normal to the surface, and neglects transverse pressure gradients across an inlet or outlet. In the definition of these tensors, the area of inlets and outlets has been assumed situated at the system boundary. The trace, the sum of the diagonal elements, of the tensors S and Ω, $\mathrm{tr}(S)$ and $\mathrm{tr}(\Omega)$, are zero.

Collecting all terms from the Eq. (3), (6) and (7), Eq. (1) may be rewritten for the i-component as

$$\partial_j \left[\rho\partial_t\phi\delta^{ij} + \rho\partial_t\epsilon^{ijk}A_k + \rho u^i u^j + p\delta^{ij} + \mu\epsilon^{ijk}\omega_k + \left(S^{ji} + P^{ji} + \Omega^{ji}\right)\delta(t-t')\right] = 0 \ , \quad (11)$$

where ϵ^{ijk} is the completely skew-symmetric Levi-Civita tensor. The Eq. (11) has the form of a divergence being zero. Now, as stated after Eq. (2), the disappearing of the divergence leads to the existence of potentials. Applying this result to Eq. (11) leads to an equation for a second rank tensor. The expression inside the brackets of Eq. (12) must be equal to a second rank tensor T satisfying $\partial_j T^{ij} = \partial_i T^{ij} = 0$. That equation may be split into its symmetric and skew-symmetric parts yielding the two equations

$$\rho\partial_t\phi\delta^{ij} + \left[\rho u^i u^j + p\delta^{ji} + P^{ij} + S^{ij}\right]\delta(t-t') = T^{ij} \ , \quad (12)$$

$$\epsilon^{ijk}\rho\partial_t A_k - \mu\epsilon^{ijk}\Delta A_k + \Omega^{ji}\delta(t-t') = \epsilon^{ijk}B_k \ , \quad (13)$$

where T is an arbitrary symmetric tensor and $\boldsymbol{B}$ an arbitrary irrotational vector. Lowering one index and contracting Eq. (12) gives the relation

$$\partial_t\rho\phi D + \rho\boldsymbol{u}^2 + pD + \mathrm{tr}(P) = \mathrm{tr}(T) \ , \quad (14)$$

where D is the space dimension of the system. This equation is employed to calculate the pressure in the flow. It remains to treat the case of the non-diagonal elements of Eq. (12), that is the case $i \neq j$, and the Eq. (13).

The off-diagonal part of Eq. (12) now reads

$$\rho u^i u^j + P^{ij} + S^{ij} = T^{ij} \ , \quad (15)$$

which yields a non-linear, but purely algebraic, equation for the velocity components. This equation has the solution $\boldsymbol{U}$ with components

$$U^i(\boldsymbol{r},t) = \pm\sqrt{\frac{\Sigma^{ij}\Sigma^{ik}}{\Sigma^{jk}}} \ , \quad (16)$$

where $\Sigma^{nm} = \frac{(-P^{nm}-S^{nm}+T^{nm})}{\rho}$ with $i \neq j \neq k$. This velocity is, in general, not irrotational.

Eq. (13) is a linear differential equation for the vector potential $\boldsymbol{A}$. To solve this equation, employ the integral kernel of the diffusion equation, $K(\boldsymbol{r},t)$, given in the form

$$(\mu\Delta - \rho\partial_t)K(\boldsymbol{r},t) = -\delta(\boldsymbol{r})\delta(\mu t) \quad \Rightarrow \quad K(\boldsymbol{r},t) = \frac{\exp\left(-\frac{\boldsymbol{r}^2}{4\nu t}\right)}{(4\pi\nu t)^{\frac{D}{2}}} \ , \tag{17}$$

where D is the space dimension and $\nu = \frac{\mu}{\rho}$ is the kinematic viscosity. Multiplied by a unit vector, K defines a solenoidal vector potential. Vortex models derived from this kind of potential have been shown to account for the decay of vortex singlets generated in a tank [10]. Models of vortex doublets derived from this kind of vector potential reproduce the energy spectrum of 2-D turbulent flows generated in the laboratory [11].

The solution of Eq. (13) then reads

$$\begin{aligned}
&\boldsymbol{A}(\boldsymbol{r},t) = \int_0^t \nu dt' \iiint d^3x' K(\boldsymbol{r}-\boldsymbol{r}',t-t')\left[\boldsymbol{\Omega}(\boldsymbol{r}',t') - \boldsymbol{B}(\boldsymbol{r}',t')\right] = \\
&\nabla \times \int_0^t \nu dt' \iint \Gamma\left(\boldsymbol{r}-\boldsymbol{r}_B,t-t'\right) d\boldsymbol{S}_B \cdot \nabla \boldsymbol{u}(\boldsymbol{r}=\boldsymbol{r}_B,t') \\
&- \int_0^t \nu dt' \iiint d^3x' K\left(\boldsymbol{r}-\boldsymbol{r}',t-t'\right)\boldsymbol{B}(\boldsymbol{r}',t') \ .
\end{aligned} \tag{18}$$

The second equality is obtained after integration over all space and using the fact that the velocity is zero on the boundary. Thus, the vector potential describes vorticity generated at solid boundaries as well as that contained in fluid entering or leaving the system.

The function Γ is a solution to $\Delta(\boldsymbol{r})\Gamma(\boldsymbol{r}-\boldsymbol{r}_B,t) = -K(\boldsymbol{r}-\boldsymbol{r}_B,t)$, and is given by $\Gamma(\boldsymbol{r},t) = G(r)\mathrm{erf}\left(\frac{r}{\sqrt{4\nu t}}\right)$, where erf is the error function.

The rotational contribution to the internal velocity field from vorticity created at the boundary, $\boldsymbol{V}$, may now be determined by taking the rotation of the vector potential of Eq. (18)

$$\begin{aligned}
&\boldsymbol{V}(\boldsymbol{r},t) = \int_0^t \nu dt' \Bigg[\iint K(\boldsymbol{r}-\boldsymbol{r}_B,t-t') d\boldsymbol{S}_B \cdot \nabla(\boldsymbol{r}_B)\boldsymbol{u}(\boldsymbol{r}_B,t') \\
&-\nabla \times \iiint d^3x' K\left(\boldsymbol{r}-\boldsymbol{r}',t-t'\right)\boldsymbol{B}(\boldsymbol{r}',t')\Bigg] \ .
\end{aligned} \tag{19}$$

This velocity field defines a rotational part of the velocity in terms of the externally applied pressure and the value of the velocity and derivatives of the velocity at boundary points.

To compute the velocity field from Eq. (16) and (19), one needs information about the velocity and velocity gradients at the boundary. One way to obtain this information is to find a solution to the equation of continuity, Eq. (2) satisfying the no-slip boundary conditions, the velocity at the boundary must be zero. One may proceed as follows. The bulk flow between inlets and outlets in an infinite space is given by the velocity field

$$\boldsymbol{v}_Q(\boldsymbol{r},t) = 2\iint d\boldsymbol{S}_Q \cdot \nabla(\boldsymbol{r})G(\boldsymbol{r}-\boldsymbol{r}_Q)\boldsymbol{v}(\boldsymbol{r}_Q,t) \ . \tag{20}$$

Here, we have employed a relation of the following kind. Suppose $F(x, y, z)$ is a function defined in a 3-D space. Then, if one approaches the plane $z = 0$ in a direction normal to a point $(x, y, 0)$,

$$\lim_{z\to\pm 0} \partial_z \iint G(x - x', y - y', z)F(x', y')\, dx'dy' = \mp\frac{F(x, y)}{2} \ . \tag{21}$$

On the boundary, the velocity normal to the surface, $\boldsymbol{v}_n$, and the tangential velocity, $\boldsymbol{v}_t$, are given by $\boldsymbol{v}_n(\boldsymbol{r}_B, t) = \boldsymbol{n}_B\,(\boldsymbol{n}_B \cdot \boldsymbol{v}_Q(\boldsymbol{r}_B, t))$ and $\boldsymbol{v}_t(\boldsymbol{r}_B, t) = \boldsymbol{v}(\boldsymbol{r}_B, t) - \boldsymbol{n}_B\,(\boldsymbol{n}_B \cdot \boldsymbol{v}_Q(\boldsymbol{r}_B, t))$, respectively. Here, $\boldsymbol{n}_B$ is a unit vector normal to the boundary surface at $\boldsymbol{r}_B$ oriented in a direction from the fluid. One may now modify Eq. (20) to get a velocity field satisfying the boundary conditions by subtracting the normal and tangential by using the integral kernels G and K,

$$\begin{aligned}\boldsymbol{v}(\boldsymbol{r}, t) = \boldsymbol{v}_Q(\boldsymbol{r}, t) - 2\iint d\boldsymbol{S}_B \cdot \nabla(\boldsymbol{r})G(\boldsymbol{r} - \boldsymbol{r}_B)\boldsymbol{v}_n(\boldsymbol{r}_B, t) \\ -2\int_0^t \nu dt' \iint d\boldsymbol{S}_B \cdot \nabla(\boldsymbol{r})K(\boldsymbol{r} - \boldsymbol{r}_B, t - t')\boldsymbol{v}_t(\boldsymbol{r}_B, t') \ .\end{aligned} \tag{22}$$

The velocity field $\boldsymbol{v}$ here describes the bulk flow and the rotational part of the velocity field created at boundaries. One may note that the last term of Eq. (22) is twice the expression of Eq. (19) if one identifies the velocities of the integrands. A factor of two is due to the split of the tensor R into symmetric and skew-symmetric tensors, Ω and S. The expression of Eq. (19) may now be determined from the last term of Eq. (22) that is, from information based on the equation of continuity and the location of boundaries, inlets and outlets.

The part of the velocity field that may still be lacking is the one stemming from vortex doublet formation, two counter-rotating vortex singlets, as observed in pipe flow subjected to an external disturbance [12] or in vortex rings just before transition towards turbulence [13]. No net vorticity can be created in the interior, but nothing prevents the formation of vortex doublets in a shearing flow. This may be coupled to another feature of the Navier-Stokes equation. It is a partial differential equation of the parabolic type, containing only single derivative terms with respect to time. Information then travels with an infinite speed, possible only in a newtonian universe equipped with an absolute and universal time. To describe turbulent features caused by local pressure fluctuations, the flow equations should be complemented by terms containing second derivatives with respect to time, in effect transforming them to wave equations.

It has been demonstrated that the flow equations by integration may be reduced to one linear partial differential equation and one algebraic equation quadratic in the velocity. This permits the computation of the velocity field and the pressure in the flow in terms of the externally applied pressure and the value of the velocity and velocity gradients at boundary points.

References

[1] Machane R, Achard J and Canot E 2000 *Int. J. Num. Meth. in Fluids* **34** 47
[2] Nardini D and Brebbia C A 1982 *Boundary Element Methods in Engineering* (Southampton, C.A. Brebbia, Computational Mechanics Publ.) 157–171
[3] Ahmad S and Banerjee P K 1986 *J. of the Eng. and Mech. Div.* ASCE **112** 682
[4] Zheng R, Phan-Thien N and Coleman J 1991 *Comp. Mech.* **8** 71
[5] Power H and Patridge P W 1994 *Int. J. Num. Meth. Eng.* **37** 1825
[6] van Heijst G J F, Clercx H J H and Molenar D 2006 *J. Fluid. Mech.* **554** 411
[7] Lighthill M J 1963 *Boundary Layer Theory* (Oxford, Oxford Univ. Press) 46–113
[8] Wu J Z and Wu J M 1998 *Theor. Comp. Fluid Dyn.* **10** 459
[9] Dassios G and Lindell I V 2002 *J. Phys. A* **35** 5139
[10] Trieling R R and van Heijst G J F 1998 *Fluid Dynamics Res.* **23** 27
[11] Tryggeson H and Lyberg M D 2007 submitted to *Phys. Rev. Lett.*
[12] Hof B, van Doorne C W H, Westerweel J and Nieuwstadt F T M 2005 *Phys. Rev. Lett.* **95** 214502
[13] Dazin A, Dupont P and Stanislas M 2006 *Exp. in Fluids* **41** 401

III

Vortex Evolution in 2-D Fluid Flows

Henrik Tryggeson and Mats D. Lyberg

Department of Physics, Växjö University, 35195 Växjö, Sweden

(Dated: February 22, 2007)

Abstract

Evolving 2-D turbulence is dominated by vortex structures. Experimental study of this phenomenon is difficult, but some methods yield information on the dynamics of 2-D vortices. Available data include information on the structure of the velocity field, the growth rate and decay rate of vortex structures, and energy spectra. It is proposed that all these features from different experimental environments may be described by singlet or doublet vortex structures derived from one unique vector potential. Predicted properties are confronted with experimental observations on forced and decaying 2-D vortex systems.

PACS numbers: 47.32.C-, 47.27.-i

How turbulence arises and what role the creation and diffusion of vorticity plays in this process is not well understood, neither in outline nor in detail. Any progress towards an understanding of the fundamentals involved could be of great practical interest, for example, for applications in astrophysics and geophysics. 2-D vortices have been observed in nature, such as high and low pressure cells in the atmosphere, and oceanic eddies. The formation of vortices is experimentally established as a distinct property of 2-D turbulent flows. The mutual advection of well-separated vortices and the merger of like-sign vortices are characteristic features.

Two common ways of experimentally generating quasi-2D turbulence are generation in a thin layer of fluid and generation in a rapidly flowing soap film. In the first case a rotational motion is induced by inserting a rotating solid object, or by introducing fluid jets. In the other flow one may introduce comb-like structures into the fluid and vorticity is generated at the boundary. For a review of experimental methods and results, see Ref. [1, 2].

Generation of vortex singlets in a tank within a layer of a stratified fluid yields vortex structures that are not exact 2-D objects, but rather flat, pancake-like structures [3]. The presence of solid boundaries act as sources of vortex filaments that by entering the flow may significantly affect the flow evolution [4].

Another way of creating rotational flow is by electromagnetically driving flows in thin, stable stratified layers [5, 6]. The flow is generated in a square cell by placing permanent magnets at the bottom below an electrically conducting fluid and applying a voltage across the fluid. In order to ensure two dimensionality, the cell is filled with layers of NaCl solutions with different densities. The interaction of an electric current driven across the cell with the magnetic field produces local stirring forces. It is possible to obtain data on the decay of 2-D vortices [5], the size and growth of and distance between vortex structures [7], as well as energy spectra [8]. With this experimental set-up, friction with the bottom may affect observations [6].

An alternative experimental approach is the use of flowing soap films [9]. Combs are positioned in the flow, or at the boundaries of the flow, of a soap film falling vertically between two wires under the influence of gravity. The teeth of the comb perpetually generate small vortices, which are then quickly swept into the center of the channel by larger vortices. The velocity fluctuations appear in the plane of the film, which has a thickness of μm, whereas the radius r of eddies produced by the combs range from sub-mm to mm. A forced,

steady turbulent state ensues. Downstream from the forcing section of the channel, the turbulence decays freely. Data on scaling effects [10] and energy spectra [11] have been obtained.

The two equations governing the flow $\boldsymbol{u}(\boldsymbol{r},t)$ of an incompressible fluid are the Navier-Stokes equation and the equation of continuity

$$\partial_t \boldsymbol{u} + (\boldsymbol{u}\cdot\nabla)\,\boldsymbol{u} = -\rho^{-1}\nabla p + \nu\nabla^2\boldsymbol{u}\ , \tag{1}$$

$$\nabla\cdot\boldsymbol{u} = 0\ . \tag{2}$$

Here, $\boldsymbol{\omega} = \nabla\times\boldsymbol{u}$ is the vorticity, p the pressure, ρ the density, ν the kinematic viscosity. To eliminate the pressure, take the rotation of Eq. (1). One then arrives at the vorticity transport equation that may be cast in the form

$$\partial_t\boldsymbol{\omega} + \boldsymbol{u}\times\Delta\boldsymbol{u} - (\nabla_u - \nabla_\omega)\,(\boldsymbol{u}\cdot\boldsymbol{\omega}) = \nu\nabla^2\boldsymbol{\omega}\ , \tag{3}$$

where the symbol ∇_u indicates that the derivatives of the nabla operator are to be applied to the components of $\boldsymbol{u}(\boldsymbol{r},t)$ only. In 2-D flows, the velocity is perpendicular to the vorticity, so $\boldsymbol{u}\cdot\boldsymbol{\omega} = 0$. We will restrict treatment to cases such that the remaining non-linear term of Eq. (3) is either exactly zero, or can be shown to be so small that it may be neglected. The equation then takes the form of the diffusion equation. The solutions may be derived from a solenoidal vector potential $\boldsymbol{A}(\boldsymbol{r},t)$. We have applied the vector potential

$$\boldsymbol{A}(\boldsymbol{r},t) = A(r,\theta,t)\boldsymbol{e} = \frac{r^n\cos n\theta}{(\nu t)^\beta}F(\xi)\boldsymbol{e}\ , \tag{4}$$

where $\xi = \frac{r}{\sqrt{\nu t}}$ and n is an integer giving the order of the vortex multiplet, $\boldsymbol{e}$ is a unit vector, β is a parameter characterizing the dynamic behaviour, F is a function of the diffusive variable ξ. It remains to determine the function F. The velocity is given by the rotation of this vector potential, and the vorticity is obtained by applying the Laplace operator to the vector potential, $\boldsymbol{\omega} = -\Delta\boldsymbol{A}$. Similar vortex models have been shown to account for the decay of vortex singlets generated in a tank [3].

Inserting the vorticity as described above, into Eq. (3) gives one solution

$$F(\xi) = \sum_j \left(\xi^2\right)^j \frac{\Gamma\left(\frac{n}{2}+j-\beta\right)}{(n+j)!j!}\ , \tag{5}$$

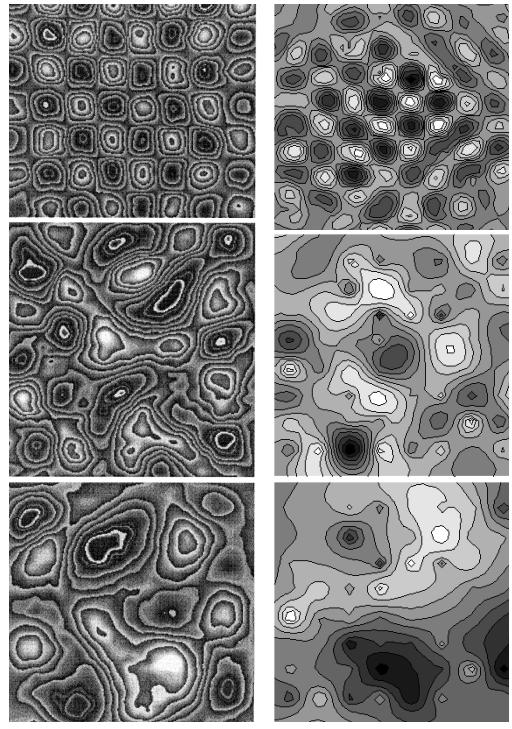

FIG. 1: Examples of calculated vorticity fields, showing the evolution of the flow from large number of small vortices, to a smaller number of larger vortices. To the left are experimentally observed evolution in [7] and to the right corresponding vorticity field given by theory. Theoretical calculations are based on vortex singlets derived from the vector potential Eq. (4). Reprinted figure with permission from [A. E. Hansen, D. Marteau and P. Tabeling, Phys. Rev. E **58**, 7261 (1998)]. Copyright (2006) by the American Physical Society.

containing three parameters, the order of the vortex multiplet n, the dynamic behavior as a power of time, β, and the lower summation index. For example, $n = 0$ gives a monopole or singlet and $n = 1$ gives a dipole or doublet. The solution presented in Eq. (5) is an even function of the variable ξ. There is, also, a similar solution odd in this variable.

To determine what representatives of this large class of vortex solutions occur in laboratory experiments, observations from some well executed experiments should be analyzed in terms of the above solution. One feature found in more than one kind of experiment is that

the energy spectral function $E(k)$, where k is the wave number, shows a $E(k) \sim k^{-3}$ behavior at least in the wave number range between 1 and 30 cm^{-1} [8, 11]. We investigate what are the conditions for velocity fields derived from the vector potential Eq. (4) to reproduce such a behavior.

The energy spectral function $E(k)$ is defined from the relation

$$2\pi k E(k) = \int_0^\infty r\, dr \int_0^{2\pi} \boldsymbol{u}^2\,(r,t)\, e^{ikr\cos\theta}\, d\theta\ . \tag{6}$$

The velocity squared derived from Eq. (4) produces terms with the angular dependence $\sin^2 n\theta$ and $\cos^2 n\theta$. Carrying out the angle integration of Eq. (6) yields terms with Bessel functions $J_{2n}(kr)$ and $J_0(kr)$. It remains to carry out the integration over r. Obviously, the velocity squared can only produce even powers of r, for example a power of $2M$. Introducing some coefficients $C(n,\beta,M)$, which may be calculated from Eq. (4), Eq. (6) may now be written

$$\begin{aligned} E(k) &= \int_0^\infty r dr \sum_M C(n,\beta,M) r^{2n-2+2M} t^{-M} \left[c_1 J_{2n}(kr) + c_2 J_0(kr)\right] \\ &= \sum_M C(n,\beta,M) k^{-3-2M}\ t^{-M} \left[c_1 \frac{2^{2n}(n+M)!}{\Gamma(n-M)} + c_2 \frac{M!}{\Gamma(-M)}\right]\ . \end{aligned} \tag{7}$$

The singularity of the Γ-function at zero and negative integers means that the contribution from vortex singlets is zero. Vortex multipoles, $n > 0$, produce the desired behavior but only for $M = 0$. Contributions from terms with powers of r greater than 0 fall off as powers of k larger than 3. Also, such terms disappear more quickly with time. Information on the rate of fall-off with time is required to determine the value of the parameter β.

We start comparison to experimental data by considering vorticity generated in layered media. In one experiment [7] vortices have been generated an 8×8 array of a bounded 2-D space, with nearest neighbors counter-rotating. It is then possible to follow the diffusion of vorticity at different times and the qualitative evolution of the flow from a large number of small vortices to a small number of large vortices. To reproduce the patterns of this evolving flow field, we carried out a simulation by placing a number of vortex singlets in the same manner as used in the experiment. We used vortex singlets derived from the vector potential Eq. (4) with a simple vortex singlet, putting $n = 0$ and $\beta = -\frac{1}{2}$. Two counter-rotating vortex singlets of this kind produce the vortex dipole $n = 1$ and $\beta = 0$.

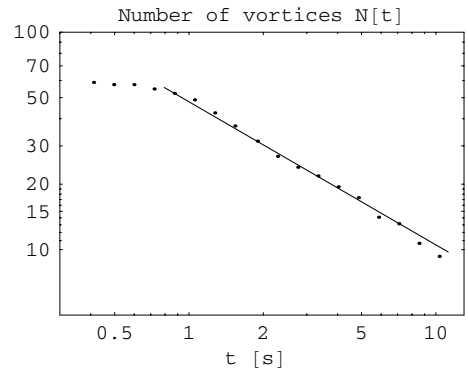

FIG. 2: Time evolution of the number of vortices in a fixed area of a layered medium. This number is proportional to the density of vortices. Solid line: $t^{-0.66}$ from simulation with vortex singlets derived from the vector potential Eq. (4). Experimental data are from Ref. [7].

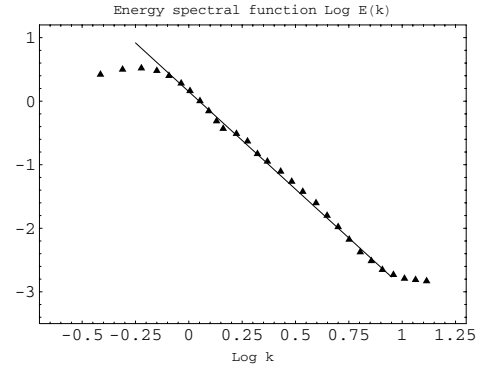

FIG. 3: Energy spectrum of the velocity field in a layered medium in a statistically stationary state. The solid line corresponds to our doublet solution. Experimental data are from Ref. [8]. The full drawn line represents a theoretical calculation based on vortex doublets derived from the vector potential Eq. (4).

The vortices have been assigned strength according to the assumption that this strength follows a normal distribution with zero mean (the sign of the vortex strength depends on the sense of rotation).

In Fig. 1, to the left, an experimentally observed evolution of a velocity field in a stratified system is shown, for details see [7]. Also in Fig. 1, but to the right, is the simulated flow

field described above. Visually, the patterns are similar. Turning to a more quantitative comparison, the number of vortices is reduced with time while their average size grows. A best fit to the vortex density $\rho(t)$ and the average vortex radius $a(t)$ obtained from the simulation gives

$$\rho(t) \sim t^{-0.66\pm0.10}, \quad a(t) \sim t^{0.30\pm0.10} \ . \tag{8}$$

The exponents determined here, -0.66 ± 0.10 for the density of vortices and 0.30 ± 0.10 for the vortex radius should be compared to those obtained experimentally in a stratified flow field [7], -0.70 ± 0.10 and 0.21 ± 0.06, respectively. Thus, there is a good agreement between experiment and theory when it regards describing the pattern of the most prominent vortex singlets. The result of this simulation is presented in Fig. 2.

Vortex singlets do not give any contribution to the energy spectrum, as noted above. This argument was based on the assumption that the vortex singlet was situated in an infinite space. As seen in Fig. 1, the vortex singlets there are rather local, and should not be expected to be of any strength outside a limited region. Therefore, there contribution to the energy spectrum may probably be neglected. In Fig 3, the experimental values of the energy spectra of a stratified system [8] are presented together with the contribution from a vortex doublet $n = 1$, $\beta = 0$, the vortex doublet derived from vortex singlets discussed in the previous two paragraphs. The vortex solution predicts quite well the slope of the experimentally statistically stationary turbulent state. For wave numbers smaller than 1 cm^{-1}, the energy spectral density is experimentally found to be flat, maybe reflecting a limitation in resolving experimentally low velocity levels at small scales [8].

One may conclude that interference between strong counter-rotating vortex singlets leads to an energy spectral function dominated by contributions from vortex dipoles.

We now turn to a discussion of results using the experimental technique a flowing soap film between partially cambered walls [11]. Regard the velocity profile as being produced by vortices. We assume that the vorticity generated at the edges of the channel decays while being carried downstream, but this is compensated for by new vorticity generated along the boundaries. With this view, the vorticity at a station should consist of vortices generated since the onset of the flow. A schematic picture presenting the above argument is given in Fig. 4. One would expect that in the absence of combs, the velocity profile would be parabolic, as for plane Poiseuille flow, generated by vortex doublets of the same kind as when

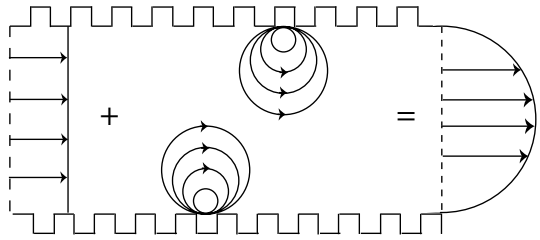

FIG. 4: Schematic picture of the assumed constituents of the flow field in a channel with combed walls. The stationary part of the flow is assumed to consist of a uniform flow represented by the arrows to the left. Vorticity is created by the combs at the boundary of system of the falling soap film. Vortex structures created at the boundary and leaving the boundary, entering the bulk flow, are assumed to be described by vortex doublets. Vortices of this structure build up a parabolic velocity profile if constantly created in the absence of combs, and the combined flow satisfies the no-slip boundary condition.

combs are present, but much weaker. The vorticity must be described as vortex doublets in order that no-slip boundary conditions are satisfied. To arrive at a parabolic profile, built up by vortex contributions from different times and the stationary uniform velocity component, one should have for the flow in the x-direction

$$u_x = \int u_\theta \left(\theta = \frac{\pi}{2}, t\right) \, dt = 1 - y^2 \ . \tag{9}$$

We apply the same vortex doublet that was used in the analysis of the layered media. Analysis of the solution gives us some predictions for the energy spectral function $E(k)$ obtained at different times t:

1. the energy spectral function $E(k)$, as a function of k, scales with $k\sqrt{\nu t}$,
2. it has an amplitude that is proportional to νt, and
3. it decays with wave number k as $E(k) \sim k^{-3}$.

In Fig. 5, the experimental energy spectra for different positions downstream from the combs are presented. This can be compered with the scaled values given in Fig. 6. For the dominant term we find the slope $E(k) \sim k^{-3}$ which is also dispayed in Fig. 5. This

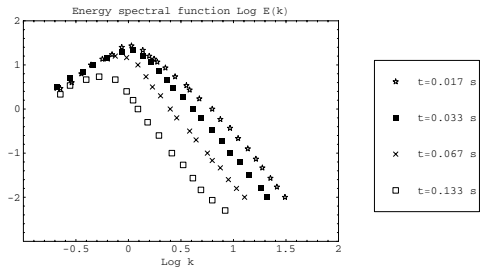

FIG. 5: Turbulent energy spectra at different positions downstream from the combs given in Ref. [11]. Relative distances to the end of the combs are 5 cm, 10 cm, 20 cm and 40 cm, respectively. This corresponds to the different times displayed in the figure.

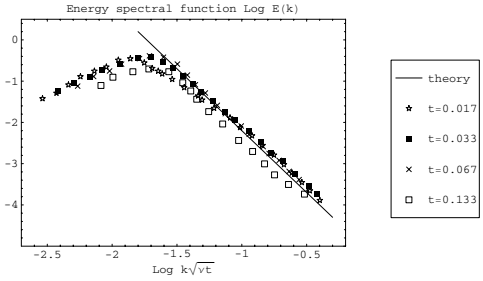

FIG. 6: Turbulent energy spectra at the same positions as in Fig. 5, but now the wave number k has been scaled by a factor $\sqrt{\nu t}$ and the amplitude divided by a factor νt as predicted by theory, creating a universal curve. The solid line represents the predicted energy spectral function from a vortex doublet discussed in the text having a slope $E(k) \sim k^{-3}$.

reproduces the experimental data in [11] for both the scaling and the slope of the energy spectra.

To conclude, the main result of this work is the theoretical prediction of the experimentally observed vortex diffusion process in 2-D stratified systems and channel flow. The model applied reproduces experimentally observed energy spectra from experiments on 2-D turbulent stratified systems and soap-films. This supports the conjecture that the turbulent flow field, as far as regards the calculation of the energy spectral function, for the case of forcing vortex singlets into a layered medium, may be viewed as consisting of isolated vortex singlets

creating vortex doublets when interfering. For the case of channel flow vortex doublets are created at the system boundary and quickly swept into the main stream by larger vortices.

[1] P. Tabeling, Phys. Rep. **362**, 1 (2002).

[2] H. Kellay and W. I. Goldburg, Rep. on Progr. in Phys. **65**, 845 (2002).

[3] R. R. Trieling and G. J. F. van Heijst, Fluid Dynamics Res. **23**, 27 (1998).

[4] G. J. F. van Heijst, H. J. H. Clercx and D. Molenaar, J. Fluid Mech. **554**, 411 (2006).

[5] O. Cardoso, D. Marteau and P. Tabeling, Phys. Rev. E **49**, 454 (1994).

[6] S. V. Danilov, V. A. Dovzhenko, F. V. Dolzhanskii and V. G. Kochina, J. Exp. Theor. Physics **95**, 48 (2002).

[7] A. E. Hansen, D. Marteau and P. Tabeling, Phys. Rev. E **58**, 7261 (1998).

[8] J. Paret, M-C. Jullien and P. Tabeling, Phys. Rev. Lett. **83**, 3418 (1999).

[9] H. Kellay, X-I. Wu and W. I. Goldburg, Phys. Rev. Lett. **74**, 3975 (1995).

[10] M. A. Rutgers, X-I. Wu, R. Bhagavatula, A. A. Petersen and W. I. Goldburg, Phys. Fluids **8**, 2847 (1996).

[11] M. A. Rutgers, Phys. Rev. Lett. **81**, 2244 (1998).

IV

Analysis of 3-D Vortex Structures in Fluids

Mats D. Lyberg and Henrik Tryggeson

Department of Physics, Växjö University, 35195 Växjö, Sweden

(Dated: February 22, 2007)

Abstract

Suppose that a vortex structure is created in the laboratory. Then, what analytical tools are available to analyze experimental data? This is the problem treated in this paper. The answer is arrived at by first finding a single-vortex solution to the flow equations, a solution that has analytical properties such that the non-linear terms in the flow equations are exactly zero. Non-linear terms removed, it is possible to apply the superposition principle to construct the velocity and vorticity of the flow field. Derived solutions are compared to some recent observations of turbulence structures.

PACS numbers: 47.27.-i, 47.37.+b

How turbulence arises and what role the creation and diffusion of vorticity plays in this process is not well understood in outline or in detail. Any progress towards an understanding of the fundamentals involved could be of great practical interest, for example, having a turbulent flow in oil and gas pipelines is not the most economical way of transporting the fuel.

The instability, reconnection, merging and breakdown of concentrated vortex structures are at the origin of intermittence in turbulent energy dissipation. Most flows are composed of vortex structures. It is nice if one can isolate a single vortex to study it, but this is difficult to achieve experimentally. However, some methods are available. Introducing disturbances into a laminar pipe flow may produce isolated vortex structures. Pushing fluid throughout a tube may generate a vortex ring where other vortex structures may appear. By sucking fluid from a flow through two opposing slots in parallel walls, a vortex may be stretched.

One method to produce vortex structures may be regarded as a large syringe that pulls water at a fixed mass flux along a precision bore tube [1, 2]. By injecting a pulsed jet of fluid tangentially into the flow, a disturbance is created. Initially, the perturbation amplitude grows linearly. Having reached a sufficient size, secondary instabilities appear due to non-linear effects [3]. Travelling vortex structures then appear at Reynolds numbers close to those typical of transition from laminar to turbulent flow in pipe flow.

Typically, these vortex structures may consist of wavy streaks, local anomalies in the stream-wise velocity, sandwiched between counter-rotating stream-wise vortices [4]. Waves travel with the fluid at a velocity slightly larger than the bulk flow but slower than the maximum laminar flow speed possible at the same volume flow. The vortex structure is reminiscent of that of vortex structures found in turbulent flows in the presence of solid boundaries. The length of the traveling structures is about twice their width.

Often several structures coexist by traveling together at the same distance from the pipe axis, evenly distributed around the axis. A twofold up to six-fold symmetry has been observed. The vortex structure transports slower fluid close to the wall towards the pipe axis, and fast fluid from the pipe center towards the wall. While low-speed central streaks exhibit a strong oscillating behavior, near wall streaks remain fairly stationary, while span-wise motions are much weaker [5].

Configurations of symmetrically positioned vortex structures appear, also, in unstable vortex rings [6, 7]. Pushing water through a cylindrical pipe creates a vortex ring. A

perturbation is amplified by a straining field near the vortex core. The perturbation initially grows linearly [6], at a later stage non-linear effects appear [7].

In the upstream part of the vortex, the instability starts with a deformation of the concentric circles of the ring. A pattern of vortex structures appears, vortices distributed in a symmetric fashion in the ring cross section. Visually, they look much like the symmetric patterns observed in the case of the pipe flow. Streamlines form, starting from the torus center, arriving at the periphery they turn back. Thus, there is an exchange of matter between the central torus and the periphery.

The study of vortex dynamics such as vortex stretching requires the formation of vortices in an environment where the elongation of the vortex is favored. A fluid flows in a laminar fashion in a channel of rectangular cross section. Boundary layers form on the four sides. Fluid is sucked out through slots situated on opposite walls [8]. Vorticity from the boundary layers is stretched by the suction. The stretching is in the same direction as the original vorticity. Initially, the vortex rolls up as a logarithmic spiral as expected from theory [9], before the stretching enhances the vorticity. The main stretching is in the core of the vortex [10].

The flow of an incompressible fluid of velocity $\boldsymbol{u}(\boldsymbol{r},t)$ is governed by the Navier-Stokes equation and by the equation of continuity. These equations read

$$\rho\partial_t\boldsymbol{u} + \rho\left(\boldsymbol{u}\cdot\nabla\right)\boldsymbol{u} \equiv \rho\partial_t\boldsymbol{u} + \rho\boldsymbol{\omega}\times\boldsymbol{u} + \frac{1}{2}\nabla\rho\boldsymbol{u}^2 = -\nabla p - \mu\nabla\times\boldsymbol{\omega}\ , \tag{1}$$

$$\rho\nabla\cdot\boldsymbol{u} = Q(\boldsymbol{r}',t')\delta(\boldsymbol{r}-\boldsymbol{r}')\delta(t-t')\ . \tag{2}$$

Here, $\boldsymbol{\omega} = \nabla\times\boldsymbol{u}$ is the vorticity, p the pressure, ρ the density, μ viscosity, and $Q(\boldsymbol{r}',t')$ the amount of fluid injected from sources or removed by sinks from the system at a specified point and time. The density and the viscosity will be treated as constants.

Taking the rotation of Eq. (1), the gradient term disappears, leaving the vorticity transport equation

$$\partial_t\boldsymbol{\omega} + \boldsymbol{u}\times\Delta\boldsymbol{u} - \left(\nabla_u - \nabla_\omega\right)\left(\boldsymbol{u}\cdot\boldsymbol{\omega}\right) = \nu\nabla^2\boldsymbol{\omega}\ , \tag{3}$$

where the symbol ∇_u indicates that the derivatives of the nabla operator are to be applied to the components of $\boldsymbol{u}$ only. It follows from Eq. (2) that the Helmholtz decomposition

applies, the velocity $\boldsymbol{u}$ is uniquely defined from an rotational part $\boldsymbol{u}_{rot}$ determined by a vector potential $\boldsymbol{A}$, and a potential part $\boldsymbol{u}_{pot}$ determined by a scalar potential ϕ as

$$\boldsymbol{u} = \boldsymbol{u}_{rot} + \boldsymbol{u}_{pot} = \nabla \times \boldsymbol{A} + \nabla\phi \ . \tag{4}$$

The vorticity is determined from the vector potential as $\boldsymbol{\omega} = \nabla(\nabla \cdot \boldsymbol{A}) - \Delta\boldsymbol{A}$. It is possible to choose $\boldsymbol{A}$ such that $\nabla \cdot \boldsymbol{A} = 0$.

To analyze experimentally observed vortex structures as those described above, one needs to find solutions of the flow equations representing them. A particular kind of simple solutions is the one where non-linear terms are explicitly zero due to properties of the solution. In finding solutions of this kind, one may be guided by the observation that non-linear terms disappear from the vorticity equation if:

1. the velocity is parallel to the vorticity, as seen from Eq. (1), or
2. the velocity is orthogonal to the vorticity and $\Delta\boldsymbol{u}$ is parallel to $\boldsymbol{u}$, as seen from Eq. (3).

The vorticity then satisfies the vector Helmholtz equation $\partial_t\boldsymbol{\omega} = \nu\Delta\boldsymbol{\omega}$.

The vortex structures observed in pipe flow, as described above, are elongated, rounded objects including vortex multipoles of finite length. This suggests finding solutions using spherical, or possibly ellipsoidal, coordinates. Consider the vector potential $\boldsymbol{V}$ describing a vortex centered at the point $\boldsymbol{r}_0$ and having a symmetry axis in the direction of $\boldsymbol{n}$

$$\boldsymbol{V}(\boldsymbol{r}, t, \boldsymbol{r}_0 = 0, \boldsymbol{n} = \boldsymbol{e}_z, l) = e^{-\frac{\nu t}{R^2}} \left[\boldsymbol{e}_r \frac{l(l+1)R}{r} j_l\left(\frac{r}{R}\right) P_l^0(\theta) \right.$$

$$\left. + \boldsymbol{e}_\theta \left(j_{l-1}\left(\frac{r}{R}\right) - \frac{lR}{r} j_l\left(\frac{r}{R}\right) \right) P_l^1(\theta) + \boldsymbol{e}_\phi j_l\left(\frac{r}{R}\right) P_l^1(\theta) \right]. \tag{5}$$

Here, R gives the length scale, j_l is a spherical Bessel function of index l, P_l^m an associated Legendre function but with magnetic number m restricted to $m = 0$ or 1. The velocity and vorticity fields derived from this vector potential possess the property that the velocity and the vorticity are parallel, $\boldsymbol{u} = \frac{\boldsymbol{V}}{R}$, $\boldsymbol{\omega} = \frac{\boldsymbol{u}}{R}$ etc. Thus, this vector potential defines an exact solution to the non-linear vorticity transport equation. Furthermore, any superposition of vortices of this kind, with the same length scale, centered at any points and with symmetry axes in any directions, also constitutes an exact solution to the vorticity equation. Some

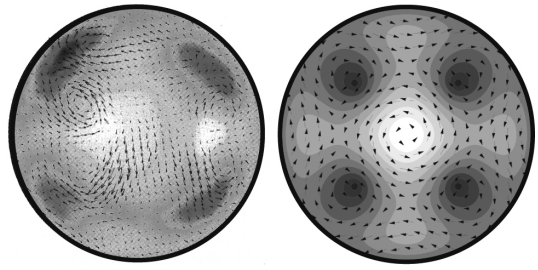

FIG. 1: Comparison of experimentally (left) and theoretically (right) observed streak patterns. Velocity components in the plane are indicated by arrows, the downstream component is indicated by color coding, where black and white signifies velocities faster or slower than the parabolic profile, respectively. Theoretical calculations are based on the assumption that the vortex structure may be reproduced by a number of vortices, derived from the vector potential Eq. (5), aligned in parallel. Reprinted with permission from [B. Hof, C. W. H. van Doorne, J. Westerweel, F. T. M. Nieuwstadt, H. Faisst, B. Eckhardt, H. Wedin, R. R. Kerswell and F. Waleffe, Science **305**, 1594 (2004)]. Copyright (2006) AAAS.

examples of applications of this kind will be given below. The crucial property, underpinning the existence of vector potentials derived from Eq. (5), is the assumption that any fluid system left undisturbed, will decay exponentially at a uniform rate. This rate is determined by the viscosity and a universal length scale, above denoted by R.

Aligning a number of counter-rotating vortex structures, derived from Eq. (5), the pattern of streaks and vortices observed in pipe flow [3, 4] may be reproduced. The result is presented in Fig. 1.

To describe a diffusive vortex structure, instead of departing from Eq. (5), it is more efficient to depart from the Green's function of the diffusion equation and define a vector potential centered at $\boldsymbol{r}_0$ and having a symmetry axis in the direction of $\boldsymbol{n}$ as (in spherical coordinates)

$$\boldsymbol{V}(\boldsymbol{r}, z, t, \boldsymbol{r}_0 = 0, \boldsymbol{n} = \boldsymbol{e}_z) = \boldsymbol{e}_z e^{-\frac{r^2}{\nu t}} (4\pi\nu t)^{-\frac{3}{2}} \ . \tag{6}$$

This kind of vector potential results in a flow field where the vorticity and the velocity are orthogonal, and this flow field decays as a power of time. We position vortices derived from Eq. (6), with the axis in the $\boldsymbol{e}_\phi$-direction, at every point of the circle of radius R with the

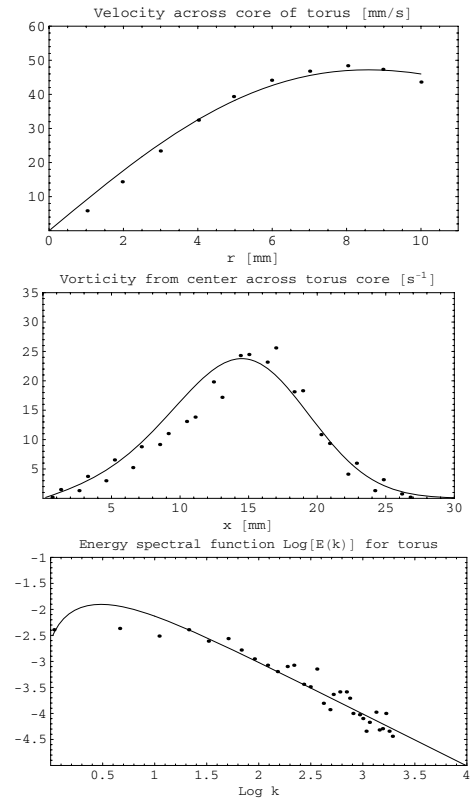

FIG. 2: Experimentally determined characteristics of a vortex ring. The top frame shows the tangential velocity as a function of the radial distance r from the center of the core. Experimental values are from Ref. [6]. The center frame shows the vorticity as a function of x, the distance from the symmetry axis of rotation in the symmetry plane across the center of the core at about $x = 15$ mm. Experimental data are from Ref. [11]. The bottom frame shows the energy spectral function as a function of the inverse length scale k. Experimental data are from Ref. [7]. In all frames, the full drawn curve represents the theoretical representation as derived from a vector potential possessing the analytical structure of Eq. (7).

center at the origin and lying in the $x - y$ plane. By carrying out an integration around this circle, the vector potential from all these contributions may be calculated

$$A(\boldsymbol{r},t)=\oint_{r'=R} d\phi \boldsymbol{V}(\boldsymbol{r},t,\boldsymbol{r}_0=\boldsymbol{r}',\boldsymbol{n}=\boldsymbol{e}_\phi)\Big|_{z'=0} W(\phi,t)\ , \tag{7}$$

where W is an arbitrary weight function. As our aim is not to study instabilities, we consider only the simplest case, we put $W=1$. The integration then results in a velocity field (spherical coordinates)

$$\boldsymbol{u}(\boldsymbol{r},t)=e^{-\frac{(r^2-R^2)}{4\nu t}}(4\pi\nu t)^{-\frac{3}{2}}\left[\frac{\cot\theta}{r}I_1\left(\frac{rR}{2\nu t}\right)\boldsymbol{e}_r\right.$$
$$\left.+\left(\frac{r}{2\nu t}I_1\left(\frac{rR}{2\nu t}\right)-\frac{R}{2\nu t}I_0\left(\frac{rR}{2\nu t}\right)\right)\boldsymbol{e}_\theta+0\ \boldsymbol{e}_\phi\right]\ , \tag{8}$$

where I_0 and I_1 are modified Bessel functions. This velocity field may now be compared to experimental data [6]. Similarly, one may derive the vorticity and the energy spectrum from Eq. (7) and compare to experimental findings [7, 11]. These comparisons to experiment have been summarized in Fig. 2.

The stretched vortex structures produced by suction [8, 10] are slender objects. Experimental results are most easily discussed in terms of a velocity field given in cylindrical coordinates (r,ϕ,z) suitable. Stretching along the z-axis by suction at the ends causes a vortex to have a stagnation point at $z=0$. One needs to satisfy boundary conditions

$$u_r(r=0,z)=0,\ u_r(r,z=0)\neq 0,\ u_\phi(r=0,z)=0,\ u_z(r=0,z)\neq 0,\ u_z(r,z=0)=0\ .$$

A possible vector potential, giving an elementary vortex structure where the vorticity and velocity are parallel, is given by the vector potential Eq. (5) multiplied by a weight function with vortex structures placed along the z-axis

$$\boldsymbol{A}(\boldsymbol{r},t)=\int dz' \sum_l c_l(z')\boldsymbol{V}(\boldsymbol{r},t,\boldsymbol{r}_0=z'\boldsymbol{e}_z,\boldsymbol{n}=\boldsymbol{e}_z,l)\ , \tag{9}$$

where the coefficients $c_l(z')$ may be arbitrarily chosen. With some restrictions from the boundary conditions, this is effectively a model with infinitely many parameters. It should then not present any difficulties to reproduce experimental data. This indicates that it should be investigated what constraints may be put on the coefficients of Eq. (9).

Starting from data on the circumferential velocity at different stations of z, one notices that the maximum velocity as a function of r increases with z in the same manner as does

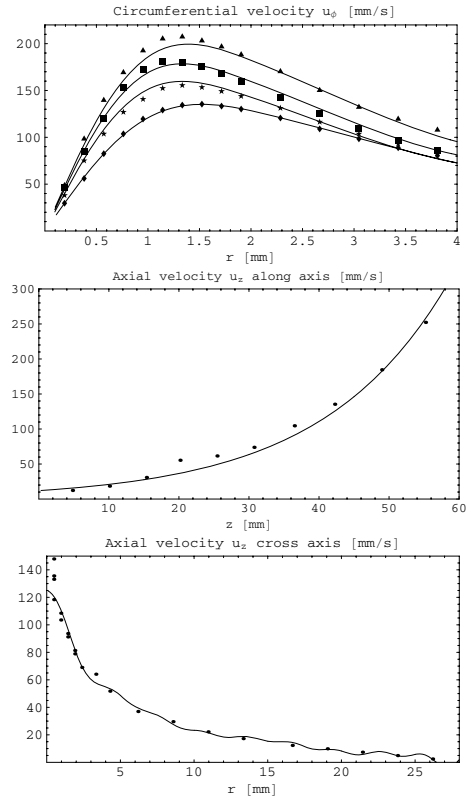

FIG. 3: Experimental characteristics of velocity components of a stretched vortex compared to theoretical representations. The top frame shows the circumferential velocity u_ϕ (cylindrical coordinates) as a function of the distance r from the axis of symmetry at different distances z from the plane of stagnation, from top to bottom $z = 7,\ 5,\ 3$ and 0 mm, respectively. Experimental data are from Ref. [10]. The center frame shows the axial velocity u_z (cylindrical coordinates) along the axis of symmetry as a function of the distance z from the plane of stagnation. Experimental data are from Ref. [8]. The bottom frame shows the axial velocity u_z in the plane of stagnation as a function of r, the distance from the axis of symmetry. Experimental data are from Ref. [8]. In all frames, the full drawn curve represents the theoretical representation as derived from a vector potential possessing the analytical structure of Eq. (9).

the axial velocity at $r = 0$. Available experimental data on the velocity field [8, 10] may be reproduced, for example, by choosing the coefficients $c_l(z')$ as polynomials in z'. The comparison to experimental data is summarized in Fig. 3.

We have discussed properties of some kind of solutions to the non-linear vorticity transport equation and how superpositions of these solutions may be used to reproduce available experimental data on properties of vortex structures. The derivation of the solutions discussed departs from the assumption that there is a universal rate of decay of vorticity for a fluid system. If this decay is exponential, there are solutions to the non-linear vorticity equation having the property that the velocity and the vorticity are parallell superpositions. If the fluid system is diffusive and decays as an inverse power of time, one may find solutions where the velocity and the vorticity are perpendicular. The solutions discussed possess degrees of freedom probably sufficient to satisfy the kind of boundary conditions commonly considered for fluid systems. However, this point needs further clarification as well as the relation between the solutions with different dynamical properties.

---

[1] B. Hof, A. Juel and T. Mullin, Phys. Rev. Lett. **91**, 2245 (2003).

[2] A. G. Darbyshire and T. Mullin, J. Fluid Mech. **289**, 83 (1995).

[3] B. Hof, C. W. H. van Doorne, J. Westerweel and T. M. Nieuwstadt, Phys. Rev. Lett. **95**, 2145 (2005).

[4] B. Hof, C. W. H. van Doorne, J. Westerweel, F. T. M. Nieuwstadt, H. Faisst, B. Eckhardt, H. Wedin, R. R. Kerswell and F. Waleffe, Science **305**, 1594 (2004).

[5] H. Faisst and B. Eckhardt, Phys. Rev. Lett. **91**, 2245 (2003).

[6] A. Dazin, P. Dupont and M. Stanislas, Exp. in Fluids **40**, 383 (2006).

[7] A. Dazin, P. Dupont and M. Stanislas, Exp. in Fluids **41**, 401 (2006).

[8] P. Petitjeans, J. H. Robres, J. E. Wesfreid and N. Kevlahan, Euro. J. Mech. B. /Fluids **17**, 549 (1998).

[9] J. C. Vassilicos and J. G. Brasseur, Phys. Rev. E **54**, 467 (1996).

[10] M. Rossi, F. Bottausci, A. Maurel and P. Petitjeans, Phys. Rev. Lett. **92**, (2004).

[11] M. Gharib, E. Rambod and K. Shariff, J. Fluid Mech. **360**, 121 (1998).

Acta Wexionensia

Nedan följer en lista på skrifter publicerade i den nuvarande Acta-serien, serie III. För förteckning av skrifter i tidigare Acta-serier, se Växjö University Press sidor på www.vxu.se

Serie III (ISSN 1404-4307)

1. *Installation Växjö universitet 1999. Nytt universitet – nya professorer. 1999*. ISBN 91-7636-233-7
2. *Tuija Virtanen & Ibolya Maricic*, 2000: Perspectives on Discourse: Proceedings from the 1999 Discourse Symposia at Växjö University. ISBN 91-7636-237-X
3. *Tommy Book*, 2000: Symbolskiften i det politiska landskapet – namn-heraldik-monument. ISBN 91-7636-234-5
4. *E. Wåghäll Nivre, E. Johansson & B. Westphal* (red.), 2000: Text im Kontext, ISBN 91-7636-241-8
5. *Göran Palm & Betty Rohdin*, 2000: Att välja med Smålandsposten. Journalistik och valrörelser 1982-1998. ISBN 91-7636-249-3
6. *Installation Växjö universitet 2000, De nya professorerna och deras föreläsningar*. 2000. ISBN 91-7636-258-2
7. *Thorbjörn Nilsson*, 2001: Den lokalpolitiska karriären. En socialpsykologisk studie av tjugo kommunalråd (doktorsavhandling). ISBN 91-7636-279-5
8. *Henrik Petersson*, 2001: Infinite dimensional holomorphy in the ring of formal power series. Partial differential operators (doktorsavhandling). ISBN 91-7636-282-5
9. *Mats Hammarstedt*, 2001: Making a living in a new country (doktorsavhandling). ISBN 91-7636-283-3
10. *Elisabeth Wåghäll Nivre & Olle Larsson*, 2001: Aspects of the European Reformation. Papers from Culture and Society in Reformation Europe, Växjö 26-27 November 1999. ISBN 91-7636-286-8
11. *Olof Eriksson*, 2001: Aspekter av litterär översättning. Föredrag från ett svensk-franskt översättningssymposium vid Växjö universitet 11-12 maj 2000. ISBN 91-7636-290-6.
12. *Per-Olof Andersson*, 2001: Den kalejdoskopiska offentligheten. Lokal press, värdemönster och det offentliga samtalets villkor 1880-1910 (Doktorsavhandling). ISBN: 91-7636-303-1.
13. *Daniel Hjorth*, 2001: Rewriting Entrepreneurship. Enterprise discourse and entrepreneurship in the case of re-organising ES (doktorsavhandling). ISBN: 91-7636-304-X.
14. *Installation Växjö universitet 2001, De nya professorerna och deras föreläsningar*, 2001. ISBN 91-7636-305-8.
15. *Martin Stigmar*, 2002. Metakognition och Internet. Om gymnasieelevers informationsanvändning vid arbete med Internet (doktorsavhandling). ISBN 91-7636-312-0.
16. *Sune Håkansson*, 2002. Räntefördelningen och dess påverkan på skogsbruket. ISBN 91-7636-316-3.
17. *Magnus Forslund*, 2002. Det omöjliggjorda entreprenörskapet. Om förnyelsekraft och företagsamhet på golvet (doktorsavhandling). ISBN 91-7636-320-1.
18. *Peter Aronsson och Bengt Johannisson (red)*, 2002. Entreprenörskapets dynamik och lokala förankring. ISBN: 91-7636-323-6.
19. *Olof Eriksson*, 2002. Stil och översättning. ISBN: 91-7636-324-4
20. *Ia Nyström*, 2002. ELEVEN och LÄRANDEMILJÖN. En studie av barns lärande med fokus på läsning och skrivning (doktorsavhandling). ISBN: 91-7636-351-1

21. *Stefan Sellbjer*, 2002. Real konstruktivism – ett försök till syntes av två dominerande perspektiv på undervisning och lärande (doktorsavhandling). ISBN: 91-7636-352-X
22. *Harald Säll*, 2002. Spiral Grain in Norway Spruce (doktorsavhandling). ISBN: 91-7636-356-2
23. *Jean-Georges Plathner*, 2003. La variabilité du pronom de la troisième personne en complément prépositionnel pour exprimer le réfléchi (doktorsavhandling). ISBN: 91-7636-361-9
24. *Torbjörn Bredenlöw*, 2003. Gestaltning – Förändring – Effektivisering. En teori om företagande och modellering. ISBN: 91-7636-364-3
25. *Erik Wångmar,* 2003. Från sockenkommun till storkommun. En analys av storkommunreformens genomförande 1939-1952 i en nationell och lokal kontext (doktorsavhandling). ISBN: 91-7636-370-8
26. *Jan Ekberg (red),* 2003, Invandring till Sverige – orsaker och effekter. Årsbok från forskningsprofilen AMER. ISBN: 91-7636-375-9
27. *Eva Larsson Ringqvist* (utg.), 2003, Ordföljd och informationsstruktur i franska och svenska. ISBN: 91-7636-379-1
28. *Gill Croona*, 2003, ETIK och UTMANING. Om lärande av bemötande i professionsutbildning (doktorsavhandling). ISBN: 91-7636-380-5
29. *Mikael Askander*, 2003, Modernitet och intermedialitet i Erik Asklunds tidiga romankonst (doktorsavhandling). ISBN: 91-7636-381-3
30. *Christer Persson*, 2003, Hemslöjd och folkökning. En studie av befolkningsutveckling, proto-industri och andra näringar ur ett regionalt perspektiv. ISBN: 91-7636-390-2
31. *Hans Dahlqvist*, 2003, Fri att konkurrera, skyldig att producera. En ideologikritisk granskning av SAF 1902-1948 (doktorsavhandling). ISBN: 91-7636-393-7
32. *Gunilla Carlsson*, 2003, Det våldsamma mötets fenomenologi – om hot och våld i psykiatrisk vård (doktorsavhandling). ISBN: 91-7636-400-3
33. *Imad Alsyouf*, 2004. Cost Effective Maintenance for Competitive Advantages (doktorsavhandling). ISBN: 91-7636-401-1.
34. *Lars Hansson*, 2004. Slakt i takt. Klassformering vid de bondekooperativa slakteriindustrierna i Skåne 1908-1946 (doktorsavhandling). ISBN: 91-7636-402-X.
35. *Olof Eriksson*, 2004. Strindberg och det franska språket. ISBN: 91-7636-403-8.
36. *Staffan Stranne*, 2004. Produktion och arbete i den tredje industriella revolutionen. Tarkett i Ronneby 1970-2000 (doktorsavhandling). ISBN: 91-7636-404-6.
37. *Reet Sjögren*, 2004. Att vårda på uppdrag kräver visdom. En studie om vårdandet av män som sexuellt förgripit sig på barn (doktorsavhandling). ISBN: 91-7636-405-4.
38. *Maria Estling Vannestål*, 2004. Syntactic variation in English quantified noun phrases with *all*, *whole*, *both* and *half* (doktorsavhandling). ISBN: 91-7636-406-2.
39. *Kenneth Strömberg*, 2004. Vi och dom i rörelsen. Skötsamhet som strategi och identitet bland föreningsaktivisterna i Hovmantorp kommun 1884-1930 (doktorsavhandling). ISBN: 91-7686-407-0.
40. *Sune G. Dufwa*, 2004. Kön, lön och karriär. Sjuksköterskeyrkets omvandling under 1900-talet (doktorsavhandling). ISBN: 91-7636-408-9
41. *Thomas Biro*, 2004. Electromagnetic Wave Modelling on Waveguide Bends, Power Lines and Space Plasmas (doktorsavhandling). ISBN: 91-7636-410-0
42. *Magnus Nilsson*, 2004, Mångtydigheternas klarhet. Om ironier hos Torgny Lindgren från *Skolbagateller* till *Hummelhonung* (doktorsavhandling). ISBN:91-7636-413-5
43. *Tom Bryder*, 2004. Essays on the Policy Sciences and the Psychology of Politics and Propaganda. ISBN: 91-7636-414-3

44. *Lars-Göran Aidemark*, 2004. Sjukvård i bolagsform. En studie av Helsingborgs Lasarett AB och Ängelholms Sjukhus AB. ISBN: 91-7636-417-8
45. *Per-Anders Svensson*, 2004. Dynamical Systems in Local Fields of Characteristic Zero (doktorsavhandling). ISBN: 91-7636-418-6
46. *Rolf G Larsson*, 2004. Prototyping inom ABC och BSc. Erfarenheter från aktionsforskning i tre organisationer (doktorsavhandling). ISBN: 91-7636-420-8
47. *Päivi Turunen*, 2004. Samhällsarbete i Norden. Diskurser och praktiker i omvandling (doktorsavhandling). ISBN: 91-7636-422-4
48. *Carina Henriksson*, 2004. Living Away from Blessings. School Failure as Lived Experience (doktorsavhandling). ISBN: 91-7636-425-9
49. *Anne Haglund*, 2004. The EU Presidency and the Northern Dimension Initiative: Applying International Regime Theory (doktorsavhandling). ISBN: 91-7636-428-3
50. *Ulla Rosén*, 2004. Gamla plikter och nya krav. En studie om egendom, kvinnosyn och äldreomsorg i det svenska agrarsamhället 1815-1939. ISBN: 91-7636-429-1
51. *Michael Strand*, 2004. Particle Formation and Emission in Moving Grate Boilers Operating on Woody Biofuels (doktorsavhandling). ISBN: 91-7636-430-5
52. *Bengt-Åke Gustafsson*, 2004. Närmiljö som lärmiljö – betraktelser från Gnosjöregionen. ISBN: 91-7636-432-1
53. *Lena Fritzén* (red), 2004. På väg mot integrativ didaktik. ISBN: 91-7636-433-X
54. *M.D. Lyberg, T. Lundström & V. Lindberg*, 2004. Physics Education. A short history. Contemporary interdisciplinary research. Some projects. ISBN: 91-7636-435-6
55. *Gunnar Olofsson (red.),* 2004. Invandring och integration. Sju uppsatser från forskningsmiljön ”Arbetsmarknad, Migration och Etniska relationer” (AMER) vid Växjö universitet. ISBN: 91-7636-437-2
56. *Malin Thor*, 2005. Hechaluz – en rörelse i tid och rum. Tysk-judiska ungdomars exil i Sverige 1933-1943 (doktorsavhandling). ISBN: 91-7636-438-0
57. *Ibolya Maricic*, 2005. Face in cyberspace: Facework, (im)politeness and conflict in English discussion groups (doktorsavhandling). ISBN: 91-7636-444-5
58. *Eva Larsson Ringqvist* och *Ingela Valfridsson* (red.), 2005. Forskning om undervisning i främmande språk. Rapport från workshop i Växjö 10-11 juni 2004. ISBN: 91-7636-450-X
59. *Vanja Lindberg*, 2005. Electronic Structure and Reactivity of Adsorbed Metallic Quantum Dots (doktorsavhandling). ISBN: 91-7636-451-8
60. *Lena Agevall*, 2005. Välfärdens organisering och demokratin – en analys av New Public Management. ISBN: 91-7636-454-2
61. *Daniel Sundberg*, 2005. Skolreformernas dilemman – En läroplansteoretisk studie av kampen om tid i den svenska obligatoriska skolan (doktorsavhandling). ISBN: 91-7636-456-9.
62. *Marcus Nilsson*, 2005. Monomial Dynamical Systems in the Field of *p*-adic Numbers and Their Finite Extensions (doktorsavhandling). ISBN: 91-7636-458-5.
63. *Ann Erlandsson*, 2005. Det följdriktiga flockbeteendet: en studie om profilering på arbetsmarknaden (doktorsavhandling). ISBN: 91-7636-459-3.
64. *Birgitta Sundström Wireklint*, 2005. Förberedd på att vara oförberedd. En fenomenologisk studie av vårdande bedömning och dess lärande i ambulanssjukvård (doktorsavhandling). ISBN: 91-7636-460-7
65. *Maria Nilsson*, 2005. Differences and similarities in work absence behavior – empirical evidence from micro data (doktorsavhandling). ISBN: 91-7636-462-3
66. *Mikael Bergström och Åsa Blom*, 2005. Above ground durability of Swedish softwood (doktorsavhandling). ISBN: 91-7636-463-1

67. *Denis Frank*, 2005. Staten, företagen och arbetskraftsinvandringen - en studie av invandringspolitiken i Sverige och rekryteringen av utländska arbetare 1960-1972 (doktorsavhandling). ISBN: 91-7636-464-X
68. *Mårten Bjellerup,* 2005. Essays on consumption: Aggregation, Asymmetry and Asset Distributions (doktorsavhandling). ISBN: 91-7636-465-8.
69. *Ragnar Jonsson*, 2005. Studies on the competitiveness of wood – market segmentation and customer needs assessment (doktorsavhandling). ISBN: 91-7636-468-2.
69. Anders Pehrsson och Basim Al-Najjar, Creation of Industrial Competitiveness: CIC 2001-2004. ISBN: 91-7646-467-4.
70. *Ali M. Ahmed*, 2005. Essays on the Behavioral Economics of Discrimination (doktorsavhandling). ISBN: 91-7636-472-0.
71. *Katarina Friberg*, 2005. The workings of co-operation.. A comparative study of consumer co-operative organisation in Britain and Sweden, 1860 to 1970 (doktorsavhandling). ISBN: 91-7636-470-4.
72. *Jonas Sjölander*, 2005. Solidaritetens omvägar. Facklig internationalism i den tredje industriella revolutionen – (LM) Ericsson, svenska Metall och Ericssonarbetarna i Colombia 1973-1993 (doktorsavhandling) ISBN: 91-7636-474-7.
73. *Daniel Silander*, 2005. Democracy from the outside-in? The conceptualization and significance of democracy promotion (doktorsavhandling). ISBN: 91-7636-475-5.
74. *Serge de Gosson de Varennes*, 2005. Multi-oriented Symplectic Geometry and the Extension of Path Intersection Indices (doktorsavhandling). ISBN: 91-7636-477-1.
75. *Rebecka Ulfgard*, 2005. Norm Consolidation in the European Union: The EU14-Austria Crisis in 2000 (doktorsavhandling). ISBN: 91-7636-482-8
76. *Martin Nilsson*, 2005. Demokratisering i Latinamerika under 1900-talet – vänstern och demokratins fördjupning (doktorsavhandling). ISBN: 91-7636-483-6
77. *Thomas Panas*, 2005. A Framework for Reverse Engineering (doktorsavhandling). ISBN: 91-7636-485-2
78. *Susanne Linnér*, 2005. Värden och villkor – pedagogers samtal om ett yrkesetiskt dokument (doktorsavhandling). ISBN: 91-7636-484-4.
79. *Lars Olsson* (red), 2005. Invandring, invandrare och etniska relationer I Sverige 1945-2005. Årsbok från forskningsmiljön AMER vid Växjö universitet. ISBN: 91-7636-488-7.
80. *Johan Svanberg*, 2005. Minnen av migrationen. Arbetskraftsinvandring från Jugoslavien till Svenska Fläktfabriken i Växjö kring 1970. ISBN: 91-7636-490-9.
81. *Christian Ackrén*, 2006. On a problem related to waves on a circular cylinder with a surface impedance (licentiatavhandling). ISBN: 91-7636-492-5.
82. *Stefan Lund*, 2006. Marknad och medborgare – elevers valhandlingar i gymnasieutbildningens integrations- och differentieringsprocesser (doktorsavhandling). ISBN: 91-7636-493-3.
83. *Ulf Petäjä*, 2006. Varför yttrandefrihet? Om rättfärdigandet av yttrandefrihet med utgångspunkt från fem centrala argument i den demokratiska idétraditionen (doktorsavhandling). ISBN: 91-7636-494-1.
84. *Lena Carlsson*, 2006. Medborgarskap som demokratins praktiska uttryck i skolan – diskursiva konstruktioner av gymnasieskolans elever som medborgare (doktorsavhandling). ISBN: 91-7636-495-X
85. *Åsa Gustafsson*, 2006. Customers´ logistics service requirements and logistics strategies in the Swedish sawmill industry (doktorsavhandling). ISBN: 91-7636-498-4.
86. *Kristina Jansson*, 2006. Saisir l'insaisissable. Les formes et les traductions du discours indirect libre dans des romans suédois et français (doktorsavhandling). ISBN: 91-7636-499-2
87. *Edith Feistner, Alfred Holl*, 2006. Mono-perspective views of multi-perspectivity : Information systems modeling and 'The bild men and the elephant'. ISBN : 91-7636-500-X.

88. *Katarina Rupar-Gadd*, 2006. Biomass Pre-treatment for the Production of Sustainable Energy – Emissions and Self-ignition (doktorsavhandling). ISBN: 91-7636-501-8.
89. *Lena Agevall, Håkan Jenner* (red.),2006. Bilder av polisarbete – Samhällsuppdrag, dilemman och kunskapskrav. ISBN: 91-7636-502-6
90. *Maud Ihrskog*, 2006. Kompisar och Kamrater .Barns och ungas villkor för relationsskapande i vardagen (doktorsavhandling). ISBN: 91-7636-503-4.
91. *Detlef Quast*, 2006. Die Kunst die Zukunft zu erfinden Selbstrationalität, asymmetrische Information und Selbstorganisation in einer wissensintensiven professionellen Non Profit Organisation. Eine informationstheoretische und organisationssoziologische Studie zum Verständnis des Verhaltens der Bibliotheksverwaltung (doktorsavhandling). ISBN: 91-7636-505-0.
92. *Ulla Johansson*, 2006. Design som utvecklingskraft. En utvärdering av regeringens designsatsning 2003-2005. ISBN: 91-7636-507-7.
93. *Klara Helstad*, 2006. Managing timber procurement in Nordic purchasing sawmills (doktorsavhandling). ISBN:91-7636-508-5.
94. *Göran Andersson, Rolf G. Larsson*, 2006. Boundless value creation. Strategic management accounting in value system configuration. ISBN: 91-7636-509-3.
95. *Jan Håkansson*, 2006. Lärande mellan policy och praktik. Kontextuella villkor för skolans reformarbete (doktorsavhandling). ISBN: 91-7636-510-7.
96. *Frederic Bill*, 2006. The Apocalypse of Entrepreneurship (doktorsavhandling). ISBN: 91-7636-513-1.
97. *Lena Fritzén*, 2006. "On the edge" – om förbättringsledarskap i hälso- och sjukvård ISBN: 91-7636-516-6
98. *Marianne Lundgren*, 2006. Från barn till elev i riskzon. En analys av skolan som kategoriseringsarena (doktorsavhandling). ISBN: 91-7636-518-2.
99. *Mari Mossberg*, 2006, La relation de concession. Étude contrastive de quelques connecteurs concessifs français et suédois (doktorsavhandling). ISBN : 91-7636-517-4.
100. *Leif Grönqvist*, 2006. Exploring Latent Semantic Vector Models Enriched With N-grams (doktorsavhandling), ISBN: 91-7636-519-0.
101. *Katarina Hjelm* (red), 2006. Flervetenskapliga perspektiv i migrationsforskning. Årsbok 2006 från forskningsprofilen Arbetsmarknad, Migration och Etniska relationer (AMER) vid Växjö universitet. ISBN: 91-7636-520-4.
102. *Susanne Thulin*, 2006. Vad händer med lärandets objekt? En studie av hur lärare och barn i förskolan kommunicerar naturvetenskapliga fenomen (licentiatavhandling), ISBN: 91-7636-521-2
103. *Per Nilsson*, 2006. Exploring Probabilistic Reasoning – A Study of How Students Contextualise Compound Chance Encounters in Explorative Settings (doktorsavhandling), ISBN: 91-7636-522-0.
104. *PG Fahlström, Magnus Forslund, Tobias Stark* (red.), 2006, Inkast. Idrottsforskning vid Växjö universitet. ISBN: 91-7636-523-9.
105. *Ulla Johansson* (red.), 2006, Design som utvecklingskraft II. Fem uppsatser om Fem uppsatser om utvalda projekt från regeringens designsatsning 2003-2005, ISBN: 91-7636-530-1.
106. *Ann-Charlotte Larsson* 2007, Study of Catalyst Deactivation in Three Different Industrial Processes (doktorsavhandling), ISBN: 978-91-7636-533-5.

107. *Karl Loxbo*, 2007,Bakom socialdemokraternas beslut. En studie av den politiska förändringens dilemman - från 1950-talets ATP-strid till 1990-talets pensionsuppgörelse (doktorsavhandling), ISBN: 978-91-7636-535-9.
108. *Åsa Nilsson-Skåve*, 2007,Hjärtat som hör det förstummade spela. Studier i Stina Aronsons berättarkonst (doktorsavhandling), ISBN: 978-91-7636-536-6.
109. *Anne Haglund Morrissey, Daniel Silander* (eds.), 2007, The EU and the Outside World - Global Themes in a European Setting, ISBN: 978-91-7636-537-3.
110. *Robert Nyqvist*, 2007, Algebraic Dynamical Systems, Analytical Results and Numerical Simulations (doktorsavhandling), ISBN: 978-91-7636-547-2.
111. *Christer Fritzell, Lena Fritzén*, 2007, Integrativ didaktik i olika ämnesperspektiv. ISBN: 978-91-7636-548-9.
112. *Torgny Klasson, Daniel Silander*, 2007. Hot och hotbilder i globaliseringens tid – en studie av den svenska säkerhetspolitiska debatten. ISBN: 978-91-7636-550-2
113. *Olof Eriksson* (red.), 2007. Översättning och Kultur. Föredrag från ett symposium vid Växjö universitet 17-18 november 2006, ISBN: 978-91-7636-552-6
114. *Henrik Tryggeson*, 2007. Analytical Vortex Solutions to Navier-Stokes Equation (doktorsavhandling), ISBN: 978-91-7636-555-7.

Växjö University Press
351 95 Växjö
www.vxu.se
vup@vxu.se